AFWAL-TR-87- 3058

ON DELAMINATION OF $(\pm\theta_m / 90_{n/2})_s$ LAMINATES SUBJECTED TO TENSILE LOADING

R. S. Sandhu
Structural Concepts Branch
G. P. Sendeckyj
Structural Integrity Branch
Structures Division

July 1987

FINAL TECHNICAL REPORT for Period March 1983 - January 1986

Approved for public release; distribution unlimited

FLIGHT DYNAMICS LABORATORY
AIR FORCE WRIGHT AERONAUTICAL LABORATORIES
AERONAUTICAL SYSTEMS DIVISION
AIR FORCE SYSTEMS COMMAND
WRIGHT-PATTERSON AIR FORCE BASE, OHIO 45433 - 6553

NOTICE

When Government drawings, specifications, or other data are used for any purpose other than in connection with a definitely Government-related procurement, the United States Government incurs no responsibility or any obligation whatsoever. The fact that the Government may have formulated or in any way supplied the said drawings, specifications, or other data, is not to be regarded by implication, or otherwise in any manner construed, as licensing the holder, or any other person or corporation; or as conveying any rights or permission to manufacture, use, or sell any patented invention that may in any way be related thereto.

This report has been reviewed by the Office of Public Affairs (ASD/PA) and is releasable to the National Technical Information Service (NTIS). At NTIS, it will be available to the general public, including foreign nations.

This report has been reviewed and is approved for publication.

Raghbir S. Sandhu

RAGHBIR S. SANDHU
Project Engineer

Larry G. Kelly

LARRY G. KELLY, Chief
Structural Concepts Branch
Structures Division

FOR THE COMMANDER

Henry A Bondaruk

HENRY A. BONDARUK, JR, Col, USAF
Chief, Structures Division
Flight Dynamics Laboratory

If your address has changed, if you wish to be removed from our mailing list, or if the addressee is no longer employed by your organization please notify AFWAL/FIBC, W-PAFB, OH 45433 to help us maintain a current mailing list.

Copies of this report should not be returned unless return is required by security consideration, cotractual obligations, or notice on a specific document.

UNCLASSIFIED

SECURITY CLASSIFICATION OF THIS PAGE

REPORT DOCUMENTATION PAGE

Form Approved OMB No. 0704-0188

1a. REPORT SECURITY CLASSIFICATION: UNCLASSIFIED	1b. RESTRICTIVE MARKINGS
2a. SECURITY CLASSIFICATION AUTHORITY	3. DISTRIBUTION/AVAILABILITY OF REPORT: Approved for public release; distribution unlimited
2b. DECLASSIFICATION/DOWNGRADING SCHEDULE	
4. PERFORMING ORGANIZATION REPORT NUMBER(S): AFWAL - TR - 87 - 3058	5. MONITORING ORGANIZATION REPORT NUMBER(S)
6a. NAME OF PERFORMING ORGANIZATION: Structural Concepts Branch Structures Division (cont'd) / 6b. OFFICE SYMBOL (If applicable): AFWAL/FIBC	7a. NAME OF MONITORING ORGANIZATION
6c. ADDRESS (City, State, and ZIP Code): Wright-Patterson Air Force Base, Ohio 45433	7b. ADDRESS (City, State, and ZIP Code)
8a. NAME OF FUNDING/SPONSORING ORGANIZATION / 8b. OFFICE SYMBOL (If applicable)	9 PROCUREMENT INSTRUMENT IDENTIFICATION NUMBER
8c. ADDRESS (City, State, and ZIP Code)	10. SOURCE OF FUNDING NUMBERS

PROGRAM ELEMENT NO	PROJECT NO	TASK NO	WORK UNIT ACCESSION NO
62201F	2401	03	66

11. TITLE (Include Security Classification)

On Delamination of $(\pm\theta_m / 90_{n/2})_s$ Laminates Subjected to Tensile Loading (Unclassified)

12. PERSONAL AUTHOR(S)

Sandhu, Raghbir S.; Sendeckyj George P.

13a. TYPE OF REPORT	13b. TIME COVERED	14. DATE OF REPORT (Year, Month, Day)	15. PAGE COUNT
Final	FROM March 1983 TO January 1986	1987 July	148

16. SUPPLEMENTARY NOTATION

17. COSATI CODES			18. SUBJECT TERMS (Continue on reverse if necessary and identify by block number)
FIELD	GROUP	SUB-GROUP	
13	13		Delamination, Laminated Composites, Stress Analysis,
11	04		Peel Stresses, Experimental Data, Acoustic Emission

19. ABSTRACT (Continue on reverse if necessary and identify by block number)

Delamination initiation investigations of symmetric laminates consisting of angle ply and 90-degree plies were conducted. Five criteria were used to determine delamination initiation for a given set m and n of angle plies and 90-degree plies. In the criteria one and two, delamination moment rates (delamination moment coefficients or DMC) relative to the applied average axial stress and strain in laminates with uncracked 90-degree plies, were maximized. The same approach was used in the criteria three and four except that the laminates had cracked 90-degree plies. The fifth criterion was based upon establishing the maximum mismatch of Poisson's ratios of angle plies and 90-degree plies. The expressions derived on the basis of the five criteria were numerically evaluated.

The results of these studies indicated that the laminates designed on the basis of the fifth criterion, namely, maximum mismatch of Poisson's ratios of angle plies and 90-degree plies had the minimum tendency to delaminate. In addition it was found that an increase in thickness of laminates (cont'd)

20 DISTRIBUTION/AVAILABILITY OF ABSTRACT	21 ABSTRACT SECURITY CLASSIFICATION
☐ UNCLASSIFIED/UNLIMITED ☒ SAME AS RPT ☐ DTIC USERS	UNCLASSIFIED

22a NAME OF RESPONSIBLE INDIVIDUAL	22b TELEPHONE (Include Area Code)	22c OFFICE SYMBOL
R. S. Sandhu	(513) 255-5864	AFWAL/FIBCA

DD Form 1473, JUN 86 — Previous editions are obsolete — SECURITY CLASSIFICATION OF THIS PAGE

UNCLASSIFIED

6. Continued

Flight Dynamics Laboratory
Air Force Wright Aeronautical Laboratories
Air Force Systems Command

19. Continued

tended to increase the delaminating tendency.

To confirm the results, four laminates A, B, C and D were selected. Laminates A, B, and C were designed in accordance with the criteria number one,two, and five respectively. Laminate D was similar to laminate A except that it was thicker and was chosen to discriminate the thickness effect.All the four laminates were analysed using the finite element method. In addition four graphite-epoxy panels corresponding to the four laminates were fabricated, cut into specimens, and were tested under uniaxial tensile loading to determine the onset of delamination.

Finite element analyses, and experimental data confirmed the approximate analytical investigations. The results shows that the delamination moment coefficient is a valid quantitative measure of the tendency of laminates to delaminate. This delamination moment coefficient concept can be used to design stacking sequences of laminates either to have a maximum tendency or a minimum tendency to delaminate. The laminates designed on the basis of DMC to have maximum tendency to delaminate were observed to fail in mixed mode, i.e., the transverse cracking of 90-degree plies combined with the edge delamination. This mixed failure mode can be avoided by imposing an additional constraint of limiting the strain in loading direction to the cracking strain (4000 μ) of 90-degree plies.

FOREWORD

This effort was initiated in September 1983 by the Structural Concepts Branch, Structures Division, Flight Dynamics Laboratory, Air Force Wright Aeronautical Laboratories, under Project No. 2401, Task No. 240103 and Work Unit No. 24010366 (Composite Fabrication, Damage Assessment and Repair), and completed in February 1986.

The specimens were fabricated by Beta Industries' on-site contractor for the Structural Concepts Branch. Mr Paul Rimer was contractor manager.

The experimental work was performed by Messrs H. D. Stalnaker, J. V. Smith and L. G. Bates of Fatigue, Fracture and Reliability Group of the Structural Integrity Branch. The Instrumentation, Data Acquisition and Data Processing Engineers were Messrs M. J. North, F. E. Hussong and B. F. Davis of the Structures Test Branch, respectively.

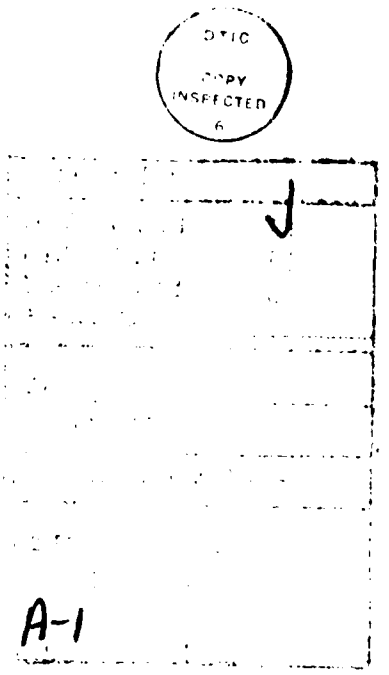

TABLE OF CONTENTS

TABLE OF CONTENTS (CONT'D)

LIST OF ILLUSTRATIONS

LIST OF ILLUSTRATIONS (CONT'D)

LIST OF ILLUSTRATIONS (CONT'D)

LIST OF ILLUSTRATIONS (CONT'D)

LIST OF ILLUSTRATIONS (CONT'D)

LIST OF TABLES

LIST OF TABLES (CONT'D)

SECTION I
INTRODUCTION

Interlaminar stresses exist in the neighborhood of the free edges of laminated plates subjected to in-plane loads. Since the time their existence was established, various numerical and analytical techniques have been used to study the nature of and the factors that influence the interlaminar stresses [1 thru 43]. These studies indicated that the interlaminar normal (peeling) stress is the dominant cause of delamination.

Pagano and Pipes [9] developed an approximate expression for the maximum peeling stress in terms of the transverse in-plane stresses in the plies based upon the classical lamination theory. In their formulation, the peeling stresses were maximized when the delamination moment (moment of transverse in-plane stresses about a point in the plane of potential delamination) is maximized. Based on examination of the expression for the delamination moment, they stated that a large Poisson's ratio mismatch tends to magnify the transverse stresses and the resulting delamination moment. They did not include the effect of accompanying changes of elastic properties. Orringer [28] used the maximum Poisson's ratio mismatch concept to design a delaminating specimen to measure the peeling stress. In addition, he conducted numerical studies. In these studies for a given laminate, he varied the ply angles and computed the maximum peeling stress per unit axial strain. He observed that the angle maximizing Poisson's ratio mismatch did not agree with the angle obtained from the numerical studies. Orringer ignored this discrepancy in favor of the design based upon the Poisson's ratio mismatch. In both studies a distribution of the peeling stresses based upon earlier experience was assumed. Sandhu [44] on the basis of experimental data suggested that no distribution pattern of the peeling stresses needed to be assumed. A simple comparison of delaminating tendency of the laminates based upon the delaminating moment per unit axial stresss was more than adequate.

In the effort reported herein the phenomena of delamination is examined in detail. The laminate system selected is angle plies with transverse plies placed at mid thickness of the laminates. The laminates are subjected to the following constraints:

a. Uncracked transverse plies and the laminates subjected to force loading.

b. Uncracked transverse plies and the laminates subjected to displacement loading.

c. Cracked transverse plies and the laminates subjected to force loading.

d. Cracked transverse plies and the laminates subjected to displacement loading.

e. Maximum Poisson's ratio mismatch.

Section II contains derivations and related analytical studies, Section III describes experiments conducted and Section IV summarizes the results and conclusions.

SECTION I I

ANALYTICAL INVESTIGATIONS

The objective of this study is to define a measure of the edge delaminating tendency of $[(\theta / -\theta)_m / 90_n / (-\theta / \theta)_m]$ laminates subjected to uniaxial loading, where m and n are integers. To meet the stated objective both analytical and experimental investigations were conducted. The analytical studies contained in this Section include:

a. Ply constitutive relations.
b. Stress resultants (for cracked and uncracked 90-degree plies).
c. Transverse stresses (for cracked and uncracked 90-degree plies)
d. Equilibrium conditions.
e. Delaminating moment (DM) and delaminating moment coefficient (DMC).
f. Delamination initiation criteria for cracked and uncracked 90-degree plies.
   (i) Maximizing DMC for force and displacement loadings.
   (ii) Maximizing Poisson's ratio mismatch of angle plies and 90-degree plies.
   (iii) Maximizing Poisson's ratio of the laminates.
g. Numerical evaluation.
h. Analytical evaluation of (g) using finite element analysis.
i. Residual thermal curing stresses.

Mechanical and thermal loads impose different constraints upon the laminates. For this reason, both types of loads were applied separately. To begin with laminates consisting of given sets of m and n plies were subjected to uniaxial loading. Using a delamination initiation criterion, ply angles maximizing the delamination tendency of these laminates were determined. These laminates were then evaluated for thermal effects.

1. Ply Constitutive Relations

Consider a single ply of fiber-reinforced composite material oriented at an angle θ with respect to a reference direction (Figure 1). Let the material axes (x_1, x_2) coincide and be perpendicular to the fiber direction. Assuming that the ply exhibits linearly thermoelastic behavior, the constitutive relations in the material coordinates system can be written as

$$e_i = S_{ij}\,\sigma_j + \alpha_i\,T$$

or

$$S_{ij}\,\sigma_j = (e_i - \alpha_i\,T) \qquad i, j = 1, 2, 6 \qquad (1)$$

where σ_j, e_i, α_i, T, and S_{ij} are the stresses, the engineering strains, linear coefficients of thermal expansion, the temperature increment and the elastic compliances.

The stresses in Equation 1 are given by

$$\sigma_i = C_{ij} (e_j - \alpha_j T) \qquad i, j = 1, 2, 6 \qquad (2)$$

The nonzero elastic stiffnesses in Equation 2 are given by

$$\begin{aligned} C_{11} &= E_{11}/(1-\mu_{12}\mu_{21}) \\ C_{22} &= E_{22}/(1-\mu_{12}\mu_{21}) \\ C_{12} &= \mu_{12} C_{22} = \mu_{21} C_{11} \\ C_{66} &= G_{12} \end{aligned} \qquad (3)$$

where E_{11}, E_{22}, G_{12}, and μ_{12} are the longitudinal Young's modulus, transverse Young's modulus, longitudinal shear modulus and major Poisson's ratio, respectively. The constitutive relations in reference coordinate system (x,y) are given by

$$\begin{bmatrix} \sigma_x \\ \sigma_y \\ \sigma_s \end{bmatrix} = \begin{bmatrix} C^{\theta}_{11} & C^{\theta}_{12} & C^{\theta}_{16} \\ C^{\theta}_{21} & C^{\theta}_{22} & C^{\theta}_{26} \\ C^{\theta}_{61} & C^{\theta}_{62} & C^{\theta}_{66} \end{bmatrix} \begin{bmatrix} e_x - \alpha_x T \\ e_y - \alpha_y T \\ e_s - \alpha_s T \end{bmatrix} \qquad (4)$$

where $C^{\theta}_{ij} = C^{\theta}_{ji}$ and

$$\begin{aligned} C^{\theta}_{11} &= U_1 + U_2 \cos (2\theta) + U_3 \cos (4\theta) \\ C^{\theta}_{12} &= U_4 - U_3 \cos (4\theta) \\ C^{\theta}_{22} &= U_1 - U_2 \cos (2\theta) + U_3 \cos (4\theta) \\ C^{\theta}_{16} &= - 0.5\, U_2 \sin (2\theta) - U_3 \sin (4\theta) \\ C^{\theta}_{26} &= - 0.5\, U_2 \sin (2\theta) + U_3 \sin (4\theta) \\ C^{\theta}_{66} &= U_5 - U_3 \cos (4\theta) \end{aligned} \qquad (5)$$

where the elastic constant invariants U_i (Reference 45) are given by

$$\begin{aligned} U_1 &= (3C_{11} + 3C_{22} + 2C_{12} + 4C_{66}) / 8 \\ U_2 &= (C_{11} - C_{22}) / 2 \\ U_3 &= (C_{11} + C_{22} - 2C_{12} - 4C_{66}) / 8 \\ U_4 &= (C_{11} + C_{22} + 6C_{12} - 4C_{66}) / 8 \\ U_5 &= (C_{11} + C_{22} - 2C_{12} - 4C_{66}) / 8 \end{aligned} \qquad (6)$$

and

$$\begin{aligned} \alpha_x &= 0.5 (\alpha_1 + \alpha_2) + 0.5 (\alpha_1 - \alpha_2) \cos (2\theta) \\ \alpha_y &= 0.5 (\alpha_1 + \alpha_2) - 0.5 (\alpha_1 - \alpha_2) \cos (2\theta) \\ \alpha_s &= 0.5 (\alpha_1 - \alpha_2) \sin (2\theta) \end{aligned} \qquad (7)$$

2. Stress Resultants

Shear coupling terms of $[(\theta / - \theta)_m / 90_n / (-\theta / \theta)_m]$ laminates are given by

$$C^{\theta}_{16} = C^{\theta}_{61} = - C^{-\theta}_{16} = - C^{-\theta}_{61}$$
$$C^{\theta}_{26} = C^{\theta}_{62} = - C^{-\theta}_{26} = - C^{-\theta}_{62}$$
$$C^{90}_{61} = C^{90}_{16} = C^{90}_{26} = C^{90}_{62} = 0$$

2.1 Stress resultants (uncracked 90 plies)

Applying the above equations and Equation 4, stress resultants for $[(\theta / - \theta)_m / 90_n / (-\theta / \theta)_m]$ laminates of uniform ply thickness t with uncracked 90-degree plies are given by

$$\begin{aligned} N_{xy}/t &= [\, 2m\, C^{\theta}_{61} + 2m\, C^{-\theta}_{61} + n\, C^{90}_{61} \,]\, e_x \\ &\quad +[\, 2m\, C^{\theta}_{62} + 2m\, C^{-\theta}_{62} + n\, C^{90}_{62} \,]\, e_y \\ &\quad +[\, 2m\, C^{\theta}_{66} + 2m\, C^{-\theta}_{66} + n\, C^{90}_{66} \,]\, e_s \\ &= [\, 2m\, C^{\theta}_{66} + 2m\, C^{-\theta}_{66} + n\, C^{90}_{66} \,]\, e_s \\ &= \lambda_4\, e_s \end{aligned} \tag{8}$$

where (using Equation 5)

$$\lambda_4 = 4m\, [\, U_5 - U_3 \cos (4\theta) \,] + n\, (U_5 - U_3) \tag{9}$$

From Equation 8 we find that Nxy = 0, if $e_s = 0$ and vice versa.

$$\begin{aligned} N_x/t &= [\, 2m\, C^{\theta}_{11} + 2m\, C^{-\theta}_{11} + n\, C^{90}_{11} \,]\, e_x \\ &\quad +[\, 2m\, C^{\theta}_{12} + 2m\, C^{-\theta}_{12} + n\, C^{90}_{12} \,]\, e_y \\ &\quad +[\, 2m\, C^{\theta}_{16} + 2m\, C^{-\theta}_{16} + n\, C^{90}_{16} \,]\, e_s \\ &= \lambda_1\, e_x + \lambda_2\, e_y \end{aligned} \tag{10}$$

where, using Equation 5,

$$\begin{aligned} \lambda_1 &= 4m\, [\, U_1 + U_2 \cos (2\theta) + U_3 \cos (4\theta) \,] \\ &\quad +n\, [U_1 - U_2 + U_3 \,] \end{aligned} \tag{11}$$

$$\lambda_2 = 4m\, [\, U_4 - U_3 \cos (4\theta) \,] + n\, [\, U_4 - U_3 \,] \tag{12}$$

$$\begin{aligned} N_y/t &= [\, 2m\, C^{\theta}_{21} + 2m\, C^{-\theta}_{21} + n\, C^{90}_{21} \,]\, e_x \\ &\quad +[\, 2m\, C^{\theta}_{22} + 2m\, C^{-\theta}_{22} + n\, C^{90}_{22} \,]\, e_y \\ &\quad +[\, 2m\, C^{\theta}_{26} + 2m\, C^{-\theta}_{66} + n\, C^{90}_{26} \,]\, e_s \\ &= \lambda_2\, e_x + \lambda_3\, e_y \end{aligned} \tag{13}$$

where, using Equation 5,

$$\begin{aligned} \lambda_3 &= 4m\, [\, U_1 - U_2 \cos (2\theta) + U_3 \cos (4\theta) \,] \\ &\quad +n\, [\, U_1 + U_2 + U_3 \,] \end{aligned} \tag{14}$$

2.2 Stress resultants (cracked 90 plies)

In the case of cracked plies, it is assumed that

$$C_{22} = C_{12} = C_{66} = 0$$

and C_{11} is not equal to zero.

Consequently ,

$$C^{90}_{66} = C^{90}_{11} = C^{90}_{12} = 0$$

$$C^{90}_{22} = E_{11}$$

The stress resultants for $[(\theta / -\theta)_m / 90_n / (-\theta / \theta)_m]$ with cracked 90-degree plies are given by

$$\begin{aligned} N^c_{xy}/t &= \lambda^c_4 \, e_s \\ N^c_x/t &= \lambda^c_1 \, e_x + \lambda^c_2 \, e_y \\ N^c_y/t &= \lambda^c_2 \, e_x + \lambda^c_3 \, e_y \end{aligned} \tag{15}$$

where

$$\begin{aligned} \lambda^c_1 &= 4m \, [\, U_1 + U_2 \cos(2\theta) + U_3 \cos(4\theta)] \\ \lambda^c_2 &= 4m \, [\, U_4 - U_3 \cos(4\theta)] \\ \lambda^c_3 &= 4m \, [\, U_1 - U_2 \cos(2\theta) + U_3 \cos(4\theta)] + n \, C_{11} \\ \lambda^c_4 &= 4m \, [\, U_5 - U_3 \cos(4\theta)] \end{aligned} \tag{16}$$

3. Equilibrium Conditions

For both uncracked and uncracked 90-degree plies the uniaxial loading of $[(\theta / -\theta)_m / 90_n / (-\theta / \theta)_m]$ laminates implies that

$$N_{xy} = N^c_{xy} = N_y = N^c_y = e_s = 0$$

and N_x, N^c_x, e_x, and e_y are not zero.

3.1 Uncracked 90 plies

Stress resultants for uncracked 90-degree plies are given by

$$\begin{aligned} N_x &= (\lambda_1 \, e_x + \lambda_2 \, e_y) \, t \\ N_y &= (\lambda_2 \, e_x + \lambda_3 \, e_y) \, t = 0 \end{aligned} \tag{17}$$

Equations 17 yield

$$\begin{aligned} e_x &= -(\lambda_3 \, e_y) / \lambda_2 \\ &= -N_x \, [\lambda_3 / (\lambda_2^2 - \lambda_1 \lambda_3)] / t \\ e_y &= N_x \, [\lambda_2 / (\lambda_2^2 - \lambda_1 \lambda_3)] / t \end{aligned} \tag{18}$$

3.2 Cracked 90 plies

Stress resultants for cracked 90-degree plies are given by

$$\begin{aligned} N^c_x &= (\lambda^c_1 \, e_x + \lambda^c_2 \, e_y) \, t \\ N^c_y &= (\lambda^c_2 \, e_x + \lambda^c_3 \, e_y) \, t = 0 \end{aligned} \tag{19}$$

Equations 19 yield

$$\begin{aligned} e_x &= -(\lambda^c_3 \, e_y) / \lambda^c_2 \\ &= -N^c_x \, [\lambda^c_3 / (\lambda^{c2}_2 - \lambda^c_1 \lambda^c_3)] / t \end{aligned}$$

$$e_y = N^c_x [\lambda^c_2 / (\lambda^c_2{}^2 - \lambda^c_1 \lambda^c_3)] / t \quad (20)$$

4. Transverse Stresses (σ_y)

Using Equation 4 and $e_s = 0$, transverse stresses (σ_y) are given by

$$\sigma^\theta_y = C^\theta_{12} e_x + C^\theta_{22} e_y \quad (21)$$

The format of transverse stresses depends upon the condition of 90-degree plies, i.e., whether 90-degree plies are uncracked or cracked.

4.1 Uncracked 90 plies

Using Equations 17 and 18, transverse stresses in terms of applied axial loads N_x and e_x for uncracked 90-degree plies are given by

$$\sigma^\theta_y = - N_x [\lambda_3 C^\theta_{12} - \lambda_2 C^\theta_{22}] / [t (\lambda_2{}^2 - \lambda_1 \lambda_3)] \quad (22)$$

and

$$\sigma^\theta_y = e_x [\lambda_3 C^\theta_{12} - \lambda_2 C^\theta_{22}] / \lambda_3 \quad (23)$$

respectively, where

$$\lambda_2{}^2 = [(4m + n) U_4 - n U_3]^2 - 8m U_3 [(4m + n) U_4 - n U_3] \cos (4\theta) + 16m^2 U_3{}^2 \cos^2 (4\theta) \quad (24)$$

$$\lambda_1 \lambda_3 = [(4m + n) U_1 + n U_3]^2 - n^2 U_2{}^2 - 16m^2 [U_2{}^2 \cos^2 (2\theta) - U_3{}^2 \cos^2 (4\theta)] - 8mn U_2{}^2 \cos (2\theta) + 8m U_3 [(4m + n) U_1 + n U_3] \cos (4\theta) \quad (25)$$

$$\lambda_2{}^2 - \lambda_1 \lambda_3 = B_1 + B_2 \cos (2\theta) + B_3 \cos (4\theta) \quad (26)$$

and

$$B_1 = [(4m + n) U_4 - n U_3]^2 - [(4m + n) U_1 + n U_3]^2 + (n^2 + 8m^2) U_2{}^2 \quad (27)$$

$$B_2 = - 8mn U_2{}^2 \quad (28)$$

$$B_3 = [8m^2 U_2{}^2 - 8m U_3 (4m + n) (U_4 + U_1)] \quad (29)$$

$$\lambda_3 C^\theta_{12} = [(4m + n) U_1 + n (U_2 + U_3)] U_4 - 4m U_2 U_4 \cos (2\theta) - [(4m + n) U_1 + n (U_2 + U_3) - 4m U_4] \times U_3 \cos (4\theta) + 4m U_2 U_3 \cos (2\theta) \cos (4\theta) - 4m U_3{}^2 \cos^2 (4\theta) \quad (30)$$

$$\lambda_2 C^\theta_{22} = [(4m + n) U_4 - n U_3] U_1 - [(4m + n) U_4 - n U_3] U_2 \cos (2\theta) + [(4m + n) U_4 - n U_3 - 4m U_1] U_3 \cos (4\theta) +$$

$$4m\,U_2\,U_3\cos(2\theta)\cos(4\theta) - 4m\,U_3^2\cos^2(4\theta) \quad (31)$$

$$\lambda_3\,C^{\theta}_{12} - \lambda_2\,C^{\theta}_{22} = B_4 + B_5\cos(2\theta) + B_6\cos(4\theta) \quad (32)$$

and

$$B_4 = n\,[\,U_1\,U_3 + U_2\,U_4 + U_3\,U_4\,] \quad (33)$$

$$B_5 = n\,[\,U_4 - U_3\,]\,U_2 \quad (34)$$

$$B_6 = -\,n\,[\,U_1 + U_2 + U_3\,] \quad (35)$$

$$\lambda_3 = B_7 + B_8\cos(2\theta) + B_9\cos(4\theta) \quad (36)$$

$$B_7 = [(4m + n)\,U_1 + n\,(U_2 + U_3)] \quad (37)$$

$$B_8 = -4m\,U_2 \quad (38)$$

$$B_9 = 4m\,U_3 \quad (39)$$

Using Equations 24 thru 39, Equations 22 and 23 become

$$\sigma^{\theta}_y = -\,N_x\,F_1/t \quad (40)$$

$$\sigma^{\theta}_y = e_x\,G_1 \quad (41)$$

where

$$F_1 = [\,B_4 + B_5\cos(2\theta) + B_6\cos(4\theta)]\,/\,[\,B_1 + B_2\cos(2\theta) + B_3\cos(4\theta)] \quad (42)$$

$$G_1 = [\,B_4 + B_5\cos(2\theta) + B_6\cos(4\theta)]\,/\,[\,B_7 + B_8\cos(2\theta) + B_9\cos(4\theta)] \quad (43)$$

4.2 Cracked 90 plies

Using Equations 19 and 20 transverse stresses in terms of applied axial loads N^c_x and e_x for cracked 90 degree plies are given by

$$\sigma^{\theta}_y = -\,N^c_x\,[\,\lambda^c_3\,C^{\theta}_{12} - \lambda^c_2\,C^{\theta}_{22}\,]\,/\,[\,t\,(\lambda^{c2}_2 - \lambda^c_1\,\lambda^c_3)] \quad (44)$$

and

$$\sigma^{\theta}_y = e^c_x\,[\,\lambda^c_3\,C^{\theta}_{12} - \lambda^c_2\,C^{\theta}_{22}\,]\,/\,\lambda^c_3 \quad (45)$$

respectively, and where

$$\lambda^{c2}_2 - \lambda^c_1\,\lambda^c_3 = B^c_1 + B^c_2\cos(2\theta) + B^c_3\cos(4\theta) \quad (46)$$

$$\lambda^c_3\,C^{\theta}_{12} - \lambda^c_2\,C^{\theta}_{22} = B^c_4 + B^c_5\cos(4\theta) \quad (47)$$

$$\lambda^c_3 = B^c_6 + B^c_7\cos(2\theta) + B^c_8\cos(4\theta) \quad (48)$$

and

$$B^c_1 = 16m^2\,(U_4^2 - U_1^2 + U_2^2/2) - 4mn\,U_1\,C_1 \quad (49)$$

$$B^c_2 = -\,4mn\,U_2\,C_{11} \quad (50)$$

$$B^c_3 = -\,[\,16m^2\,(2\,U_3\,U_4 + 2\,U_1\,U_3 - U_2^2/2) +$$

$$4mn\, U_3\, C_{11} \tag{51}$$

$$B^c_4 = n\, C_{11}\, U_4 \tag{52}$$

$$B^c_5 = -\, n\, C_{11}\, U_3 \tag{53}$$

$$B^c_6 = 4m\, U_1 + n\, C_{11} \tag{54}$$

$$B^c_7 = -\, 4m\, U_2 \tag{55}$$

$$B^c_8 = 4m\, U_3 \tag{56}$$

Using Equations 46 thru 56, Equations 44 and 45 become

$$\sigma^\theta{}_y = -\, N^c_x\, F^c_1 / t \tag{57}$$

$$\sigma^\theta{}_y = e^c_x\, G^c_1 \tag{58}$$

where

$$F^c_1 = [\, B^c_4 + B^c_5 \cos(4\theta)] / [\, B^c_1 + B^c_2 \cos(2\theta) + B^c_3 \cos(4\theta)] \tag{59}$$

$$G^c_1 = [\, B^c_4 + B^c_5 \cos(4\theta)] / [\, B^c_6 + B^c_7 \cos(2\theta) + B^c_8 \cos(4\theta)] \tag{60}$$

5. Delaminating Moment (DM) and Delaminating Moment Coefficient (DMC)

In the $[(\theta / -\theta)_m / 90_n / (-\theta / \theta)_m]$ laminates subjected to the uniaxial loading, the stress resultant, N_y, is zero, i.e.,

$$4m\, \sigma^\theta{}_y + n\, \sigma^{90}{}_y = 0$$

or

$$\sigma^{90}{}_y = 4m\, \sigma^\theta{}_y / n \tag{61}$$

where $\sigma^\theta{}_y$ = Stress in θ plies

and $\sigma^{90}{}_y$ = Stress in 90-degree plies

These $\sigma^{90}{}_y$ and $\sigma^\theta{}_y$ transverse stresses form a delaminating moment resisted by a moment formed by peeling stresses. This delaminating moment, DM, at the mid surface of the laminates is given by

$$DM = [\, 2mt\,(mt + nt/2) - (4m/n)(nt/2)(nt/4)\,]\, \sigma^\theta{}_y$$

$$= m(4m + n)\,(t^2/2)\, \sigma^\theta{}_y \tag{62}$$

To evaluate the effects of the delaminating moment, DM, upon the peeling stress (σ_z), finite element and finite difference techniques can be used. Both the techniques are expensive in time and effort for preliminary investigations. For initial studies an approximate technique is desirable. Such approximate assessment of the effects is feasible using the approaches of References 9 and 44. In one approach (Reference 9), a distribution (based upon experience) of peeling stress is assumed and the resulting moment calculated. Using $\sigma^\theta{}_y$ from one of

Equations 40, 41, 57, and 58, this moment is equated to DM of Equation 62 to obtain an explicit expression for the peeling stress σ_z in terms of elastic constants and loading.

The other approach uses directly DM of Equation 62 and requires no distribution assumption of the peeling stress (Reference 44). In this technique, the rate change of DM (not the magnitude) with respect to the average axial stress σ_o or strain e_o defined as the delaminating moment coefficient (DMC) is used. The delaminating moment coefficients based upon the axial stress and the axial strain are respectively given by

$$DMC_s = DM / \sigma_o = m (4m + n)^2 (t^2 / 2) (\sigma^{\theta}_{y} / \sigma_o) \quad (63)$$

$$DMC_e = DM / e_o = m (4m + n) (t^2 / 2) (\sigma^{\theta}_{y} / e_o) \quad (64)$$

Equation 63 was used in Reference 44 to differentiate delaminating / non-delaminating laminates among a group of thirty one laminates of different stacking sequences. For these laminates values of DMC_s ranged from $0.32 \times 10^{-5}(in)^3$ to $37.88 \times 10^{-5}(in)^3$. The test data showed that laminates with $DMC_s < 10.23 \times 10^{-5}(in)^3$ did not show any signs of delamination. The data indicate that for a given material system there is a critical DMC below which delamination is unlikely. This aspect of DMC has a potential of being used to determine stacking sequences of designed laminates which have DMC_s less than the critical value. The concept of determining the stacking sequence for designed laminates will be discussed in detail in Section IV.

In the subsequent paragraph, we will use the DMC to evaluate quantitatively delaminating tendency of the $[(\theta / - \theta)_m / 90_n / (- \theta / \theta)_m]$ laminates. Maximization of DMC of cracked and uncracked laminates for force and displacement loadings for a given set of m and n will yield the angle θ resulting in laminates with the maximum tendency to delaminate. For the purpose of comparison, the angle θ maximizing the mismatch of Poisson's ratios and the Poisson's ratio of the laminates are determined.

6. Angle θ Maximizing Delamination Tendencies for Various Criteria

6.1 Maximizing DMC_s for uncracked 90 plies and N_x loading

Using Equations 40 and $N_x = (4m+n) \sigma_o$, Equation 63 can be written as

$$DMC_s = -m (4m+n)^2 (t^2 / 2) F_1 \quad (65)$$

DMC_s attains the maximum value when

$$dF_1 / d\theta = d / d\theta \{ [B_4 + B_5 \cos (2\theta) + B_6 \cos (4\theta)] / [B_1 + B_2 \cos (2\theta) + B_3 \cos (4\theta)] \} = 0 \quad (66)$$

On simplification Equation 66 yields

$$a_1 \cos^2 (2\theta) + b_1 \cos (2\theta) + c_1 = 0 \quad (67)$$

where

$$a_1 = 2 (B_2 B_6 - B_3 B_5)$$

$$b_1 = 4 (B_1 B_6 - B_3 B_4)$$

$$c_1 = (B_1 B_5 + B_2 B_6 - B_2 B_4 - B_3 B_5) \quad (68)$$

The solution of Equation 67 yields

$$\theta_{1,2} = 0.5 \text{ Arc cos } [(- b_1 \pm \sqrt{} (b_1^2 - 4 a_1 c_1)) / (2 a_1)] \quad (69)$$

6.2 Maximizing DMC_e for uncracked 90 plies and e_o loading

Using Equations 41 and $e_x = e_o$, Equation 64 can be written as

$$DMC_e = G_1 \quad (70)$$

DMC_e attains the maximum value when

$$dG_1 / d\theta = d / d\theta \{ [B_4 + B_5 \cos (2\theta) + B_6 \cos (4\theta)] / [B_7 + B_8 \cos (2\theta) + B_9 \cos (4\theta)] \} = 0 \quad (71)$$

On simplification Equation 71 yields

$$a_2 \cos^2 (2\theta) + b_2 \cos (2\theta) + c_2 = 0 \quad (72)$$

where

$$a_2 = 2 (B_8 B_6 - B_9 B_5)$$

$$b_2 = 4 (B_7 B_6 - B_9 B_4)$$

$$c_2 = (B_7 B_5 + B_8 B_6 - B_8 B_4 - B_9 B_5) \quad (73)$$

The solution of Equation 72 yields

$$\theta_{1,2} = 0.5 \text{ Arc cos } [(- b_2 \pm \sqrt{} (b_2^2 - 4 a_2 c_2)) / (2 a_2)] \quad (74)$$

6.3 Maximizing DMC_s for cracked 90 plies and N_x loading

Using Equations 57 and $N_x = (4m+n) \sigma_o$, Equation 63 can be written as

$$DMC_s = -m (4m+n)^2 (t^2 / 2) F^c_1 \quad (75)$$

DMC_s attains the maximum value when

$$dF^c_1 / d\theta = d / d\theta \{ [B^c_4 + B^c_5 \cos (4\theta)] / [B^c_1 + B^c_2 \cos (2\theta) + B^c_3 \cos (4\theta)] \} = 0 \quad (76)$$

On simplification Equation 76 yields

$$a_3 \cos^2 (2\theta) + b_3 \cos (2\theta) + c_3 = 0 \quad (77)$$

where

$$a_3 = 2 B^c_2 B^c_5$$

$$b_3 = 4 (B^c_1 B^c_5 - B^c_3 B^c_4)$$

$$c_3 = B^c_2 B^c_5 - B^c_2 B^c_4 \quad (78)$$

The solution of Equation 77 yields

$$\theta_{1,2} = 0.5 \text{ Arc cos } [(- b_3 \pm \sqrt{} (b_3^2 - 4 a_3 c_3)) / (2 a_3)] \quad (79)$$

6.4 Maximizing DMC_e for cracked 90 plies and e_o loading

Using Equations 58 and $e_x = e_o$, Equation 64 can be written as

$$DMC_e = G^c_1 \quad (80)$$

DMC_e attains the maximum value when

$$dG^c_1 / d\theta = d / d\theta \{ [B^c_4 + B^c_5 \cos (4\theta)] / [B^c_6 + B^c_8 \cos (2\theta) + B^c_9 \cos (4\theta)] \} = 0 \quad (81)$$

On simplification Equation 81 yields

$$a_4 \cos^2 (2\theta) + b_4 \cos (2\theta) + c_4 = 0 \qquad (82)$$

where

$$a_4 = 2 B^c_7 B^c_5$$

$$b_4 = 4 (B^c_6 B^c_5 - B^c_8 B^c_4)$$

$$c_4 = B^c_7 B^c_5 - B^c_7 B^c_4 \qquad (83)$$

The solution of Equation 82 yields

$$\theta_{1,2} = 0.5 \text{ Arc cos } [(- b_4 \pm \sqrt{} (b_4^2 - 4 a_4 c_4)) / (2 a_4)] \qquad (84)$$

6.5 Maximizing mismatch of Poisson's ratios of $\pm\theta_m$ and 90_n plies

Poisson's ratio of 90_n is minimum. For maximum mismatch of Poisson's ratios of $\pm\theta_m$ and 90_n, Poisson's ratio of $\pm\theta_m$, $\mu_\theta = e_y / e_x$, must be maximum.

Using Equations 18, 11, and 14 along with n = 0, Poisson's ratio μ_θ can be written as

$$\mu_\theta = [U_4 - U_3 \cos (4\theta)] / [U_1 - U_2 \cos (2\theta) + U_3 \cos (4\theta)] \qquad (85)$$

The Poisson's ratio, μ_θ, attains the maximum value when

$$d\mu_\theta / d\theta = 0 \qquad (86)$$

On simplification Equations 85 and 86 yield

$$a_5 \cos^2 (2\theta) + b_5 \cos (2\theta) + c_5 = 0 \qquad (87)$$

where

$$a_5 = 2 U_2 U_3$$

$$b_5 = - 4 U_3 (U_1 + U_4)$$

$$c_5 = U_2 (U_3 + U_4) \qquad (88)$$

The solution of Equation 87 yields

$$\theta_{1,2} = 0.5 \text{ Arc cos } [(- b_5 \pm \sqrt{} (b_5^2 - 4 a_5 c_5)) / (2 a_5)] \qquad (89)$$

6.6 Maximizing Poisson's ratio of $[(\theta / -\theta)_m / 90_n / (-\theta / \theta)_m]$ laminates

The Poisson's of $[(\theta / -\theta)_m / 90_n / (-\theta / \theta)_m]$ laminates (using Equations 12,14, and 18) is given by the following expression:

$$\mu_\theta = e_y / e_x = \lambda_2 / \lambda_3 = [\, 4m \{ U_4 - U_3 \cos(4\theta) \} + n (U_4 - U_3)] / [\, 4m \{ U_1 - U_2 \cos(2\theta) + U_3 \cos(4\theta) \} + n (U_1 + U_2 + U_3)] \quad (90)$$

The Poisson's ratio, $\mu_{\theta,.}$ of the laminates attains the maximum value when

$$d\mu_\theta / d\theta = 0 \quad (91)$$

On simplification Equations 90, and 91 yield

$$a_6 \cos^2(2\theta) + b_6 \cos(2\theta) + c_6 = 0 \quad (92)$$

where

$$a_6 = 8m\, U_2\, U_3$$

$$b_6 = -4\, U_3 [(4m + n)(U_1 + U_4) + n\, U_2]$$

$$c_6 = U_2 [(4m + n)\, U_4 + (4m - n)\, U_3] \quad (93)$$

The solution of Equation 87 yields

$$\theta_{1,2} = 0.5 \text{ Arc cos } [(-b_6 \pm \sqrt{(b_6^2 - 4\, a_6\, c_6)}) / (2\, a_6)] \quad (94)$$

Equations 68,73,78,83,88, and 93 have a general form expressed as

$$\theta_{1,2} = 0.5 \text{ Arc cos } [(-b \pm \sqrt{(b^2 - 4\, a\, c)}) / (2\, a)]$$

where a, b, and c for various delamination criteria are given in Table 1.

7. Delamination Criteria Evaluation

In paragraph 6 of this Section, six criteria were used to derive expressions to determine the angle, θ, maximizing the delaminating tendency. An examination of these expressions shows that the criteria 6.2 and 6.6 are not independent.It can easily be shown that

$$a_2 = n\, a_6 (U_1 + U_2 + U_3)$$

$$b_2 = n\, b_6 (U_1 + U_2 + U_3)$$

$$c_2 = n\, c_6 (U_1 + U_2 + U_3) \qquad (95)$$

As a consequence of Equation 95, we have only to consider five criteria, namely, the maximum mismatch of Poisson's ratios (para 6.5), and the maximum delaminating moment coefficients for uncracked and cracked 90-degree plies subjected to force and displacement loadings.

To evaluate the five criteria, three studies were conducted. These studies are:

a. Numerical evaluation of the derived equations.

b. Finite element analyses of selected combinations of m, n, and elastic properties.

c. Experimental verification of the results of the numerical evaluation and the finite element analyses.

7.1 Numerical evaluation

The numerical investigation was conducted in two parts. In the first part, the parameters m and n were varied to determine the derived parameters θ, μ, $\sigma^{\theta}_{y} / \sigma_o$, DMC_s,and DMC_e for each of the five criteria. For the determination of the parameters assumed elastic constants were:

$$E_{11} = 19.26 \times 10^6 \text{ psi}$$
$$E_{22} = 1.32 \times 10^6 \text{ psi}$$
$$G_{12} = 0.83 \times 10^6 \text{ psi}$$
$$\mu_{12} = 0.35 \qquad (96)$$

The results of this study are tabulated in Tables 2 thru 6. The data presented is for criteria 6.1 thru 6.5. In the case of criteria 6.1, and 6.3 when N_x loading is applied, only the values of DMC_s are shown.For criteria 6.2, 6.4, and 6.5 with e_x loading, in addition to the related values of DMC_e, the corresponding values of DMC_s are included. The data show the following:

a. DMC for all the five criteria increases with the increasing parameters m and n.

b. DMC increases as m / n decreases.

c. For the same ratio of m / n, (for example $m_1 = 5$, $n_1 = 1$, and $m_2 = 10$, $n_2 = 2$) the computed values of θ, μ, and $\sigma^{\theta}_{y} / \sigma_o$ for all the criteria are the same. However, $DMC_{s2} = DMC_{s1} (m_2 / m_1)^2$.

In the second part, the parameters θ, μ, $\sigma^{\theta}_{y} / \sigma_o$, DMC_s, and DMC_e, for the maximum delamination moments under N_x, and e_x loading and the maximum mismatch of Poisson's ratios were calculated, for a given set of m = 5, and n = 2, and various values of E_{11}, E_{22}, G_{12}, and μ_{12}. The results are tabulated in Table VII. The tabulated data show that:

a. The changes in the Poisson's ratio have minimal effect upon the DMC.

b. Increasing the shear Young's modulus G_{12} causes the DMC to decrease.

c. Increasing the transverse Young's modulus, E_{22}, causes the DMC to change but not very appreciably.

d. Increasing the longitudinal Young's modulus, E_{11}, increases DMC dramatically.

7.2 Analytical-experimental evaluation of paragraph 7.1

The data of Tables 2 thru 6 indicate that for the same set of values of m and n, the five criteria yield different values of θ, μ, $\sigma^{\theta}_{y} / \sigma_o$, and DMC. To establish the credibility of the findings of Tables 2 thru 6, an analytical-experimental study was conducted. The analytical part of the study is described in the subsequent paragraphs whereas experimental investigations are included in Section III.

The laminates selected for the analytical and experimental investigations were:

Type	Stacking Sequence	Plies	Criterion
A	$[(49.8 / -49.8)_5 / 90]_s$	22	6.1
B	$[(30.8 / -30.8)_5 / 90]_s$	22	6.2
C	$[(25.5 / -25.5)_5 / 90]_s$	22	6.5
D*	$[(47.9 / -47.9)_{10} / 90]_s$	42	6.1

The laminate D* is similar to the laminate A except for the number of m plies.

The specimen laminates A, B, and C were selected to discriminate between the delamination initiation criteria. The specimen type D was selected to check the observed increase in the delamination tendency (Table 2) as compared to that of the specimen type A resulting from the increase in thickness.

To conduct the analytical studies, we modelled half of the width using constant generalized strain elements as shown in Figures (2a) and (3a). The plies were modelled using single elements through the ply thickness. Thus, 770 elements were used for specimens A, B, and C and 1470 elements were used for specimen D. The nodal displacements, centroidal stresses and strains were obtained for a longitudinal applied average stress of 100 psi. The interlaminar stresses at z=0 were obtained by Lagrangian interpolation of the σ_z values at the element centroids. These σ_z values were then extrapolated to estimate the maximum interlaminar normal stress at the free edge.

The finite element analysis results are presented in Figures 2 thru 4 and Table 8. Figure 2 shows exaggerated views of the displacement fields in specimens A, B, and C. This figure shows that for the same applied average axial stress of 100 psi, specimen A undergoes the greatest distortion near the free edge, while specimen C undergoes the least distortion. These results can be interpreted to indicate that specimen A has the greatest tendency for edge delamination of the three specimens and the delamination will be initiated at the lowest applied axial stress. Figure 3 shows the distortion of specimen D. By comparing the distortions near the free edge of all the specimens, we conclude that laminate D has the greatest tendency for edge delamination followed by laminates A, B, and C in descending order. This confirms the predictions based upon DMC_s for these specimens.

The conclusions drawn in the preceding paragraph are confirmed by the entries (column 1) of Table 4 and the plots of σ_z shown in Figure 4. Figure 4 and the Table 4 show that for the same applied axial stresss, the value of normal stress σ_z at the free edge is the highest for specimen D followed by specimens A, B, and C. Both the distortions and the values of normal

stress σ_z near the free edge of the specimens confirms the delamination tendency predicted by DMC_s.

The delamination moment coefficients (based upon stress) for laminates A, B, C, and D are 48.67, 27.43, 19.72, and 109.3 x 10^{-5} $(in)^3$ (Table 2 for Criteia 6.1,Table 3 for Criterion 6.2, Table 6 for Criterion 6.5) respectively, and the corresponding normal stresses σ_z at the free edges of the specimens are 107.74, 67.65, 51.12, and 126.22 psi (Table 8). The ratios of DMCs are 2.48 : 1.39 : 1.0 : 5.54 while the ratios of the normal stress σ_z are 2.11 : 1.32 : 1.0 : 2.47.The ratios of DMC_s are consistent with the ratios of the normal stress σ_z for specimens A, B, and C. The results for specimen D show a different trend. The delaminating moment in a laminate is resisted by the normal stresses σ_z and the shearing stresses τ_{zy}. The shearing stresses obtained by the finite technique for all the four laminates A, B, C, and D are tabulated in Tables 9 thru 12. The tables show the shearing stresses in elements relative to free edges and mid planes. The discrepancy between the normal stress ratios and the DMC_s ratios observed above may be due to the fact that the DMC_s approach ignores the presence of the shearing stresses while the finite element method does not.

8. Effects of Residual Thermal Curing Stresses

To evaluate residual thermal curing stresses present in cured laminates with and without applied loads, it is assumed that:

(a) Thermal and elastic properties remain unchanged during the cooling process.

(b) Re-distribution of thermal stresses in composites due to the presence of the matrix does not occur.

(c) Young's moduli of elasticity are the same as in Equation 96.

(d) Temperature change is equal to -250° F.

(e) Coefficients of linear expansion in the fiber α_0 and transverse direction α_{90} are -0.2 x 10^{-6} and 16.0 x 10^{-6} in / in per °F respectively.

In this study, m assumes values 1, 5, 10, 40, and 100, and n assumes values 1, 2, and 4. The criteria used are 6.1, 6.2, and 6.5, namely, maximizing DMC_s for uncracked 90 plies with N_x loading, maximizing DMC_e for uncracked 90 plies with e_o loading,and maximizing mismatch of Poisson's ratios of $\pm\theta_m$ and 90_n plies. The results of the investigation are summarized in Tables13 thru 15. The tables contain thermal stresses (distinguished by T) in angle and 90 plies and DMC in X and Y directions.

From the tabulated data (Tables 13 thru 15), we find the following trends in the cured and unloaded laminates:

(a) The stress $\sigma^{\theta T}{}_x$ is compressive for all values of m and n for all the three design conditions, namely, criteria 6.1, 6.2, and 6.5 which causes the DMC to be negative.This indicates that cured laminates corresponding to the three criteria are unlikely to delaminate along the edges normal to X-axis.

(b) The effects of stresses $\sigma^{\theta T}{}_y$ and $\sigma^{90T}{}_y$ acting upon edges normal to Y-axis appear to be different for the three criteria. In the case of the condition of the maximum mismatch of Poisson's ratios, the stresses $\sigma^{\theta T}{}_y$ and $\sigma^{90T}{}_y$ are tensile and compressive respectively. For this condition the laminates have a tendency to delaminate along edges parallel to X-axis. This tendency increases with thickness of the laminates. A similar trend is seen for Criterion 6.2. It is less severe for $m < 10$, but for $m > 40$ ($n < 4$) this condition tends to create delamination conditions of magnitudes similar to Criterion 6.5. For Criterion 6.1, two trends are observed. In the case of $m<10$, the stresses $\sigma^{\theta T}{}_y$ and $\sigma^{90T}{}_y$ are compressive and tensile respectively except for $m = 10$ and $n = 1$. Within this range, laminates are less likely to delaminate under thermal residual stresses. However, for $m > 40$ laminates have tendency to delaminate but it is far less severe than the one of the other two criteria.

SECTION III

EXPERIMENTAL INVESTIGATION

The experimental study was performed to validate the results obtained in Section II. This study is described in the following paragraph.

1. Material System

The material system used in the study was AS4/3501-6, graphite-epoxy, supplied by Hercules Incorporated in the form of a 12-inch-wide prepreg tape roll. This supplied roll (no. 29) belonged to the batch number 3233 fabricated in October 1984.

2. Panels and Cure Cycle

Using the manufacturer's recommended cure cycle, four panels were fabricated. The four panels had the following stacking sequences:

Panel	Stacking Sequence	Plies
A	$(\pm 49.8_5 / 90)_s$	22
B	$(\pm 30.8_5 / 90)_s$	22
C	$(\pm 25.5_5 / 90)_s$	22
D	$(\pm 47.9_{10} / 90)_s$	42

The rationale for selecting the stacking sequences for the panels has been described in Section II. The panels (12 inches x 18 inches) were laid up using 12-inch wide prepreg tape. After curing, the panels were subjected to ultrasonic through-transmission C-scan inspection for flaws. The inspection did not reveal significant defects.

3. Specimens

The cured and inspected panels were trimmed along their long edges and then tabbed using straight-sided 2-inch wide glass-phenolic tabs. The tabbed panels were machined from both edges into 1-inch wide specimens of dimensions shown in Figure 5. The

material left over from the central region was used to determine the composition of the panels by the nitric acid digestion method. Table 16 shows that the panels were essentially porosity free and had fiber volumes varying from 66 to 62 percent.

The specimens cut from the panels were designated as A-1, B-1, C-1, and D-1 thru A-14, B-14, C-14, and D-14. The widths and thicknesses of the specimens were determined at three locations using a flat-headed micrometer. The cross-section areas were determined by averaging the measurements. These average cross-section areas were used to determine the stresses from the loads.

4. Instrumentation

The following techniques were used to determine the onset of edge delamination:

(a) Strain Gage Rosettes Centrally mounted, back-to-back strain gage rosettes were used on specimens A-1, B-1, C-1, and D-1. The rosettes provided strain data up to the maximum applied loads, but failed to register the onset of edge delamination (Figures 6 thru 9). Hence, their use was discontinued in subsequent tests.

(b) Transverse Strain Gages Single element strain gages were bonded to three groups of specimens at locations shown in Figure 10. These gages did register the onset of delamination at the locations where they were bonded to the specimens (Figures 11 thru 30). Since edge delaminations initiate at random locations along specimen edges, the use of transverse strain gages at a limited number of locations is of doubtful value. To get meaningful results, transverse strain gages would have to be bonded at all locations along the specimen length. Since this is uneconomical, the use of transverse strain gages was discontinued after three sets of tests.

(c) Cracked Silver Ink Instrumentation Cracked silver ink instrumention was used in some of the tests. The edges of the specimens were coated with a brittle lacquer or hysol to provide electrical insulation from the conducting graphite fibers. After the lacquer or hysol dried, silver paint ink was used to draw a zigzag line along the specimen edge as shown in

Figure 10. The ends of the conducting line were connected to a power source and a buzzer. The silver paint line cracked upon delamination initiation, causing an electrical discontinuity and sounding of the buzzer. This technique gave erratic results. Moreover, the thin lacquer coating tended to provide some edge reinforcement and the delamination tended to initiate along the uncoated edge. As a result, this technique was used in only some of the tests (for example Figures 11b, 12b, 13b, and 14b).

(d) Acoustic Emission Instrumentation An Acoustic Emission Technology (AET) linear Locator Model 3000 was used in most of the tests to monitor acoustic emission during loading. Two acoustic emission sensors were mounted as close to the tabs as possible (Figure 31). The RMS acoustic emission activity from the sensor near the upper grip was recorded as a function of the applied load. The acoustic emission from the region between the two sensors was also recorded and stored at preselected load levels. Plots of both of these activities are shown in Figures 32 thru 69. Since the instrumentation did not permit continuous recording of the acoustic emission from between the sensors, only the RMS acoustic emission from the upper sensor was used in data reduction. An arbitrary RMS acoustic emission activity of 1000 counts was used as an indication of the occurrence of damage. Isolated RMS acoustic emission events with more than 1000 counts were assumed to correspond to matrix cracking. More than two RMS acoustic emission events with at least 1000 counts corresponding to consecutive load points were taken as an indication of the onset of edge delamination. This edge delamination initiation criterion was used in all tests for which the acoustic emission monitoring instrumentation was used.

(e) Visual Observation To observe the onset of edge delamination, one edge of each specimen was sprayed with Fluoro Finder FD-32 Developer, marketed by Testing Systems Inc. The spray dried quickly to give a uniform white coating on the edge of the specimen. This white coating provided an excellent background against which the edge delamination could be seen. The coated edge of the specimen was monitored visually and the load at which delaminations initiated was recorded manually. Since the reaction time of the

observer (GPS) was slow in some tests, the stresses for delamination initiation determined by visual observation are an upper bound. High resolution black and white macro photographs were used to document the occurrence of matrix cracks in specimens from panels A and D prior to edge delamination initiation. The matrix cracks appeared as pits in the white coating as will be discussed later.

After the tests were completed, the edges of the specimens were photographed and the specimens were inspected using tetrabromoethane (TBE) enhanced x-ray radiography. During the x-raying of the specimens, we discovered that the coating that was sprayed on the specimens left a residue that showed up in the x-ray negatives. All attempts to completely remove the residue proved futile and, as a result, the TBE enhanced x-ray photographs turned out to be useable, but of poor quality.

5. Testing and Test Data

The specimens were loaded in tension using a screw-driver test frame (INSTRON Floor Model TT-115) with 1 inch-wide self-aligning wedge-action grips. The tests were performed at a crosshead speed of 0.02 inches per minute at room temperature and ambient humidity. The load, strain, acoustic emission, and cracked silver ink data were recorded using an in-house data acquisition system. The data were sampled sufficiently often to give a load resolution of 10 pounds. Most of the tests were conducted until delaminations were observed visually along one edge of the specimen. Some of the tests were terminated prior to the onset of delamination to document the occurrence of pre-delamination damage.

The test results are summarized in Tables 17 thru 20, which give the specimen numbers, cross-sectional areas, strains, and stresses for the initiation of edge delaminations determined by transverse gages, cracked silver ink, acoustic emission and visual observation. The table also contains stresses for initiation of matrix cracking as determined from the RMS acoustic emission data and maximum applied stresses. Of all the techniques used, the acoustic emission method appear to be consistent and dependable. The average

initial delamination stresses for laminates A, B, C, and D are 19.2, 23.3, 26.4, and 18.6 ksi respectively. The corresponding average initial matrix cracking stresses are 15.5, 21.7, 25.1, and15.3 ksi. These results are consistent with those obtained using DMC and finite element techniques described in Section II.

Edge views of some of the typical specimens after and during tests are shown in Figures 70 thru 75. Figure 70 is the edge view of specimen A-9 which was loaded to the extent that a large delaminated section could be seen.Specimen A-13 (Figure 71) on the other hand was loaded to the extent that the formation of black dots on white paint could be observed during and after the test. Specimens B-9,and C-9 (Figures 72 and 73) did not develop black dots. In both these specimens, slits were observed in loaded and unloaded conditions. The behavior of specimens D-9 and D-14 (Figures 74 and 75) was similar to that of specimens A-9 and A-13, i.e., the appearance of black dots prior to the formation of longitudinal cracks. Enhanced x-ray photographs of the specimens discussed in this paragraph are shown in Figure 76. In the figure extensive matrix cracking of specimens type A and D can easily be observed whereas matrix cracking is barely visible in specimens type B and C.

SECTION IV

DISCUSSION OF RESULTS AND CONCLUSIONS

The analytical and experimental investigations of Sections II and III have yielded some significant results. These results correspond to the following aspects of the studies:

(a) Delamination moment coefficient (DMC) as the measure of delaminating tendency of laminates.

(b) DMC as the technique to design a stacking sequence.

(c) Free edge failure modes.

1. DMC - The Measure of Delaminating Tendency of Laminates

Five distinct criteria have been developed for determining the angle that maximizes the edge delamination tendency of $(\pm\theta_m / 90_{n/2})_s$ laminates. Of these criteria, three are based on the assumption that matrix cracking does not occur in the 90-degree plies prior to edge delamination. Criterion 6.1 maximizes stress based DMC_s. It yields a laminate that delaminates at the lowest applied axial load N_x. Criterion 6.2 maximizes strain based DMC_e. This criterion is computationally equivalent to maximizing the Poisson's ratio of the laminate. Criterion 6.5, maximizing the Poisson's ratio mismatch between the $\pm\theta$ and 90 degree sublaminates (Reference 9), gives a laminate that delaminates at neither the lowest applied axial stress nor the lowest applied axial strain. This observation was confirmed both experimently and numerically by finite element determination of the peeling stresss σ_z near the free edge of the laminates designed in accordance with Criteria 6.1, 6.2 and 6.5.

Since Criterion 6.5 (Reference 9) has been used extensively since the mid-70s to design delamination prone specimens, we tried to determine how it came about. Upon re-examining the derivations, we found that the expressions of Reference 9 for delamination moment agree with our expressions. For the sake of completeness, the derivations of Reference 9 are reproduced in the following paragraph.

Let us consider a laminate consisting of two sets of angle ply laminates ($\pm\theta_1$ and $\pm\theta_2$) having thicknesses h_1 and h_2 subjected only to the applied axial load N_x (no thermal loading). Using Equation 4, stress resultants (average axial stress σ_o) for the laminate are given by

$$N^P_x = A_{11}\, e_x + A_{12}\, e_y$$

$$N^P_y = A_{12}\, e_x + A_{22}\, e_y$$

where

$$A_{11} = C^{\theta 1}_{11}\, h_1 + C^{\theta 2}_{11}\, h_2$$

$$A_{12} = C^{\theta 1}_{12}\, h_1 + C^{\theta 2}_{12}\, h_2$$

$$A_{22} = C^{\theta 1}_{22}\, h_1 + C^{\theta 2}_{22}\, h_2$$

and

$$N^P_x = (h_1 + h_2)\, \sigma_o$$

Since there is no applied transverse load, we get

$$N^P_y = \sigma^{\theta 1}_y\, h_1 + \sigma^{\theta 2}_y\, h_2 = 0$$

From the above equations and Equation 4, we get

$$\begin{aligned}
\sigma^{\theta 1}_y &= -\,(h_2 / h_1)\, \sigma^{\theta 2}_y \\
&= -\,(h_2 / h_1)\, [\, C^{\theta 2}_{12}\, e_x + C^{\theta 2}_{22}\, e_y \,] \\
&= -h_2\, (h_1 + h_2)\, \sigma_o / (A_{11} A_{22} - A^2_{12}) \\
&\quad [\, C^{\theta 2}_{12}\, C^{\theta 1}_{22} - C^{\theta 2}_{22}\, C^{\theta 1}_{12} \,] \\
&= -h_2\, (h_1 + h_2)\, \sigma_o / (A_{11} A_{22} - A^2_{12}) \\
&\quad [\, \nu^{\theta 2}_{12} - \nu^{\theta 1}_{12} \,]\, C^{\theta 1}_{22}\, C^{\theta 2}_{22}
\end{aligned} \qquad (97)$$

Equation 97 is exactly the same as the equation 9 of Reference 9 if we equate

$$\nu^{\theta 2}_{12} = \nu^2_{12}$$

$$\nu^{\theta 1}_{12} = \nu^1_{12}$$

$$C^{\theta 1}_{22} = Q^1_{22}$$

$$C^{\theta 2}_{22} = Q^2_{22}$$

$$C^{\theta 1}_{12} = Q^1_{12}$$

$$C^{\theta 2}_{12} = Q^2_{12}$$

In Reference 9, instead of actually maximizing the delamination moment, it was postulated that a large Poisson's ratio mismatch [$\nu^{\theta 2}{}_{12} - \nu^{\theta 1}{}_{12}$] between the angle ply units tended to magnify the stress $\sigma^{\theta 1}{}_{y}$. An examination of Equation 97 shows that maximization of the Poisson's ratio mismatch [$\nu^{\theta 2}{}_{12} - \nu^{\theta 1}{}_{12}$] alone ignores $C^{\theta 1}{}_{22}\, C^{\theta 2}{}_{22}$ and ($A_{11}A_{22} - A^2{}_{12}$) which are also functions of θ_1 and θ_2. This partial maximization of the stress $\sigma^{\theta 1}{}_{y}$ leads to inconsistent results because it fails to yield maximum peeling stresses.

The remaining two criteria, namely, 6.3 and 6.4 are similar to criteria 6.1 and 6.2 respectively except for the cracked and uncracked states of 90 degree plies. A perusal of Tables 2 thru 5 indicates that cracking of 90-degree plies tends to increase the delamination moment coefficients.

2. DMC - The Technique to Design a Stacking Sequence

In a laminate, ply orientations and their number are determined by design requirements. The plies can be stacked in variety of ways in the laminate. In the case of laminates with free edges, delamination is a possibility. For these conditions, the DMC technique can be used to determine the stacking sequence with the least tendency to delaminate before attempting the expensive finite element technique.

To illustrate the technique, les us consider a 24-ply laminate with $(\pm 45_5, 90_4, 0_{10})$ ply orientations designed to have $E_{xx} = 10.17 \times 10^6$ psi and $\mu_{xy} = 0.34$. These requirements can be met by a variety of sequences. Of these, two typical sequences are:

(a) $(\pm 45, 90_2, \pm 45, 0_5, -45, 45, 0_5, -45, 45, 90_2, -45, 45)$

(b) $(\pm 45, 0, 90, \pm 45, 0_4, 90, -45, 45, 90, 0_4, -45, 45, 90, 0, -45, 45)$

The delamination moment coefficients computed at the interfaces of the plies of both the sequences are shown in Table 21. From the data, we find that the maximum DMC_s for the sequence (a) and the sequence (b) are 1.83×10^{-5} $(in)^3$ and 7.99×10^{-5} $(in)^3$ respectively. These maxima occur between plies 4 and 5 for the sequence (a) and between

plies 11 and 12 for the sequence (b). Sequence (b) is more prone to delamination than the sequence (a). This tendency can also be seen in Figure 77 showing the deformed state obtained by the finite element technique and the undeformed state of sequences (a) and (b).

The actual edge delamination will depend upon whether the DMC of the laminate is greater than the critical DMC or not. For example in Reference 44, laminates with DMC greater than 10.0×10^{-5} $(in)^3$ delaminated before failure and the other did not. For the material system of Reference 44, the critical DMC appears to have a value (8.0 to 10.0) x 10^{-5} $(in)^3$. If we apply the critical DMC to the laminates of Tables 2 thru 6, we find that the first two laminates in Table 2 and 3, the first one in Table 4, the first two in Table 5 and the first three in Table 6 have DMC values less than the critical one. It means that these laminates will not delaminate before failure. One must have sufficient number of m and n plies to yield DMC value greater than the critical one.

Hence, we find the DMC technique is a viable procedure for preliminary selection of the stacking sequence in laminates.

3. Free Edge Failure Modes

In this study four types of specimens A, B, C and D (paragraph 7.2,Section II) were tested under tensile loading. Typical failure modes observed are shown in Figures 70 thru 76.

Specimens B and C failed by splitting each of the laminates into two sub-laminates approximately at the mid plane and without matrix cracking. The mid-plane splitting was accomplished in a series of steps with increasing load.

The failure modes of specimens A and D were different. The onset of failure was marked by the appearance of dots along the mid plane. With increasing loads, the density of the dots increased till they collapsed into mid plane splits. It appears that the failure process begins by matrix cracking. The local matrix cracking increases the tendency of the

laminate towards delamination (para 1, Section IV) and local delamination results in the appearance of dots. This matrix cracking and delamination causes unloading of the fiber tips and release of energy. During tests we observed that the formation of the dot was accompanied by a whiff (seen on videotape) of the white powder being blown away locally from the painted edge of the specimens.

Specimens A and D, though having the greatest tendency to delaminate, have mixed modes of failure (matrix cracking and delamination). On the other hand, in specimens B and C initiation of delamination is not accompanied by matrix cracking. For the same number of m and n plies the angle θ for specimen A is greater than the angle θ of specimens B and C. Probably $(\pm 40.0_m / 90_{n/2})_s$ laminates will satisfy the condition that no matrix cracking occurs before initiation of delamination while having delamination tendency greater than that of specimens B and C designed for Criteria 6.2 and 6.5. In the following paragraph we examine the possibility of using $(\pm 40.0_m / 90_{n/2})_s$ laminates by studying the data of laminates A, B, and C.

Laminates A, B, and C with the layup of $(\pm \theta_5 / 90)_s$ have initial matrix cracking stresses 15.5, 21.7,and 25.1 ksi and delamination initiation stresses 19.2, 23.3, and 26.4 ksi (Tables 17 thru 19) respectively. These stresses were plotted (Figure 78) against the experimental delamination and matrix crack initiation stresses as functions of $\pm\theta$. From the plot, matrix crack initiation stress data was obtained for angles other than those corresponding to laminates A, B, and C. Using SQ5 (point stress program), axial strains pertaining to matrix crack initiation stress and DMC_s data were calculated and plotted. From Figure 78, we find that an angle slightly greater than 40 degrees will develop an axial strain of 4000 μ in/in. To prevent matrix cracking, we need to limit the axial strain to 4000 μ in/in. The laminate with layup of $(\pm 40_5 / 90)_s$ is probably the best choice because it has the greatest tendency to delaminate without developing mixed edge delamination modes of failure.

REFERENCES

1. D. W. Oplinger, "Edge Effects in Angle Ply Laminates," AMMRC TR-71-62, Army Materials and Mechanics Research Center, December 1971.

2. A. H. Puppo and H. A. Evensen, "Interlaminar Shear in Laminate Composites Under Generalized Plane Stress," Journal of Composite Materials, Vol. 4, 1970, page 214.

3. R. L. Foye and D. J. Baker, "Design of Orthotropic Laminates," presented at the 11th Annual AIAA Structures, Structural Dynamics, and Materials Conference, Denver, Colorado, April 1970.

4. R. B. Pipes and N. J. Pagano, "Interlaminar Stresses in Composite Laminates Under Uniform Axial Tension," Journal of Composite Material Vol. 4, 1970, pages 538-548.

5. N. J. Pagano and R. B. Pipes, "Influence of Stacking Sequence on Laminate Strength," Journal of Composite Materials, Vol. 5, 1971, Pages 51-57.

6. R. B. Pipes and I. M. Daniel, "Moire Analysis of the Interlaminar Shear Edge Effect in Laminated Composites," Journal of Composite Materials, Vol. 5, 1971, pages 255-259.

7. G. Isakson and A. Levy, "Finite Element Analysis of Interlaminar Shear in Fibrous Composites," Journal of Composite Materials, Vol. 5, 1971, pages 273-276.

8. E. F. Rybicki, "Approximate Three-Dimensional Solution for Symmetric Laminates Under Inplane Loading," Journal of Composite Materials, Vol. 5, 1971, page 354.

9. N. J. Pagano and R. B. Pipes, "Some Observations on the Interlaminar Strength of Composite Laminates," International Journal of Mehanical Sciences, Vol. 15, 1973, pages 679-688.

10. J. M. Whitney, "Free Edge Effects in Characterization of Composite Materials," ASTM, STP 521, "The Test Methods for High Modulus Fibers and Composites," 1973, pages 167-179.

11. R. B. Pipes, B. E. Kaminski, and N. J. Pagano, "Influence of the Free Edge upon the Strength of Angle-Ply Laminates," ASTM, STP 521, "The Test Methods for High Modulus Fibers and Composites," 1973, pages 218-226.

12. D. W. Oplinger, B. S. Parker, F. P. Chiang, "Edge Effect Studies in Fiber-Reinforced Laminates," AMMRC TR 73-41, Army Materials and Mechanics Research Center, September 1973.

13. N. J. Pagano, "On Calculation of Interlaminar Normal Stress in Composite Laminates," Journal of Composite Materials, Vol. 8, January 1974, pages 65-82.

14. R. B. Pipes and N. J. Pagano, "Interlminar Stresses in Composite Laminates An Approximate Elasticity Solution," Journal of Applied Mechanics, Vol. 41, No. 3, September 1974, pages 668-672.

15. S. Tang, "Boundary Layer Theory - Part I: Laminated Composites in Plane Stress," Journal of Composite Materials, Vol. 9, January 1975, pages 33-41.

16. S. Tang, "Boundary Layer Theory - Part II: Laminated Composites in Plane Stress," Journal of Composite Materials, Vol. 9, January 1975, pages 42-52.

17. S. Tang, "Interlaminar Stresses of Uniformly loaded Rectangular Composite Plates," Journal of Composite Materials, Vol. 10, 1976, pages 69-78.

18. A. S. D. Wang and F. W. Crossman, "Some New Results on Edge Effects in Symmetric Composite Laminates," Journal of Composite Materials, Vol. 11, January 1977, pages 92-106.

19. A. S. D. Wang and F. W. Crossman, "Edge Effects on Thermally Induced Stresses in Composite Laminates," Journal of Composite Materials, Vol. 11, 1977, pages 300-312.

20. N. J. Pagano," Free Edge Stress Fields in Composite Laminates," AFML-TR-77-113, Wright-Patterson Air Force Base, Ohio, August 1977.

21. N. J. Pagano, "Stress Field in Composite Laminates," AFML-TR-77-114, Wright-Patterson AFB, Ohio, August 1977.

22. J. M. Whitney and R. Y. Kim, "Effect of Stacking Sequence on Notched Strength of Laminated Composites," ASTM STP 617, "Composite Materials Testing and Design (Fourh Conference)," 1977, pages 229-242.

23. K. L. Reifsnider, E. G. Hennke II, and W. W. Stinchcomb, "Delamination in Quasi-Isotropic Graphite-Epoxy Laminates," ASTM STP 617, "Composite Materials - Testing and Design (Fourth Conference)," 1977, pages 93-105.

24. P. W. Hsu and C. T. Herakovich," A Perturbation Solution for Interlaminar Stresses in Bidirectional Laminates," ASTM STP 617, "Composite Materials: Testing and Design (Fourth Conference)," 1977, pages 296-316.

25. P. W. Hsu and C. T. Herokovich," Edge Effects in Angle-Ply Composites Laminates," Journal of Composite Materials, Vol. 11, 1977, pages 422-428.

26. E. F. Rybicki, D. W. Schmueser and J. Fox," An Energy Release Rate Approach for Stable Crack Growth in the Free-Edge Delamination Problem," Journal of Composite Materials, Vol. 11 1977, pages 470-487.

27. S. S. Wang and J. F. Mandell, "Analysis of Delamination in Unidirectional and Crossplied Fiber-Composites Containing Surface Cracks," NASA CR-135248, NASA Lewis Research Center, May 1977.

28. O. Orringer, "Analytical and Experimental Evaluation of Two Designs for Graphite/Epoxy Antenna Feed Truss for Communications Satellite," AFFDL-TR-78-78, Wright-Patterson Air Force Base, Ohio, June 1978.

29. E. F. Rybicki and D. W. Schmueser, "Effect of Stacking Sequence and Lay-up Angle on Free Edge Stresses Around a Hole in Laminated Plate Under Tension," Journal of Composite Materials, Vol. 12, 1978, page 300-313.

30. J. T. S. Wang and J. H. Dickson, "Interlaminar Stresses in Symmetric Composite Laminates," Journal of Composite Materials, Vol. 12, 1978, pages 390-402.

31. K. L. Reifsnider, E. G. Hennke, and W. W. Stinchcomb, "Defect-Property Relationships in Composite Materials," AFML-TR-76-81 Part IV, Wright-Patterson Air Force Base, Ohio, June 1979.

32. R. L. Spilker and S. C. Chou, "Edge Effects in Symmetric Composite Laminates: Importance of Satisfying the Traction-Free-Edge Condition," Journal of Composite Materials, Vol. 14, 1980, pages 2-20.

33. E. Altus, A. Rotem and M. Shmueli, "Free Edge Effect in Angle Ply Laminates - A New Three Dimensional Finite Difference Solution," Journal of Composite Materials, Vol. 14, 1980, pages 21-30.

34. E. L. Stanton and L. M. Crain, "An Analysis of Interlaminar Stress Gradients and Impact Damage in Graphite-Epoxy Laminates," Report No. NADC-80135-60, Naval Air Development Center, March 1980.

35. I. S. Raju, J. D. Whitcomb and J. G. Goree, "A New Look at Numerical Analysis of Free-Edge Stresses in Composite Laminates," NASA Technical Paper 1751, NASA Langley Research Center, December 1980.

36. C. T. Herakovich, "On the Relationship Between Engineering Properties and Delamination of Composite Materials," Journal of Composite Materials, Vol. 15, 1981, pages 336-348.

37. A. S. D. Wang and M. Slomiana, "Fracture Mechanics of Delamination - Initiation and Growth," Report No. NADC- 79056-60, Naval Air Development Center, January 1982.

38. S. S. Wang, "Edge Delimination in Angle-Ply Composite Laminates," NASA CR-165439, NASA Lewis Research Center, February 1981.

39. F. W. Crossman and A. S. D. Wang, "The Dependence of Transverse Cracking and Delamination on Ply Thickness Graphite/Epoxy Laminates," ASTM, STP 775, "Damage in Composite Materials," 1982, pages 118-139.

40. T. K. O'Brien, "Characterization of Delamination Onset and Growth in a Composite Laminate," ASTM, STP 775, "Damage in Composite Materials," 1982, pages 140-167.

41. T. K. O'Brien, N. J. Johnston, D. H. Morris and R. A. Simonds, "A Simple Test for the Interlaminar Fracture Toughness of Composites," SAMPE Journal July/August 1982, pages 8-15.

42. T. K. O'Brien, "Mixed - Mode Strain - Energy - Release Rate Effects on Edge Delamination of composites," NASA Technical Memorandum 84592, January 1983.

43. T. K. O'Brien, I. S. Raju, and D. P. Garber, "Residual Thermal and Moisture Influence on Strain Energy Release Rate Analysis of Edge Delamination," Journal of Composite Technology and Research, Vol 8, No. 2, summer 1986, pages 37-47.

44. R. S. Sandhu, "Analytical-Experiment Correlation of the Behavior of 0^o, $\pm 45^o$, 90^o Family of AS/3501-5 Graphite-Epoxy Composite-Laminates under Uniaxial Tensile Loading," AFFDL - TR-79-3064, Wright-Patterson Air Force Base, Ohio, May 1979.

45. S. W. Tsai and N. J. Pagano, "Invariant Properties of Composite Materials," Composite Materials Workshop, S. W. Tsai, J. C. Halpin and N. J. Pagnano, Editors, Technomic Publishing Co., Inc., 1968, pages 233-253.

TABLE 1

Constants Defining the Critical Angle θ

Criterion	Equation	a	b	c
1	68	$2 (B_2 B_6 - B_3 B_5)$	$4 (B_1 B_6 - B_3 B_4)$	$B_1 B_5 + B_2 B_6 - B_2 B_4 - B_3 B_5$
2	73	$2 (B_8 B_6 - B_9 B_5)$	$4 (B_7 B_6 - B_9 B_4)$	$B_7 B_5 + B_8 B_6 - B_8 B_4 - B_9 B_5$
3	78	$2 B^c_2 B^c_5$	$4 (B^c_1 B^c_5 - B^c_3 B^c_4)$	$B^c_2 (B^c_5 - B^c_4)$
4	83	$2 B^c_7 B^c_5$	$4 (B^c_6 B^c_5 - B^c_8 B^c_4)$	$B^c_7 (B^c_5 - B^c_4)$
5	88	$2 U_2 U_3$	$- 4 U_3 (U_1 + U_4)$	$U_2 (U_3 + U_4)$
6	93	$8 m U_2 U_3$	$- 4 U_3 [(4m + n) x (U_4 + U_1) + n U_2]$	$U_2 [(4m + n) U_4 + (4m - n) U_3]$

TABLE 2

Dependence of Angles; Delaminating Moment Coefficients; and Laminate Poisson's Ratios on m and n for $[(\theta / -\theta)_m / 90_n]_s$ Graphite-epoxy Laminates, Criterion 6.1

Plies		Uncracked 90-Degree Plies N_x loading			
m	n	θ	μ	$\sigma^{\theta}_y/\sigma_0$	DMC_s
(1)	(2)	(3)	(4)	(5)	(6)
1	1	52.6	0.32	0.59	4.05
1	2	54.2	0.23	0.87	7.16
1	4	54.8	0.16	1.21	13.33
5	1	47.9	0.56	0.19	27.32
5	2	49.8	0.46	0.32	48.67
5	4	52.0	0.35	0.51	84.71
10	1	46.5	0.64	0.10	59.27
10	2	47.9	0.56	0.19	109.30
10	4	49.8	0.46	0.32	194.68
40	1	45.1	0.72	0.03	256.34
40	2	45.6	0.69	0.06	498.46
40	4	46.5	0.64	0.10	948.35
100	1	44.7	0.74	0.01	652.52
100	2	45.0	0.73	0.02	1289.30
100	4	45.4	0.70	0.05	2519.79

TABLE 3

Dependence of Angles; Delaminating Moment Coefficients; and Laminate Poisson's Ratios on m and n for $[(\theta / -\theta)_m / 90_n]_s$ Graphite-epoxy Laminates, Criterion 6.2

Plies		Uncracked 90-Degree Plies e_x Loading				
m	n	θ	μ	$\sigma^{\theta}_y/\sigma_0$	DMC_e	DMC_s
(1)	(2)	(3)	(4)	(5)	(6)	(7)
1	1	34.3	0.50	0.34	15.85	2.37
1	2	37.2	0.33	0.54	24.36	4.46
1	4	39.7	0.20	0.83	38.47	9.16
5	1	28.7	0.96	0.11	132.04	15.26
5	2	30.8	0.77	0.18	219.04	27.43
5	4	33.4	0.56	0.30	344.81	48.95
10	1	27.3	1.12	0.06	299.91	33.06
10	2	28.7	0.96	0.11	528.14	61.06
10	4	30.8	0.77	0.18	876.15	109.71
40	1	26.0	1.28	0.02	1353.37	143.20
40	2	26.5	1.22	0.03	2592.12	278.22
40	4	27.3	1.12	0.06	4798.58	528.97
100	1	27.5	1.32	0.01	3478.56	364.79
100	2	25.9	1.29	0.01	6828.62	720.41
100	4	26.3	1.24	0.03	13181.40	1406.85

TABLE 4

Dependence of Angles; Delaminating Moment Coefficients; and Laminate Poisson's Ratios on m and n for $[(\theta / -\theta)_m / 90_n]_s$ Graphite-epoxy Laminates, Criterion 6.3

Plies		Cracked 90-Degree Plies N_x loading			
m	n	θ	μ	$\sigma^{\theta}_y/\sigma_0$	DMC_s
(1)	(2)	(3)	(4)	(5)	(6)
1	1	54.9	0.28	0.68	4.68
1	2	57.8	0.19	1.12	9.24
1	4	60.2	0.11	1.88	20.70
5	1	48.8	0.53	0.20	28.66
5	2	51.2	0.43	0.35	52.32
5	4	54.0	0.32	0.58	95.61
10	1	47.2	0.61	0.11	61.43
10	2	48.8	0.53	0.20	114.65
10	4	51.2	0.43	0.35	209.28
40	1	45.6	0.70	0.03	263.39
40	2	46.2	0.67	0.06	513.64
40	4	47.2	0.61	0.11	982.93
100	1	45.3	0.72	0.01	669.35
100	2	45.5	0.71	0.02	1324.02
100	4	46.0	0.68	0.05	2593.54

TABLE 5

Dependence of Angles; Delaminating Moment Coefficients; and Laminate Poisson's Ratios on m and n for $[(\theta / -\theta)_m / 90_n]_s$ Graphite-epoxy Laminates, Crioterion 6.4

Plies		Cracked 90-Degree Plies e_x Loading				
m	n	θ	μ	$\sigma^{\theta}{}_y/\sigma_0$	DMC_e	DMC_s
(1)	(2)	(3)	(4)	(5)	(6)	(7)
1	1	34.5	0.49	0.36	16.13	2.50
1	2	37.4	0.31	0.60	24.87	4.94
1	4	40.1	0.19	1.01	39.42	11.11
5	1	28.8	0.96	0.11	133.66	15.54
5	2	30.9	0.76	0.18	222.14	28.17
5	4	33.6	0.55	0.30	350.57	51.22
10	1	27.4	1.11	0.06	303.25	33.51
10	2	28.8	0.96	0.11	534.65	62.16
10	4	30.9	0.76	0.18	888.54	112.69
40	1	26.0	1.28	0.02	1366.91	144.72
40	2	26.5	1.22	0.03	2619.10	281.45
40	4	27.4	1.11	0.06	4852.00	536.24
100	1	25.7	1.32	0.01	3512.45	368.43
100	2	25.9	1.29	0.01	6896.35	727.89
100	4	26.3	1.24	0.03	13316.54	1422.62

TABLE 6

Dependence of Angles; Delaminating Moment Coefficients; and Laminate Poisson's Ratios on m and n for $[(\theta / -\theta)_m / 90_n]_s$ Graphite-epoxy Laminates, Criterion 6.5

Plies		Maximum Mismatch of Poisson's Ratios				
m	n	θ	μ	$\sigma^{\theta}_{y}/\sigma_0$	DMC_e	DMC_s
(1)	(2)	(3)	(4)	(5)	(6)	(7)
1	1	25.5	0.44	0.20	13.89	1.37
1	2	25.5	0.27	0.27	19.59	2.19
1	4	25.5	0.16	0.36	28.77	4.00
5	1	25.5	0.94	0.86	129.02	12.50
5	2	25.5	0.73	0.13	206.82	19.72
5	4	25.5	0.50	0.18	307.00	29.91
10	1	25.5	1.11	0.05	297.57	29.54
10	2	25.5	0.94	0.09	516.06	49.98
10	4	25.5	0.73	0.13	827.26	78.90
40	1	25.5	1.28	0.02	1352.50	138.81
40	2	25.5	1.22	0.03	2586.08	261.99
40	4	25.5	1.11	0.05	4761.19	472.66
100	1	25.5	1.32	0.01	3478.18	360.18
100	2	25.5	1.29	0.01	6825.76	702.56
100	4	25.5	1.24	0.02	13161.01	1339.90

TABLE 7

Dependence of Critical Angles and Delamination Moment Coefficients
for $[\pm\theta_5 / 90]_s$ Laminates on Ply Elastic Constants

E_{11}	E_{22}	G_{12}	μ_{12}	Maximum DMC_s			Maximum DMC_e			Maximum Mismatch of μs		
(msi)	(msi)	(msi)		θ_c	DMC_s	DMC_e	θ_c	DMC_s	DMC_e	θ_c	DMC_s	DMC_e
19.26	1.32	0.83	0.25	49.89	48.72	127.84	31.16	27.58	216.52	25.98	19.88	204.57
			0.30	49.84	48.69	128.18	30.97	27.50	217.71	25.74	19.80	205.64
			0.35	49.80	48.67	128.58	30.78	27.43	219.04	25.49	19.72	206.82
			0.40	49.77	48.67	129.02	30.59	27.36	220.48	25.24	19.65	208.09
19.26	1.32	0.60	0.35	49.88	63.06	138.07	30.90	32.26	239.00	25.68	22.56	225.49
		0.70		49.85	56.06	133.89	30.85	30.03	230.12	25.60	21.27	217.21
		0.90		49.78	45.30	125.77	30.74	26.15	213.26	25.43	18.95	201.39
19.26	1.00	0.83	0.35	51.07	49.71	119.05	30.34	27.18	221.87	24.09	18.31	202.97
	2.00			48.15	47.22	142.22	31.65	27.98	213.88	27.69	21.93	207.60
	2.50			47.40	46.46	148.38	32.53	28.55	208.94	29.32	23.31	204.82
6.00	1.32	0.83	0.35	44.32	11.85	28.38	31.52	9.82	34.15	29.03	9.10	33.90
12.00				47.70	29.95	76.56	31.42	20.22	110.82	27.46	16.57	107.88
24.00				50.84	59.44	158.74	30.50	30.52	290.40	24.51	20.41	271.77

TABLE 8

Values of σ_Z obtained using Finite Element Method
for
Laminates A, B, C, and D**

Laminate	σ_Z* psi Acting upon Mid Plane										
	Location from Edge in Terms of Ply Thickness										
	(11)	(10)	(9)	(8)	(7)	(6)	(5)	(4)	(3)	(2)	(1)
	9.5	8.5	7.5	6.5	5.5	4.5	3.5	2.5	1.5	0.5	0.
A	-3.55	-3.33	-2.95	-2.36	-1.46	0.0	2.52	7.37	18.54	56.35	107.74
B	-2.26	-2.68	-2.36	-1.86	-1.13	0.0	1.86	5.22	12.72	36.78	67.65
C	-2.31	-2.15	-1.91	-1.52	-0.95	-0.07	1.36	3.93	9.61	27.81	51.12
D	-1.65	-1.24	-0.68	0.13	1.31	3.16	6.26	12.10	25.21	68.32	126.22

* Applied Axial Stress = 100.0 psi

** A = $[(+49.8/-49.8)_5 / 90]_s$ Laminate

B = $[(+30.8/-30.8)_5 / 90]_s$ Laminate

C = $[(+25.5/-25.5)_5 / 90]_s$ Laminate

D = $[(+47.9/-47.9)_5 / 90]_s$ Laminate

TABLE 9

Shear Stresses τ_{yz} at Centroids of Finite Elements
Laminate A: $(\pm 49.8_5 / 90)_s$*

Shear Stress τ_{yz} psi at Centroids of Elements from the Left Free Edge
Elements Numbers from Left to Right

Element Number Increasing from the Mid-plane	1	2	3	4	5	6	7	8
1	16.09	19.43	16.87	14.04	11.63	9.70	8.16	6.94
2	24.13	30.93	28.43	24.78	21.37	18.45	16.01	13.97
3	3.35	15.06	19.27	19.78	18.87	17.46	15.93	14.45
4	1.21	6.48	10.89	13.11	13.89	13.87	13.42	12.75
5	0.43	3.12	6.08	8.26	9.55	10.20	10.41	10.34
6	0.01	1.37	3.25	4.98	6.29	7.17	7.70	7.98
7	-0.19	0.33	1.46	2.74	3.88	4.78	5.45	5.91
8	-0.39	-0.38	0.26	1.17	2.11	2.95	3.64	4.17
9	-0.54	-0.84	-0.53	0.10	0.85	1.58	2.23	2.75
10	-0.57	-0.98	-0.90	-0.50	0.05	0.63	1.16	1.60
11	-0.24	-0.60	-0.64	-0.46	-0.18	0.11	0.37	0.57

* Applied Axial Stress = 100.0 psi

TABLE 10

Shear Stresses τ_{yz} at Centroids of Finite Elements
Laminate B: $(\pm 30.8_5 / 90)_s$*

Shear Stress τ_{yz} psi at Centroids of Elements from the Left Free Edge
Elements Numbers from Left to Right

Element Number Increasing from the Mid-plane	1	2	3	4	5	6	7	8
1	7.24	10.26	9.22	7.80	6.56	5.55	4.74	4.10
2	15.28	17.85	15.84	13.65	11.77	10.21	8.93	7.87
3	3.18	11.06	12.93	12.48	11.41	10.25	9.17	8.21
4	1.27	5.27	8.37	9.52	9.58	9.14	8.52	7.85
5	0.57	2.73	4.97	6.52	7.26	7.44	7.30	7.00
6	0.21	1.35	2.84	4.17	5.11	5.65	5.87	6.87
7	-0.00	0.50	1.45	2.48	3.37	4.03	4.45	4.67
8	-0.19	-0.01	0.05	1.27	2.03	2.68	3.18	3.51
9	-0.29	-0.04	-0.08	0.44	1.04	1.61	2.09	2.44
10	-0.30	-0.05	-0.37	-0.05	0.38	0.81	1.18	1.46
11	-0.13	-0.03	-0.28	-0.15	0.02	0.22	0.39	0.51

* Applied Axial Stress = 100.0 psi

TABLE 11

Shear Stresses τ_{yz} at Centroids of Finite Elements
Laminate C: $(\pm 25.5_5 / 90)_s$*

Shear Stress τ_{yz} psi at Centroids of Elements from the Left Free Edge
Elements Numbers from Left to Right

Element Number Increasing from the Mid-plane	1	2	3	4	5	6	7	8
1	4.98	7.39	6.67	5.64	4.74	4.02	3.44	2.98
2	11.50	13.03	11.43	9.81	8.45	7.33	6.42	5.67
3	2.54	8.55	9.73	9.23	8.34	7.43	6.62	5.91
4	1.02	4.14	6.53	7.30	7.22	6.80	6.27	5.74
5	0.47	2.16	3.93	5.12	5.63	5.69	5.52	5.22
6	0.18	1.08	2.27	3.32	4.04	4.54	4.54	4.48
7	-0.00	0.43	1.18	2.00	2.71	3.21	3.51	3.64
8	-0.13	-0.00	0.45	1.06	1.66	2.17	2.55	2.78
9	-0.20	-0.26	-0.01	0.41	0.88	1.33	1.70	1.96
10	-0.20	-0.34	-0.62	-0.02	0.35	0.68	0.97	1.18
11	-0.09	-0.20	-0.18	-0.03	0.05	0.19	0.32	0.41

* Applied Axial Stress = 100.0 psi

TABLE 12

Shear Stresses τ_{yz} at Centroids of Finite Elements
Laminate D: $(\pm 47.8_5 / 90)_s$*

Shear Stress τ_{yz} psi at Centroids of Elements from the Left Free Edge
Elements Numbers from Left to Right

Element Number Increasing from the Mid-plane	1	2	3	4	5	6	7	8
1	16.82	20.66	18.09	15.16	12.61	10.64	9.03	7.74
2	26.12	33.37	30.76	26.95	23.40	20.35	17.78	15.63
3	3.99	16.97	21.62	22.22	21.25	19.73	18.07	16.46
4	1.64	7.81	12.91	15.47	16.38	16.36	15.84	15.07
5	0.81	4.29	7.91	10.51	12.05	12.78	12.99	12.86
6	0.48	2.55	5.06	7.23	8.80	9.81	10.37	10.62
7	0.29	1.60	3.39	5.04	6.44	7.48	8.19	8.63
8	0.17	1.02	2.24	3.54	4.72	5.68	6.41	6.94
9	0.09	0.64	1.50	2.48	3.44	4.24	4.98	5.52
10	0.03	0.37	0.97	1.71	2.48	3.19	3.82	4.35
11	-0.02	0.17	0.58	1.12	1.73	2.33	2.89	3.38
12	-0.06	0.01	0.27	0.67	1.14	1.63	2.12	2.56
13	-0.10	-0.12	0.03	0.30	0.67	1.07	1.48	1.88
14	-0.13	-0.23	-0.18	0.01	0.28	0.61	0.95	1.30
15	-0.16	-0.33	-0.34	-0.23	-0.03	0.23	0.52	0.83
16	-0.19	-0.41	-0.48	-0.42	-0.28	-0.01	0.17	0.44
17	-0.21	-0.46	-0.57	-0.56	-0.47	-0.31	-0.11	0.12
18	-0.22	-0.48	-0.61	-0.64	-0.58	-0.46	-0.30	-0.11
19	-0.20	-0.45	-0.58	-0.63	-0.61	-0.53	-0.40	-0.24
20	-0.13	-0.33	-0.46	-0.52	-0.53	-0.48	-0.39	-0.27
21	-0.01	-0.12	-0.21	-0.25	-0.26	-0.24	-0.20	-0.15

* Applied Axial Stress = 100.0 psi

TABLE 13

Thermal Residual Stresses and DMC_s in $[(\theta / -\theta)_m / 90_n]_s$
Graphite-epoxy Laminates, Criterion 6.1

Plies		Uncracked 90-Degree Plies Thermal DMC_s and Stresses (psi)					
m	n	$\sigma^{\theta T}{}_x$	$\sigma^{\theta T}{}_y$	$\sigma^{90T}{}_x$	$\sigma^{90T}{}_y$	$DMC^T{}_{sx}$	$DMC^T{}_{sy}$
(1)	(2)	(3)	(4)	(5)	(6)	(7)	(8)
1	1	-906.07	-1192.42	3624.28	4769.67	-0.31	-0.41
1	2	-1590.04	-2351.96	3180.09	4703.89	-0.79	-1.17
1	4	-2716.11	-3945.77	2716.11	3945.77	-2.40	-3.48
5	1	-220.68	-48.10	4413.60	962.03	-6.71	-1.46
5	2	-413.15	-318.86	4131.52	3188.56	-13.78	-10.63
5	4	751.76	-913.98	3758.79	4569.91	-29.84	-36.28
10	1	-114.98	34.05	4599.33	-1361.94	-26.64	7.89
10	2	-220.68	-48.10	4413.60	962.03	-53.65	-11.69
10	4	-413.15	-318.86	4131.52	3188.56	-110.23	-85.07
40	1	-29.80	27.22	4767.95	-4366.39	-425.81	388.96
40	2	-58.86	39.76	4708.46	-3180.69	-851.47	575.19
40	4	-114.98	34.05	4599.33	-1361.94	-1704.80	504.82
100	1	-12.01	12.93	4805.38	-5173.09	-2662.17	2866.00
100	2	-23.90	23.09	4780.38	-4617.55	-5323.00	5141.97
100	4	-47.32	36.25	4731.84	-3625.15	-10643.39	8154.23

TABLE 14

Thermal Residual Stresses and DMC_s in $[(\theta / -\theta)_m / 90_{n/2}]_s$
Graphite-epoxy Laminates, Criterion 6.2

Plies		Uncracked 90-Degree Plies Thermal DMC_s and Stresses (psi)					
m	n	$\sigma^{\theta T}{}_x$	$\sigma^{\theta T}{}_y$	$\sigma^{90T}{}_x$	$\sigma^{90T}{}_y$	$DMC^T{}_{sx}$	$DMC^T{}_{sy}$
(1)	(2)	(3)	(4)	(5)	(6)	(7)	(8)
1	1	-1216.37	1740.64	4865.46	-6962.55	-0.42	0.60
1	2	-2307.50	1095.94	4614.99	-2191.88	-1.14	0.54
1	4	-4172.64	-299.62	4172.14	299.62	-3.68	-0.26
5	1	-246.36	1339.48	4927.14	-26789.52	-7.49	40.70
5	2	-496.69	1728.18	4966.94	-17281.82	-16.57	57.64
5	4	-982.31	1814.95	4911.56	-9074.77	-38.99	72.04
10	1	-121.23	886.05	4849.30	-35442.12	-28.09	205.27
10	2	-246.36	1339.48	4927.14	-26789.52	-59.89	325.63
10	4	-496.69	1728.18	4966.94	-17281.82	-132.52	461.09
40	1	-29.55	286.13	4728.08	-45780.69	-422.24	4088.49
40	2	-59.72	522.48	4777.55	-41798.69	-863.96	7558.70
40	4	-121.23	886.05	4849.30	-35442.12	-1797.45	13137.00
100	1	-11.73	121.27	4692.54	-48509.06	-2599.63	26874.55
100	2	-23.58	233.30	4716.77	-46659.04	-5252.29	51957.34
100	4	-47.59	433.15	4759.08	-43314.57	-10704.92	97428.41

TABLE 15

Thermal Residual Stresses and DMC_s in $[(\theta / -\theta)_m / 90_{n/2}]_s$
Graphite-epoxy Laminates, Criterion 6.5

Plies		Uncracked 90-Degree Plies Thermal DMC_s and Stresses (psi)					
m	n	$\sigma^{\theta T}{}_x$	$\sigma^{\theta T}{}_y$	$\sigma^{90T}{}_x$	$\sigma^{90T}{}_y$	$DMC^T{}_{sx}$	$DMC^T{}_{sy}$
(1)	(2)	(3)	(4)	(5)	(6)	(7)	(8)
1	1	-1225.52	2864.52	4902.10	-11458.09	-0.42	0.99
1	2	-2417.35	3039.41	4834.70	-6078.81	-1.20	1.51
1	4	-4646.61	2821.32	4646.61	-2821.32	-4.10	2.49
5	1	-241.14	1534.72	4822.88	-30694.49	-7.33	46.64
5	2	-487.91	2187.98	4879.14	-21879.82	-16.27	72.97
5	4	-981.12	2738.15	4905.62	-13690.75	-38.94	108.68
10	1	-119.15	956.08	4765.98	-38243.25	-27.60	221.49
10	2	-241.14	1534.72	4822.88	-30694.49	-58.62	373.09
10	4	-487.91	2187.98	4879.14	-21879.82	-130.18	583.76
40	1	-29.36	292.30	4697.02	-46768.20	-419.46	4176.68
40	2	-59.04	544.29	4723.52	-43543.52	-854.18	7874.32
40	4	-119.15	956.08	4765.98	-38243.25	-1766.54	14175.28
100	1	-11.70	122.34	4678.98	-48936.69	-2592.05	27111.31
100	2	-23.46	237.35	4691.20	-47469.84	-5223.91	52860.04
100	4	-47.13	447.80	4713.41	-44779.88	-10601.79	100724.20

TABLE 16

Resin Content and Density *

Panel	Ply Thickness	Density	Resin Wt. %	Percent Volume		
				Resin	Fiber	Voids
A	0.00506	1.6083	26.37	33.52	66.13	0.35
B	0.00508	1.5960	28.03	35.37	64.14	0.49
C	0.00505	1.6091	28.84	36.68	63.95	-0.63
D	0.00499	1.5963	29.52	37.25	62.87	-0.12

* Assumed Resin Density = 1.2650 gm / cc

Assumed Fiber Density = 1.7881 gm / cc

TABLE 17

Strains; Initial Delamination Stresses; Initial Matrix Cracking Stress; and Maximum Stresses for Laminate A

Specimen	Area	Strain x 10^{-6}		Initial Delamination Stress (ksi)				Initial Matrix Cracking	Maximum Stress
		Axial	Transverse	Gages	Silver Ink	Accoustic Emission	Visual		
(1)	(2)	(3)	(4)	(5)	(6)	(7)	(8)	(9)	(10)
A*-1	0.1125	6099.	-6415	N*	17.1				27.5
A - 2	0.1151		-5000.	21.0	18.1				22.7
A - 3	0.1152					18.4		13.2	20.3
A - 4	0.1138		-5050.	19.8		19.7	17.9	14.7	21.8
A - 5	0.1121		-4500.	20.4		19.6		15.2	21.7
A - 6	0.1133				18.1	18.1	18.0	11.0	21.1
A - 7	0.1129				14.2	19.9	20.4	15.6	20.9
A - 8	0.1152				18.8	18.8	17.4	15.0	21.9
A - 9	0.1172				19.3	19.1	15.4	14.8	20.5
A - 10	0.1125				N*	N*	16.5	17.3	17.3
A - 11	0.1131				N*	N*		17.5	17.8
A - 12	0.1138				10.2	20.0		15.7	20.7
A - 13	0.1145				19.2	18.6	18.0	17.3	19.5
A - 14	0.1156				19.7	19.6	17.0	18.5	20.0
AVERAGE				20.4	17.2	19.2	18.1	15.5	

A* = $[(49.8 / -49.8)_5 /90]_s$ Laminate

N* = Not Indicated

TABLE 18

Strains; Initial Delamination Stresses; Initial Matrix Cracking Stress; and Maximum Stresses for Laminate B

Specimen	Area	Strain x 10^{-6}		Initial Delamination Stress (ksi)				Initial Matrix Cracking	Maximum Stress
		Axial	Transverse	Gages	Silver Ink	Accoustic Emission	Visual		
(1)	(2)	(3)	(4)	(5)	(6)	(7)	(8)	(9)	(10)
B*-1	0.1165	3300.	-3000.	22.0	24.5				27.5
B - 2		This specimen was not tested							
B - 3	0.1139		-2700	25.5	25.5				25.6
B - 4	0.1153		-2700.	23.6		23.3	23.4	19.8	26.5
B - 5	0.1151		-2500.	23.7		23.8		22.7	25.2
B - 6	0.1144				24.2	23.2	<24.2	20.3	24.9
B - 7		This specimen was discarded							
B - 8	0.1129				24.8	23.5	24.8	22.2	26.2
B - 9	0.1138				24.1	25.1	23.9	22.7	25.7
B - 10	0.1140					23.7	23.8	21.5	24.0
B - 11	0.1138					N*	24.3	24.2	24.4
B - 12	0.1143					21.3	21.7	20.3	22.0
B - 13	0.1142					22.1	22.1	20.2	22.3
B - 14	0.1141					23.3	23.6	23.1	23.4
			AVERAGE	23.7	24.6	23.3	23.5	21.7	

B* = $[(30.8 / -30.8)_5 /90]_s$ Laminate

N* = Not Indicated

TABLE 19

Strains; Initial Delamination Stresses; Initial Matrix Cracking Stress; and Maximum Stresses for Laminate C

Specimen	Area	Strain x 10^{-6}		Initial Delamination Stress (ksi)				Initial Matrix Cracking	Maximum Stress
		Axial	Transverse	Gages	Silver Ink	Accoustic Emission	Visual		
(1)	(2)	(3)	(4)	(5)	(6)	(7)	(8)	(9)	(10)
C*-1	0.1135	2900.	-2400.	20.4	25.8		22.0		29.8
C - 2	0.1168		-1700.	20.6	27.4		22.3		28.0
C - 3	0.1152				23.4	26.2		24.0	27.1
C - 4	0.1143		-1700.	23.5		21.1	22.7	21.1	26.2
C - 5	0.1155		-2000.	23.8		24.9		24.2	27.2
C - 6	0.1137				22.9	25.0	22.9	24.0	27.6
C - 7	0.1114					28.7	29.9	24.3	29.9
C - 8	0.1106					29.0	29.1	28.5	29.2
C - 9	0.1119					27.4	27.4	26.4	27.6
C - 10	0.1119					27.9	28.0	27.6	28.0
C - 11	0.1150					N*	24.8	25.3	25.3
C - 12	0.1138					26.3	26.3	26.3	26.4
C - 13	0.1147					27.3	30.6	25.9	30.6
C - 14	0.1129					N*	24.2	24.0	24.3
			AVERAGE	22.1	24.9	26.4	25.9	25.1	

A* = $[(25.5 / -25.5)_5 /90]_s$ Laminate

N* = Not Indicated

TABLE 20

Strains; Initial Delamination Stresses; Initial Matrix Cracking Stress; and Maximum Stresses for Laminate D

Specimen	Area	Strain x 10^{-6}		Initial Delamination Stress (ksi)				Initial Matrix Cracking	Maximum Stress
		Axial	Transverse	Gages	Silver Ink	Accoustic Emission	Visual		
(1)	(2)	(3)	(4)	(5)	(6)	(7)	(8)	(9)	(10)
D*-1	0.2140			22.1	18.2		22.1		22.1
D - 2	0.2186				17.9		16.2		18.4
D - 3	0.2176				20.0				21.9
D - 4	0.2143			21.3		16.0	21.0	13.9	21.8
D - 5	0.2162			18.2		18.3	16.2	13.3	19.5
D - 6	0.2176				18.0	18.4		11.8	21.5
D - 7	0.2137					20.1	21.4	16.7	21.0
D - 8	0.2150					19.8	22.4	15.2	20.2
D - 9	0.2169					N*	16.4	17.4	16.5
D - 10	0.2148					N*	17.1	15.8	17.1
D - 11	0.2160					18.2	17.1	16.6	19.4
D - 12	0.2163					19.3	21.5	15.6	21.5
D - 13	0.2180					20.5	19.7	15.6	21.8
D - 14	0.2175					17.0	19.9	16.8	20.3
			AVERAGE	20.5	18.5	18.6	19.3	15.3	

D* = $[(47.9 / -47.9)_5 / 90]_s$ Laminate

N* = Not Indicated

TABLE 21

Stacking Sequences and DMC of ($\pm 45_5 / 90_4 / 0_{10}$) Laminates

Ply Number	Stacking Sequence I Angle	Stacking Sequence I $DMC_S \times 10^{-5}(in)^3$	Stacking Sequence II Angle	Stacking Sequence II $DMC_S \times 10^{-5}(in)^3$
1	45.0		45.0	
		0.33		0.33
2	-45.0		-45.0	
		1.33		1.33
3	90.0		0.	
		1.83		2.66
4	90.0		90.0	
		0.65		3.16
5	45.0		45.0	
		-1.03		3.16
6	-45.0		-45.0	
		-2.04		3.82
7	0.		0.	
		-2.72		4.81
8	0.		0.	
		-3.40		5.81
9	0.		0.	
		-4.07		6.81
10	0.		0.	
		-4.74		7.82
11	0.		90.0	
		-5.40		7.99
12	45.0		45.0	
		-5.74		7.66
13	-45.0		-45.0	
		-5.40		7.99
14	0.		90.0	
		-4.74		7.82
15	0.		0.	
		-4.06		6.82
16	0.		0.	
		-3.40		5.82

TABLE 21 (CONT'D)

Stacking Sequences and DMC of ($\pm 45_5 / 90_4 / 0_{10}$) Laminates

Ply Number	Stacking Sequence I Angle	Stacking Sequence I $DMC_s \times 10^{-5}(in)^3$	Stacking Sequence II Angle	Stacking Sequence II $DMC_s \times 10^{-5}(in)^3$
17	0.		0.	
		-2.71		4.82
18	0.		0.	
		-2.03		3.82
19	-45.0		-45.0	
		-1.02		3.16
20	45.0		45.0	
		0.66		3.17
21	90.0		90.0	
		1.84		2.67
22	90.0		0.	
		1.34		1.34
23	-45.0		-45.0	
		0.34		0.34
24	45.0		45.0	
		0.		0.

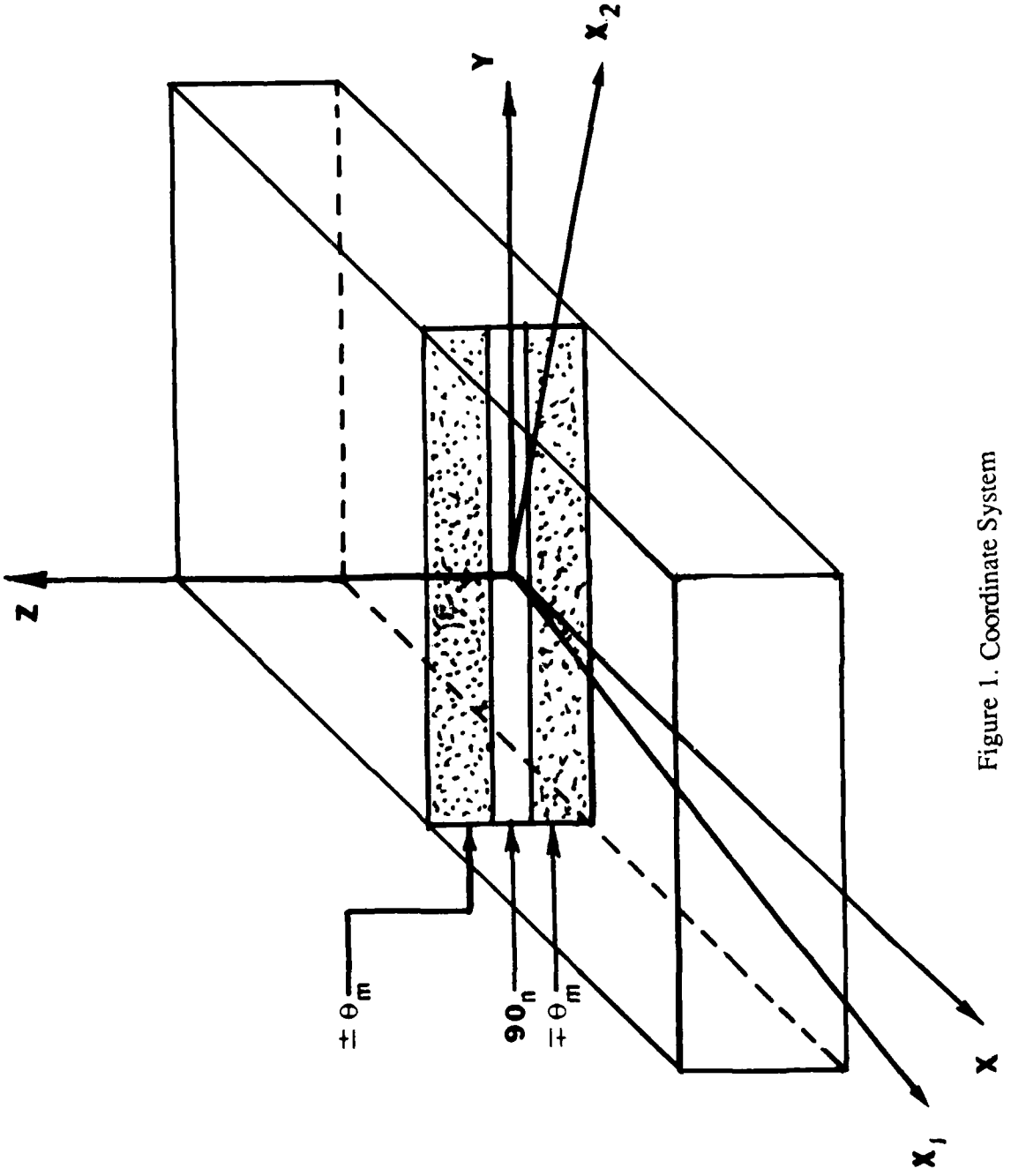

Figure 1. Coordinate System

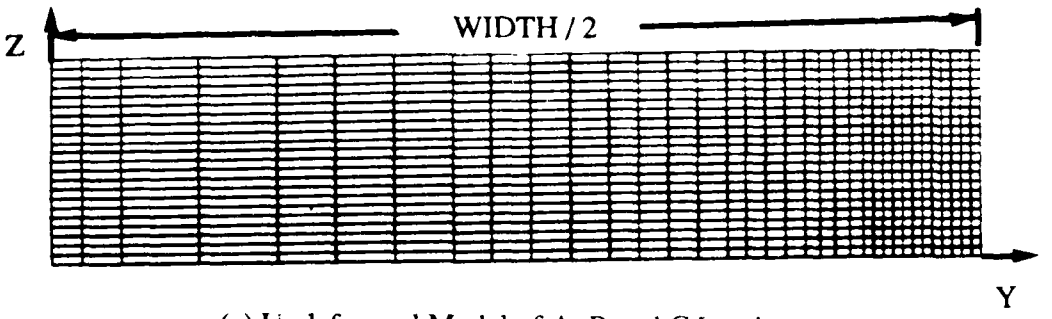

(a) Undeformed Model of A, B and C Laminates

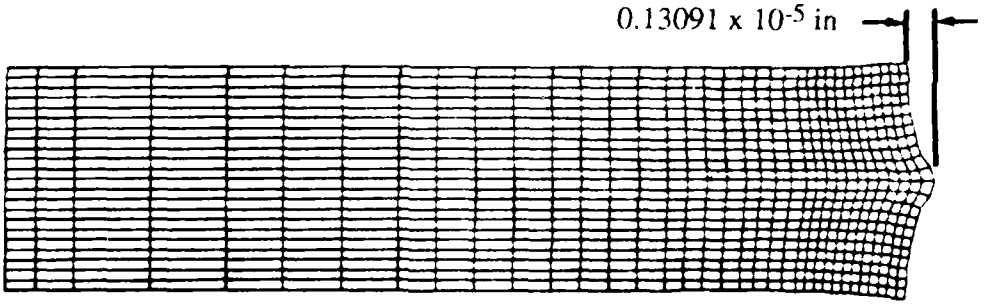

(b) Deformed Model of A Laminate *

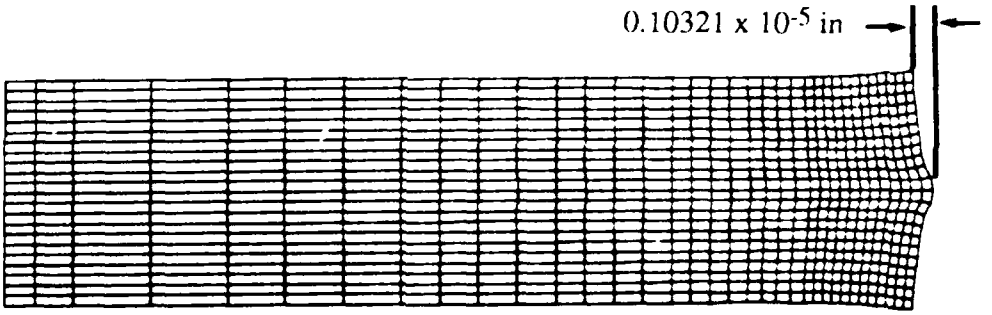

(c) Deformed Model of B Laminate *

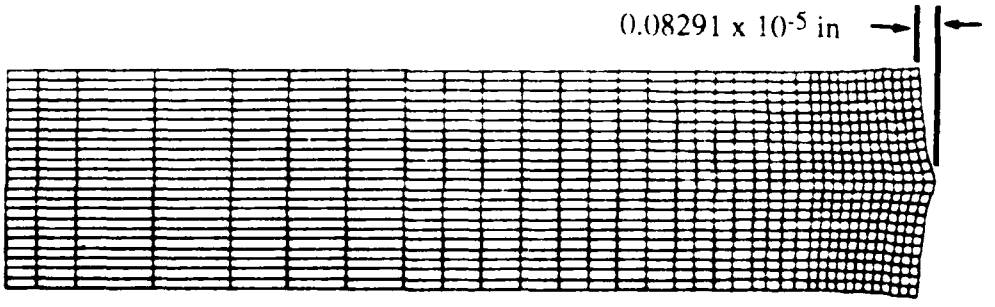

(d) Deformed Model of C Laminate *

* Applied Axial Stress of 100 psi

Figure 2. Finite Element Models of A, B and C Laminate Specimens

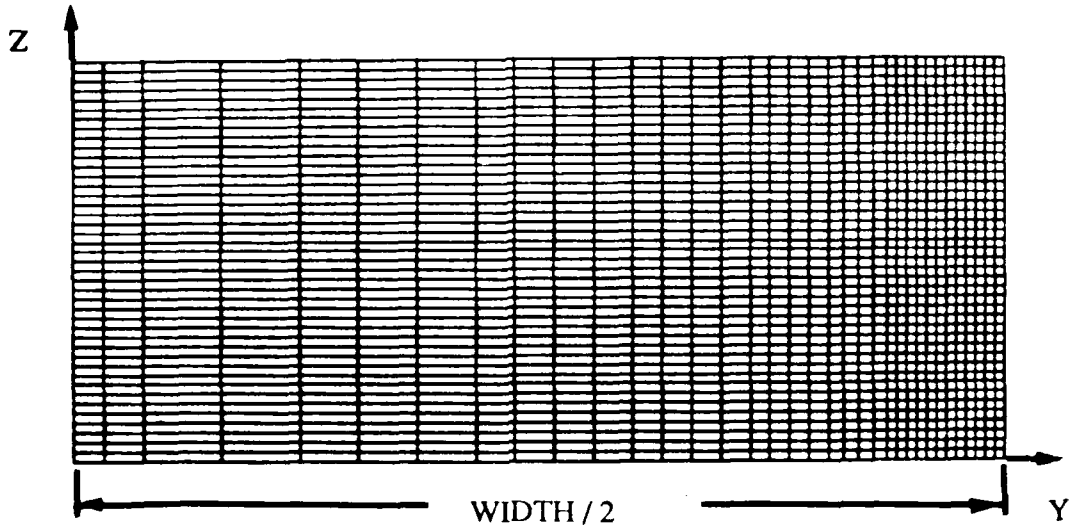

(a) Undeformed Model

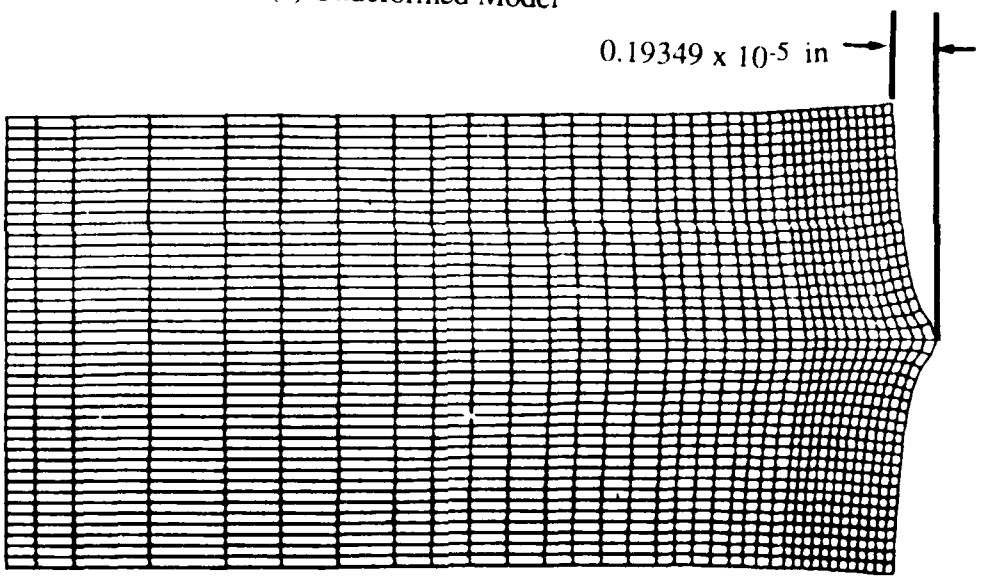

(b) Deformed Model of D Laminate *

* Applied Axial Stress of 100 psi

Figure 3. Finite Element Model of Laminate D Specimen

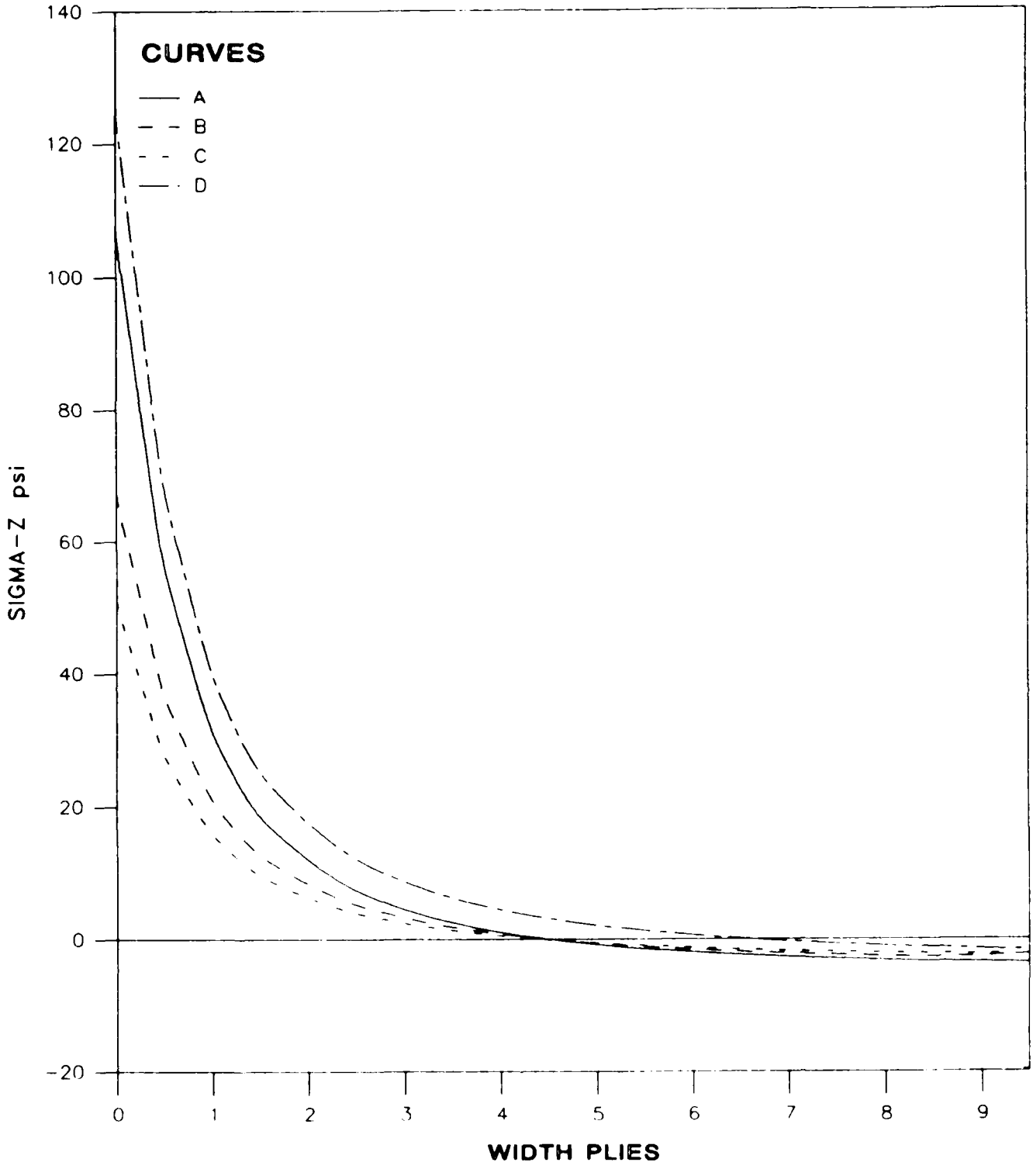

Figure 4. Normal Stress σ_z at Mid-Plane for Width of 10 Plies of Specimens A, B, C, and D

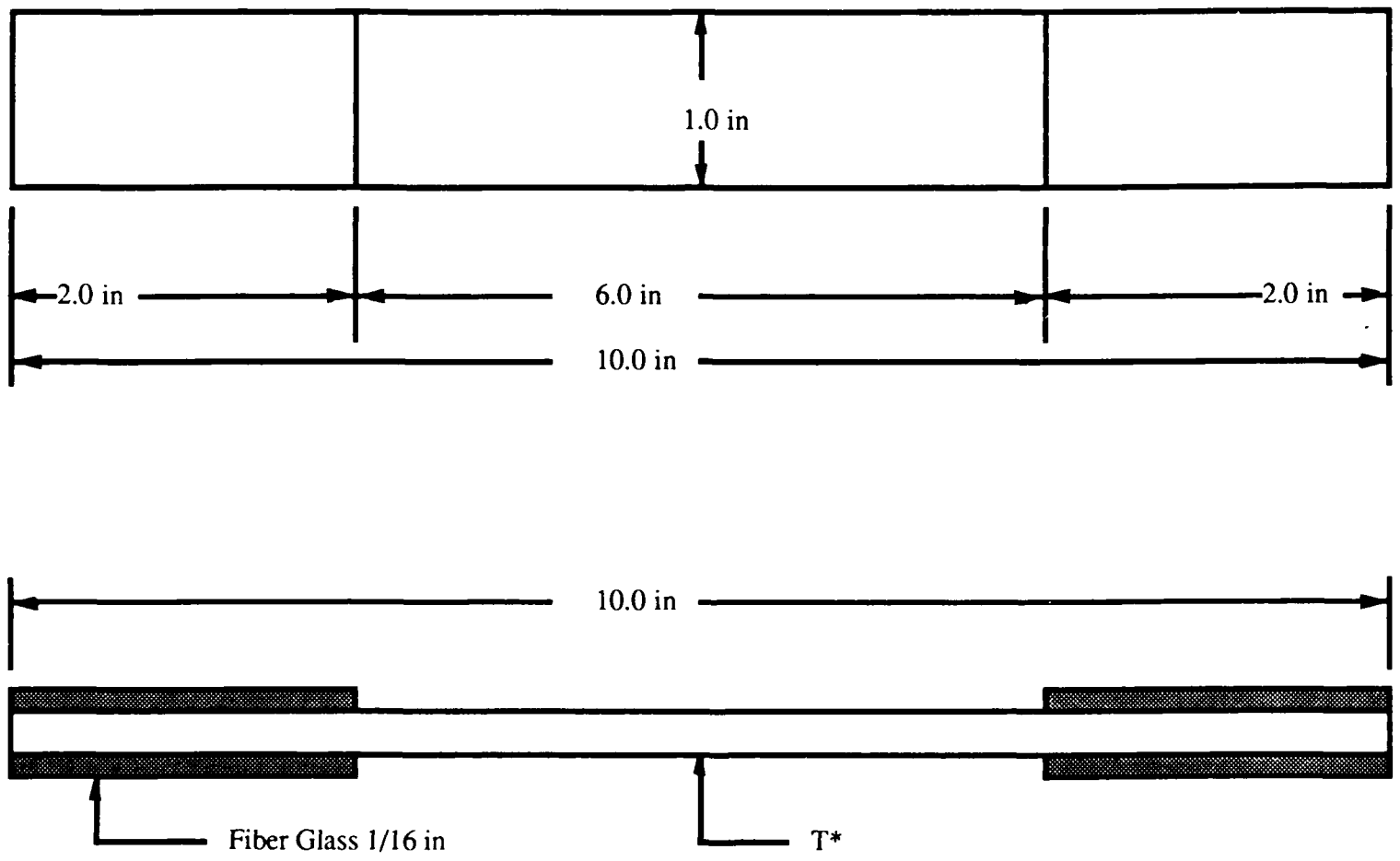

* T = A ($\pm 49.8_5 / 90)_S$; B ($\pm 30.8_5 / 90)_S$; C ($\pm 25.5_5 / 90)_S$; D ($\pm 47.9_{10} / 90)_S$

Figure 5. Specimen Geometry

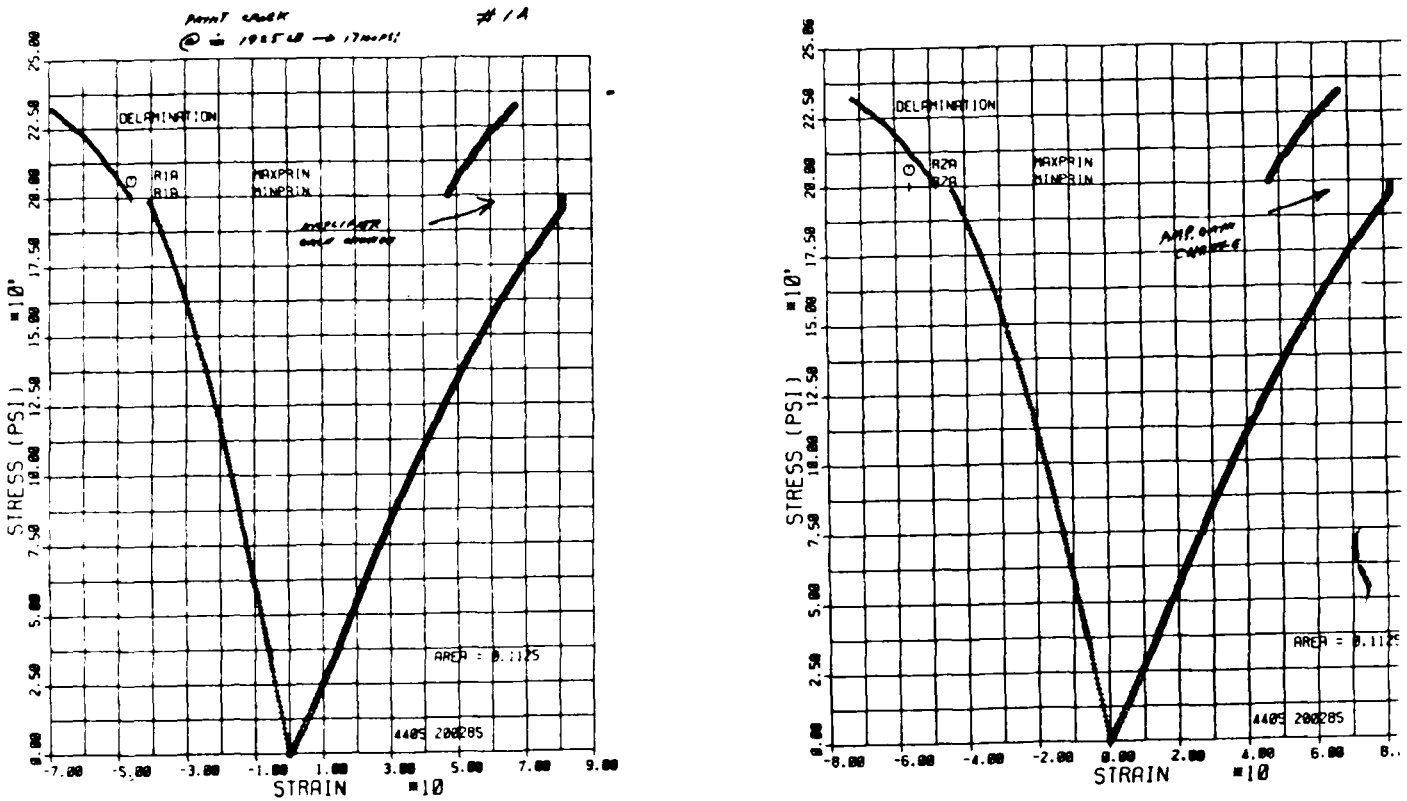

(a) Rosette 1

(b) Rosette 2

Figure 6. Stress-Strain Curves of Back to Back Rosettes Bonded to Specimen A-1

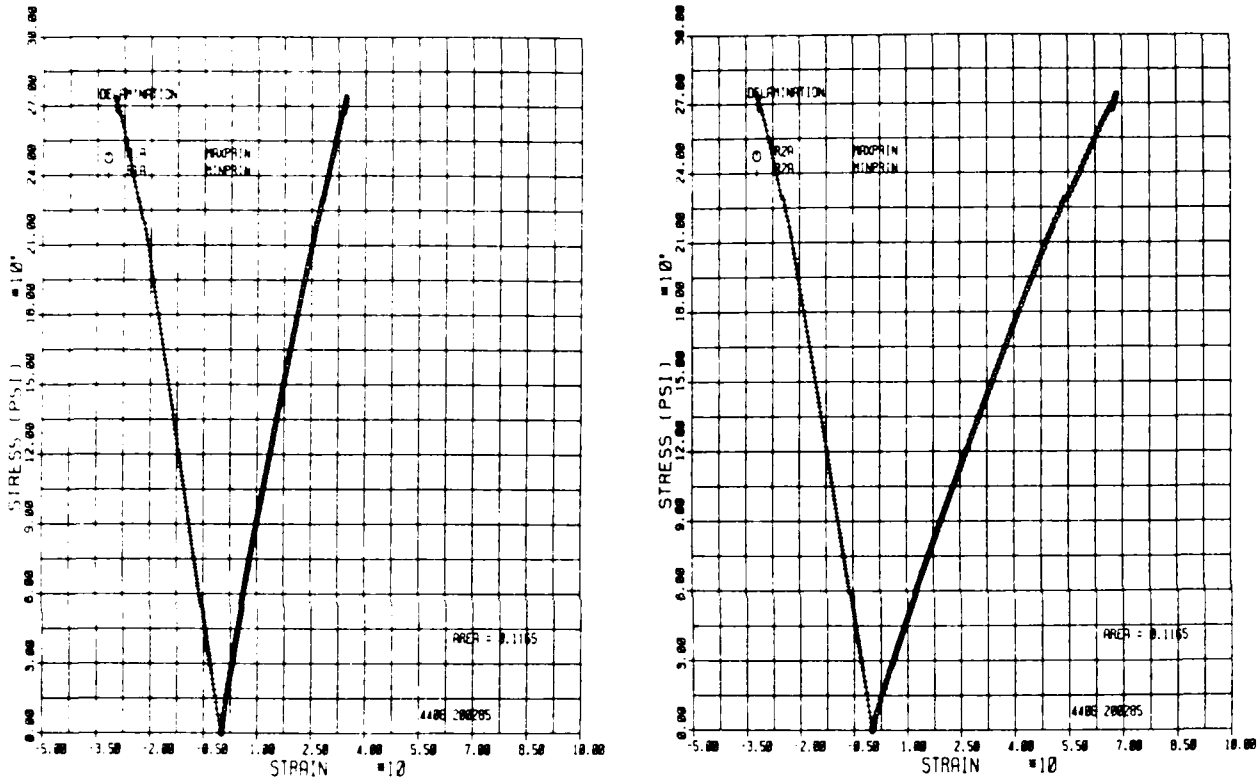

(a) Rosette 1

(b) Rosette 2

Figure 7. Stress-Strain Curves of Back to Back Rosettes Bonded to Specimen B-1

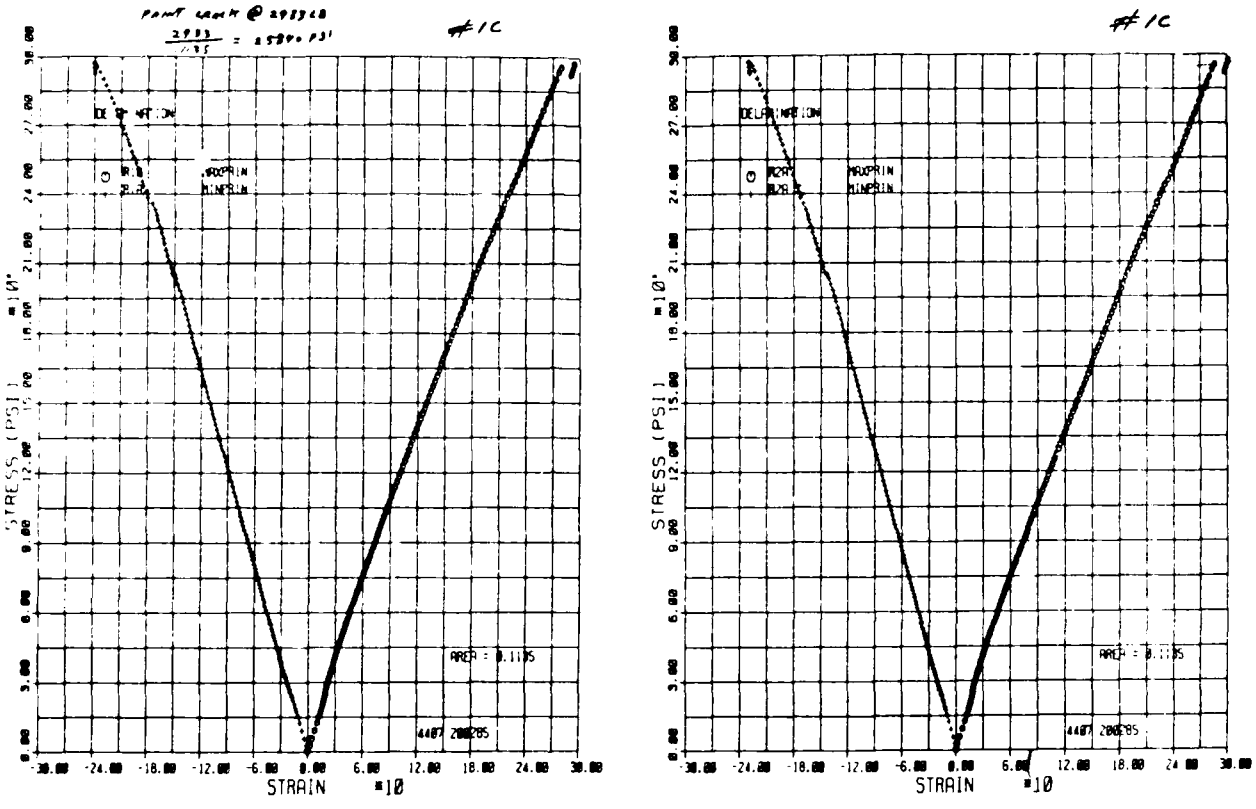

(a) Rosette 1

(b) Rosette 2

Figure 8. Stress-Strain Curves of Back to Back Rosettes Bonded to Specimen C-1

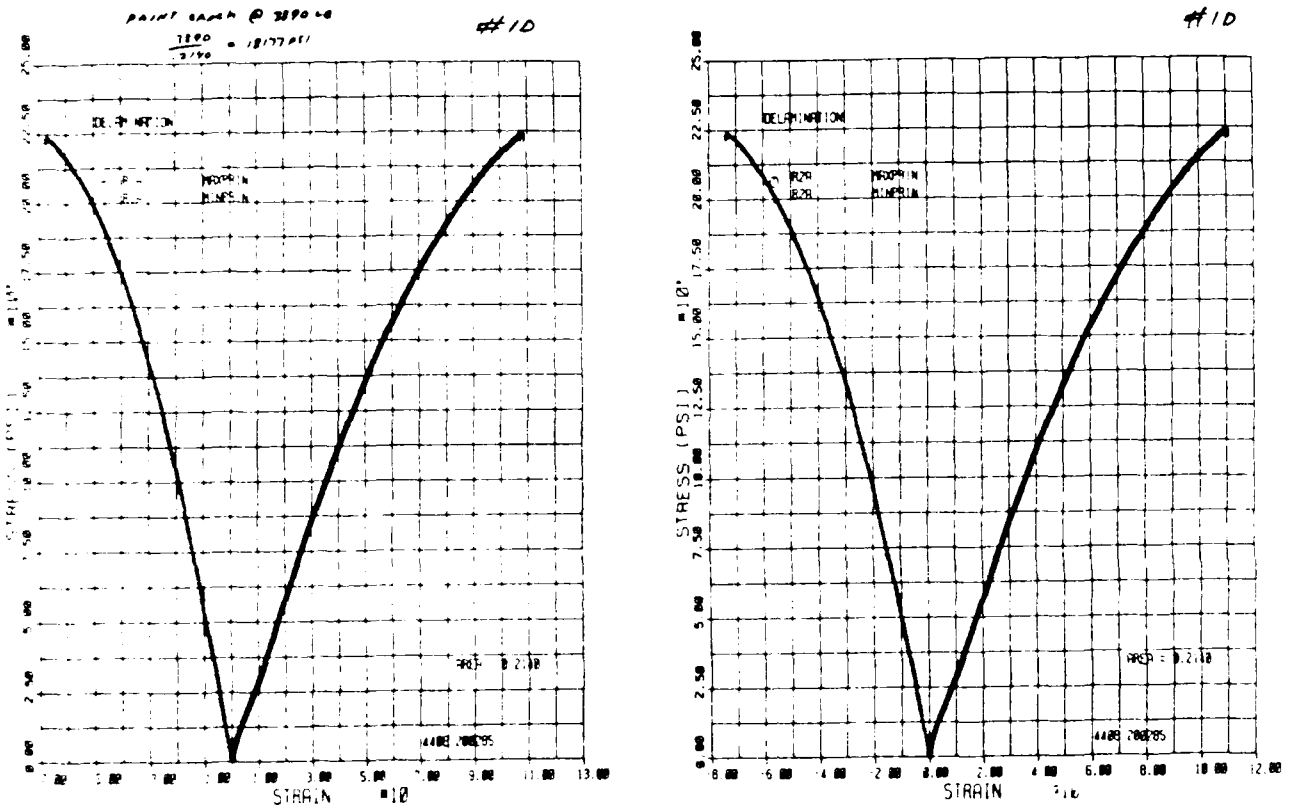

(a) Rosette 1

(b) Rosette 2

Figure 9. Stress-Strain Curves of Back to Back Rosettes Bonded to Specimen D-1

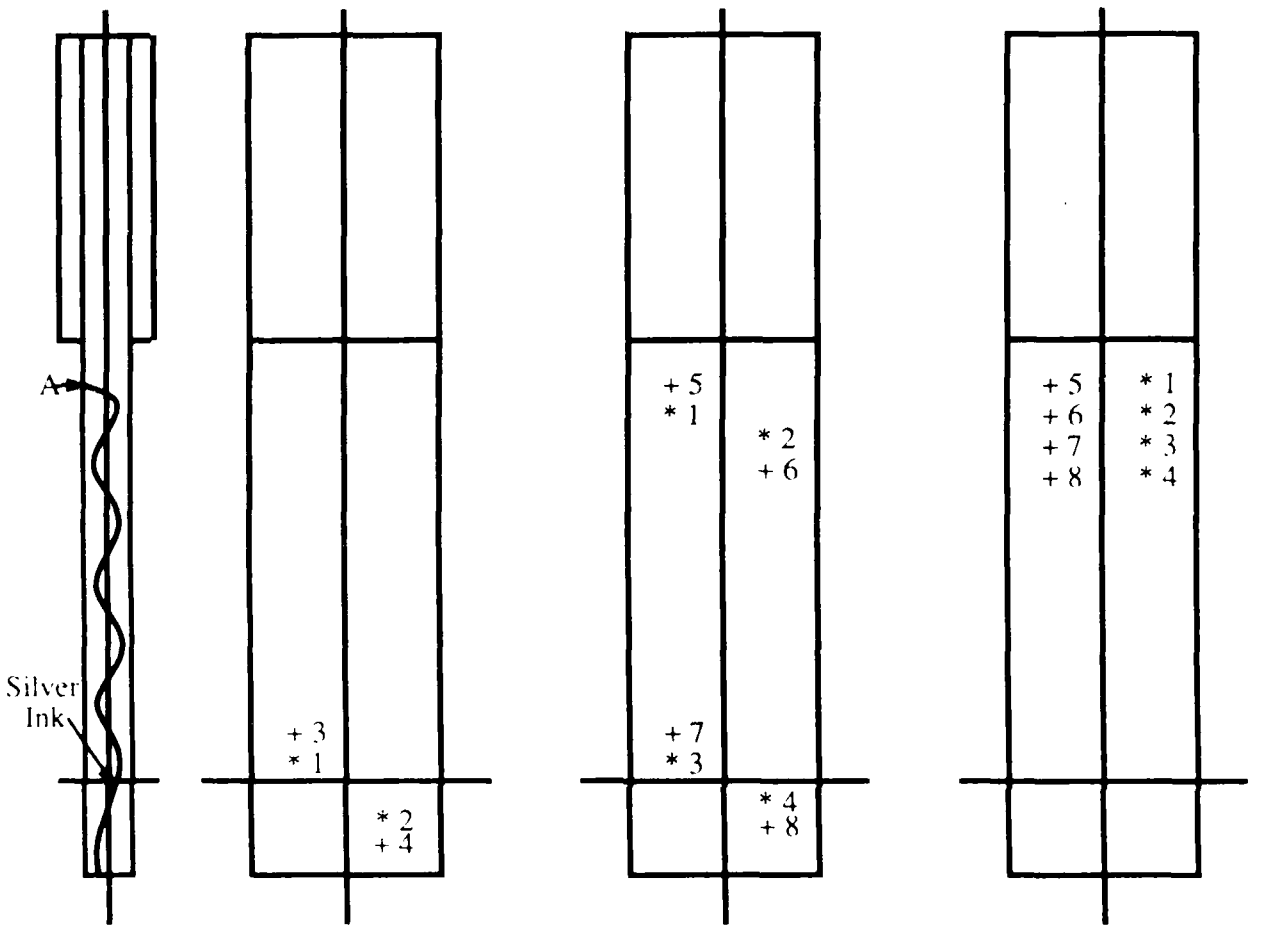

Figure 10. Locations of Single Element Gages Bonded Transversely and of Silver Ink

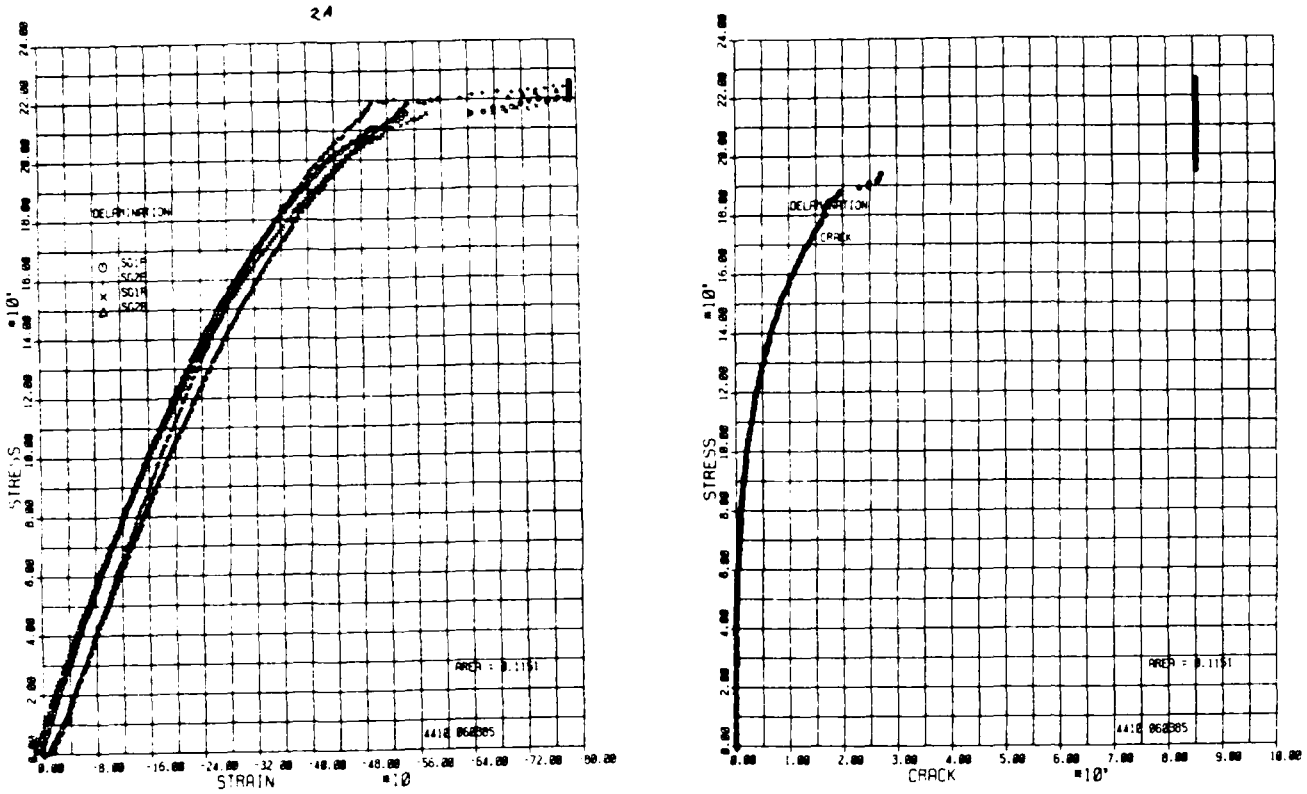

(a) Transverse Gages

(b) Silver Ink

Figure 11. Stress-Strain Curves for Transverse Gages and Response of Silver Ink of Specimen A-2

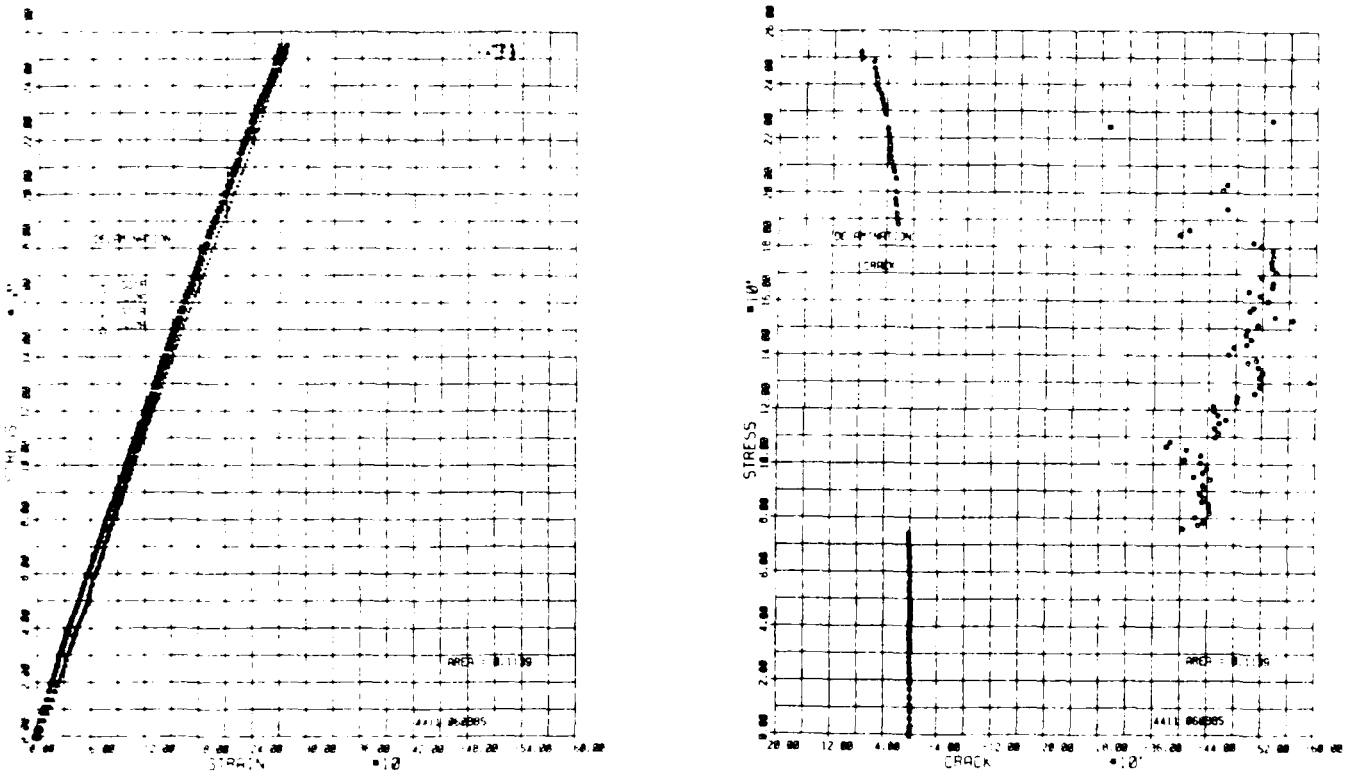

(a) Transverse Gages

(b) Silver Ink

Figure 12. Stress-Strain Curves for Transverse Gages and Response of Silver Ink of Specimen B-3

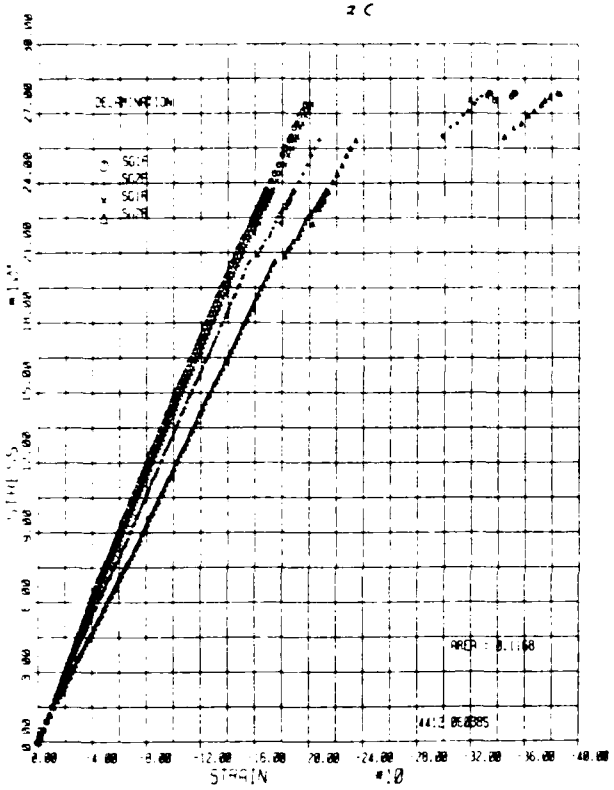

(a) Transverse Gages

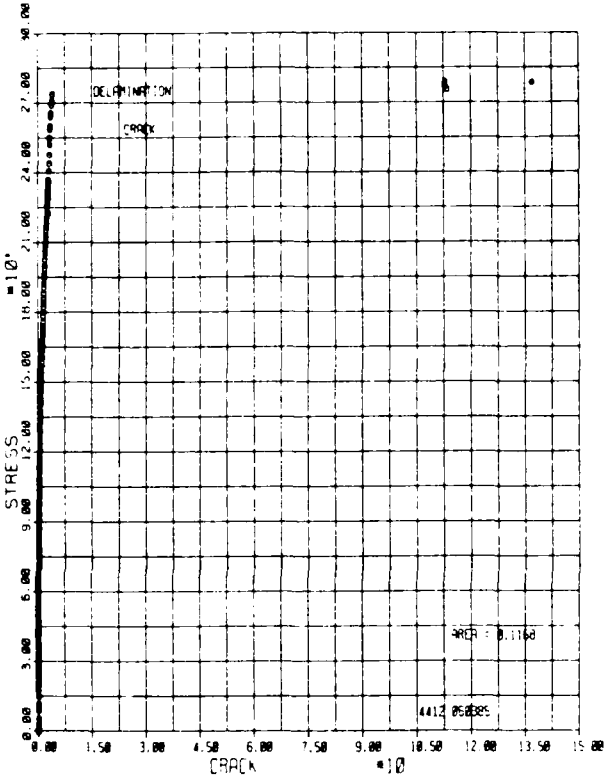

(b) Silver Ink

Figure 13. Stress-Strain Curves for Transverse Gages and Response of Silver Ink of Specimen C-2

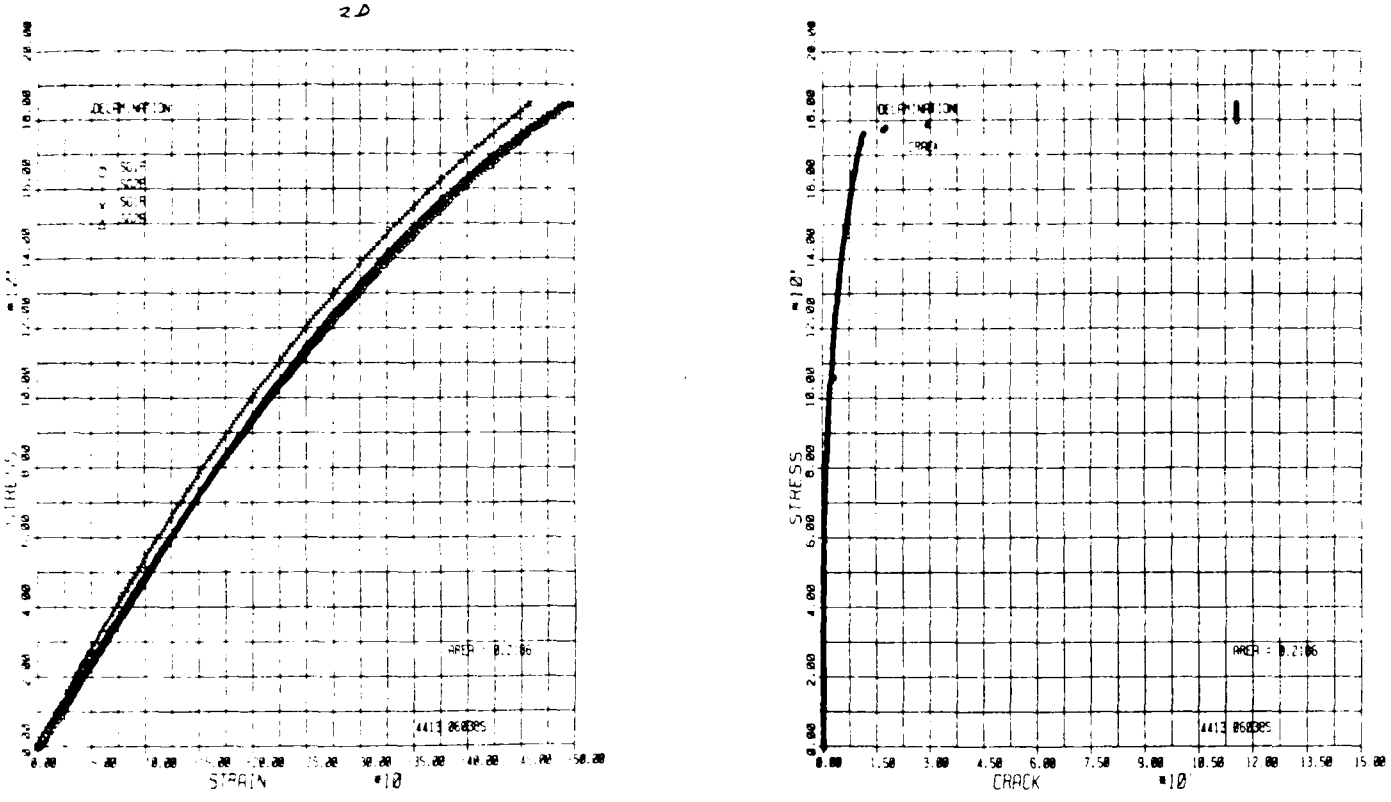

(a) Transverse Gages

(b) Silver Ink

Figure 14. Stress-Strain Curves for Transverse Gages and Response of Silver Ink of Specimen D-2

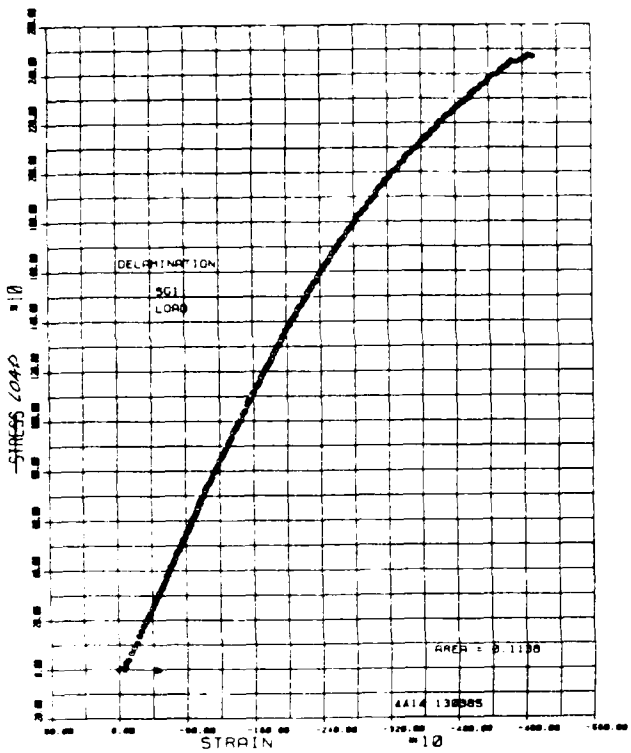

(a) Transverse Gage 1

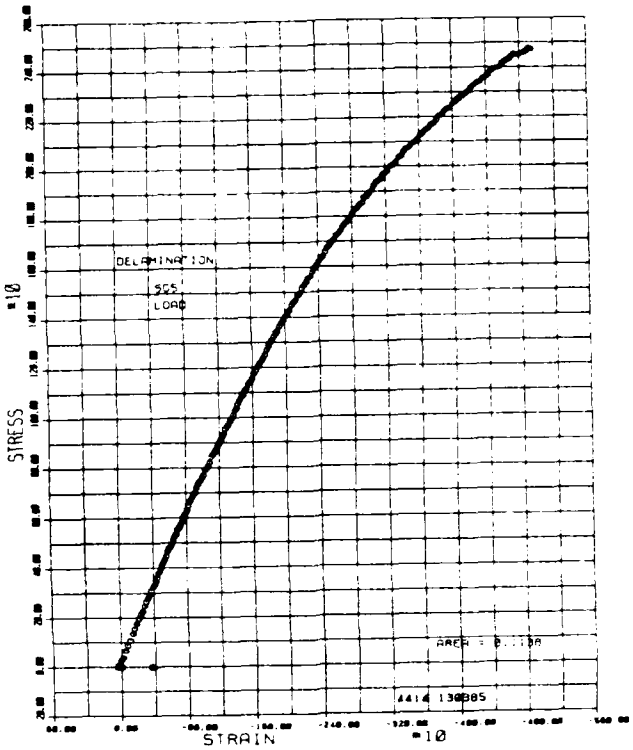

(b) Transverse Gage 5

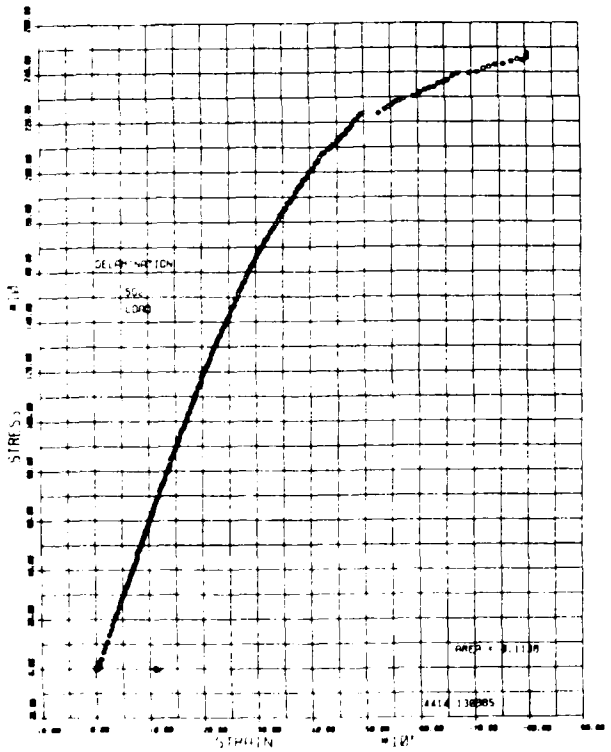

(c) Transverse Gage 2

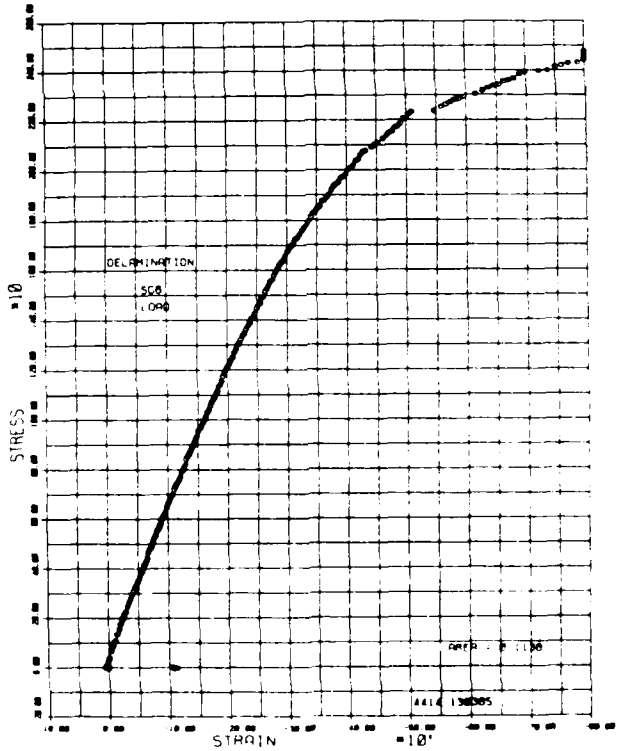

(d) Transverse Gage 6

Figure 15. Stress-Strain Curves of Transverse Gages of Specimen A-4

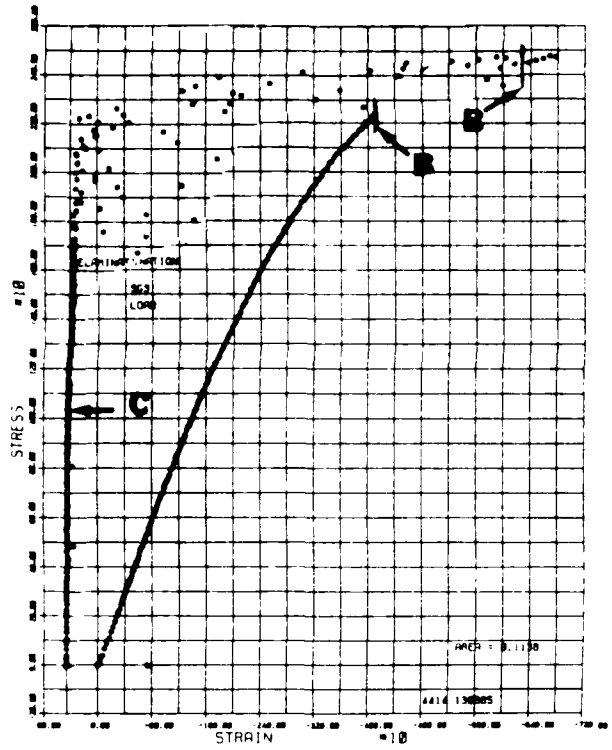

(a) Transverse Gage 3 (B) and Acoustic Emission (C)

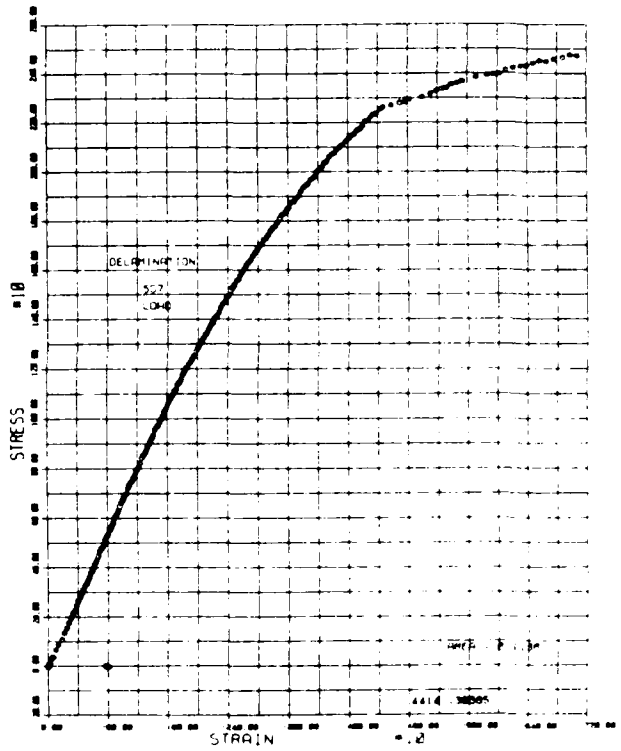

(b) Transverse Gage 7

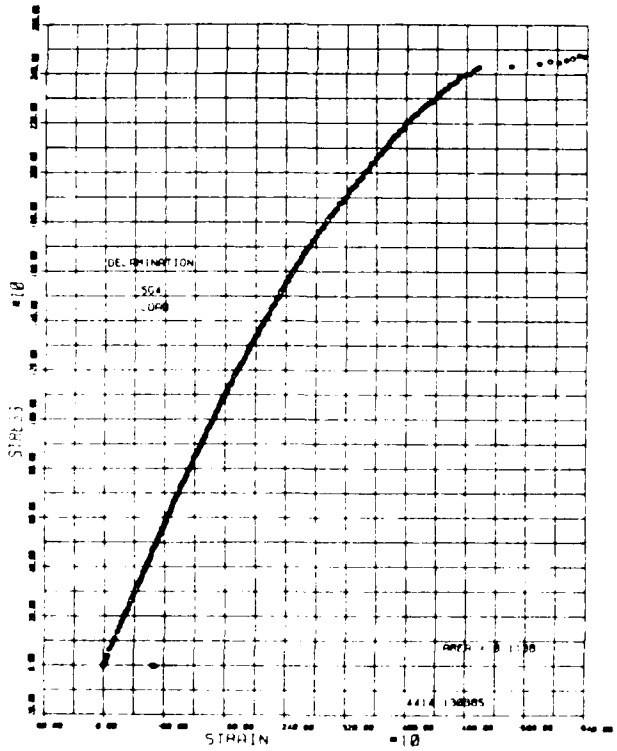

(c) Transverse Gage 4

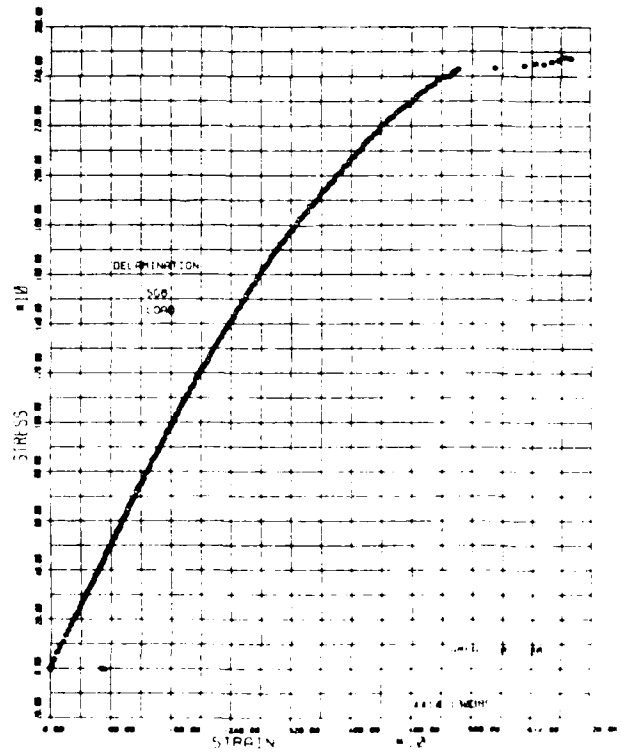

(d) Transverse Gage 8

Figure 16. Stress-Strain Curves of Transverse Gages and Acoustic Emission of Specimen A-4

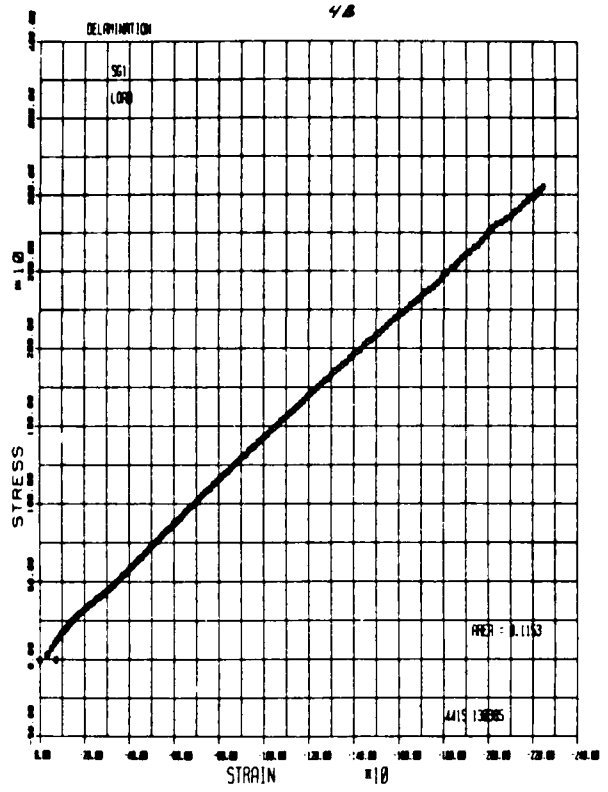

(a) Transverse Gage 1

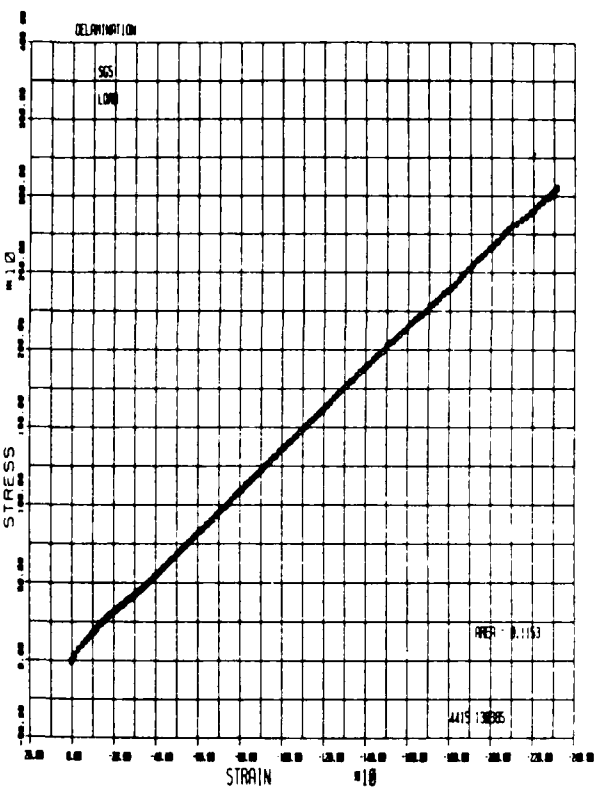

(b) Transverse Gage 5

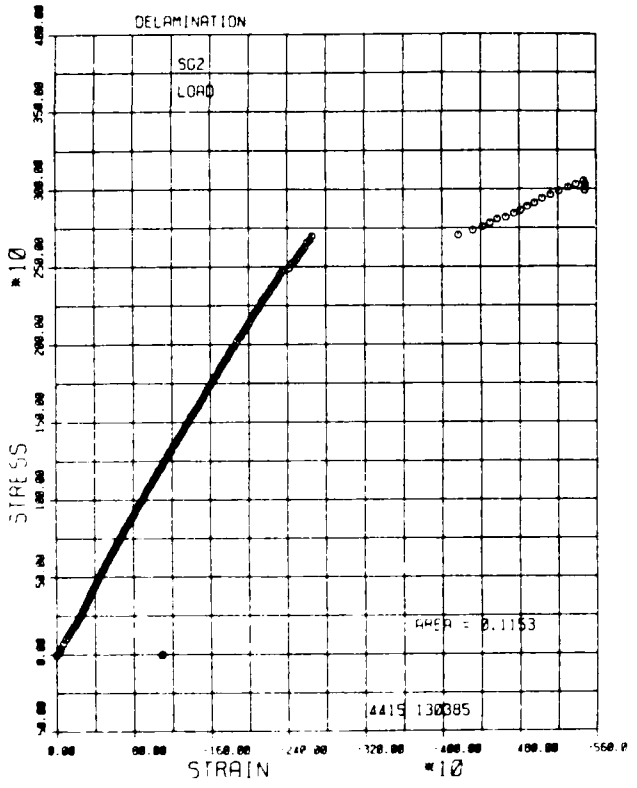

(c) Transverse Gage 2

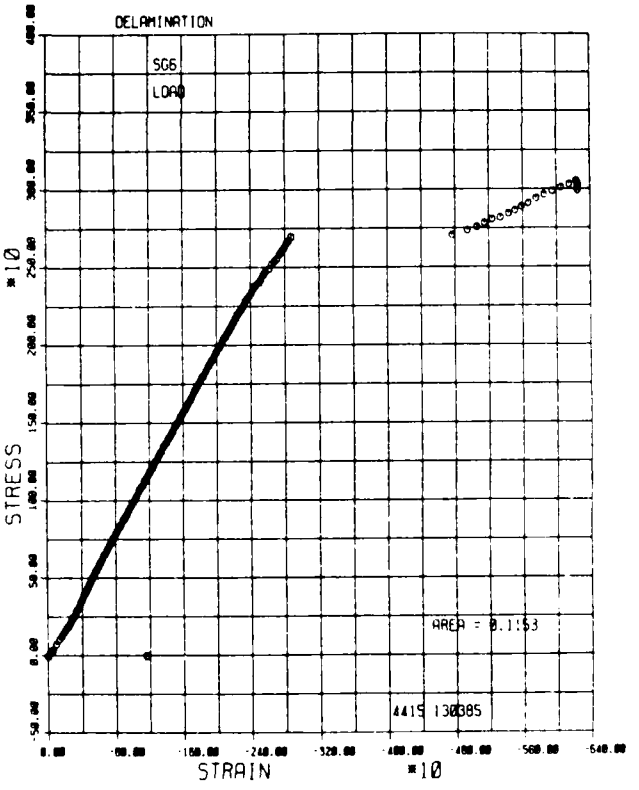

(d) Transverse Gage 6

Figure 17. Stress-Strain Curves of Transverse Gages of Specimen B-4

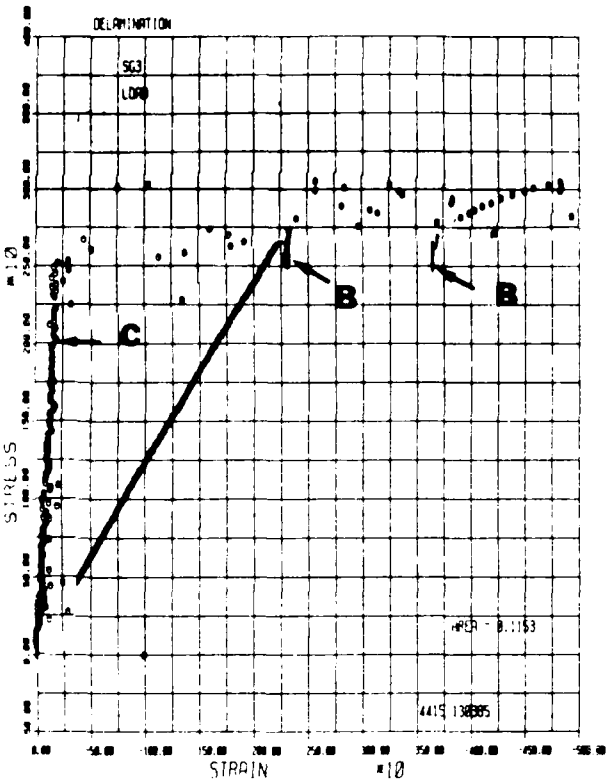

(a) Transverse Gage 3 (B) Acoustic Emission (C)

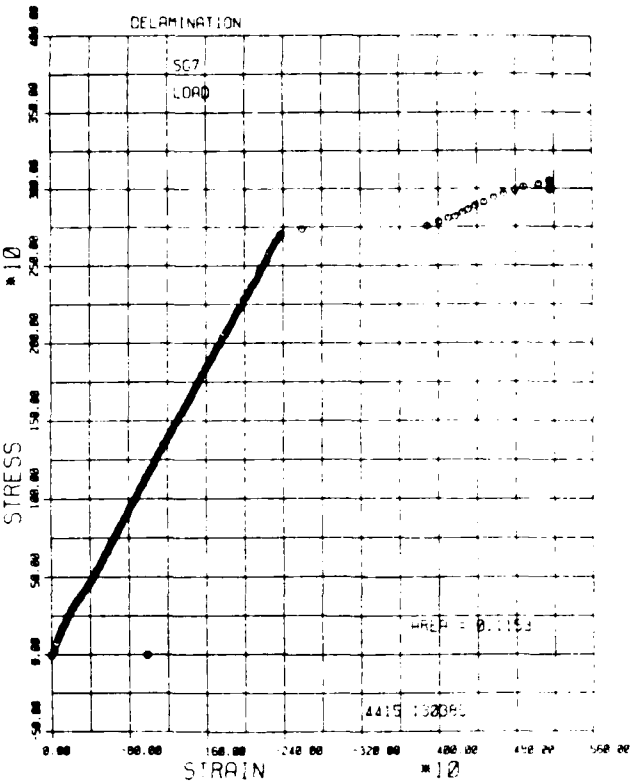

(b) Transverse Gage 7

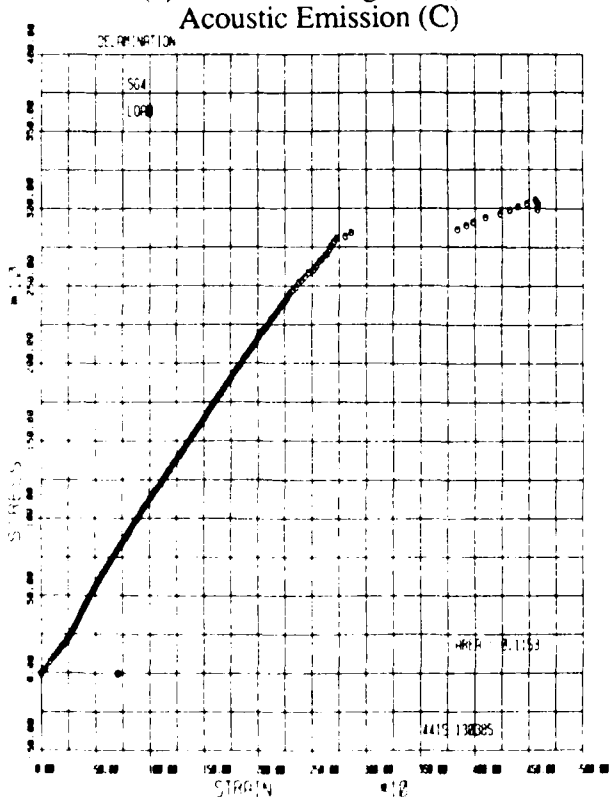

(c) Transverse Gage 4

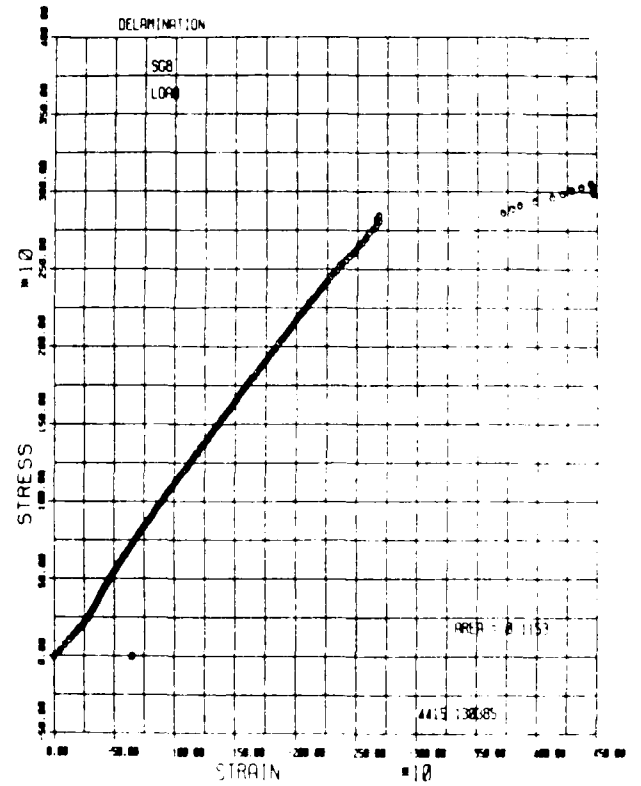

(d) Transverse Gage 8

Figure 18. Stress-Strain Curves of Transverse Gages and Acoustic Emission of Specimen B-4

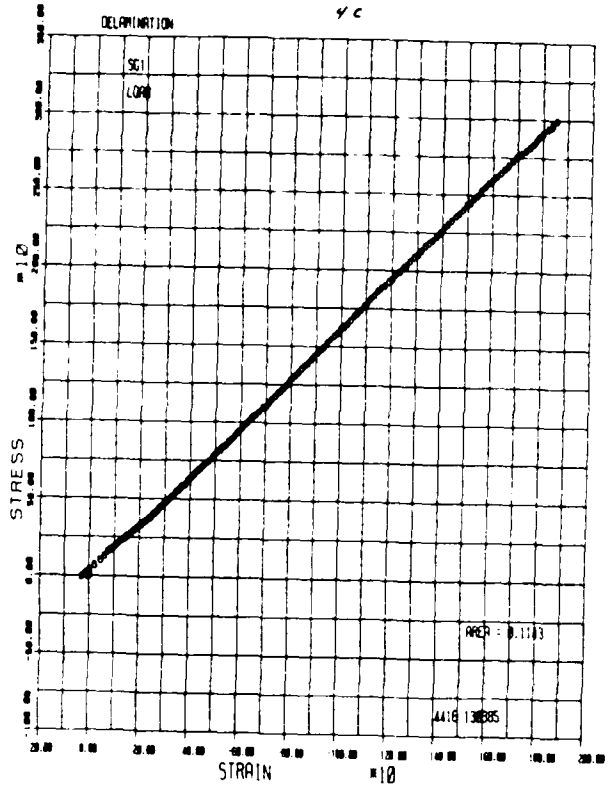

(a) Transverse Gage 1

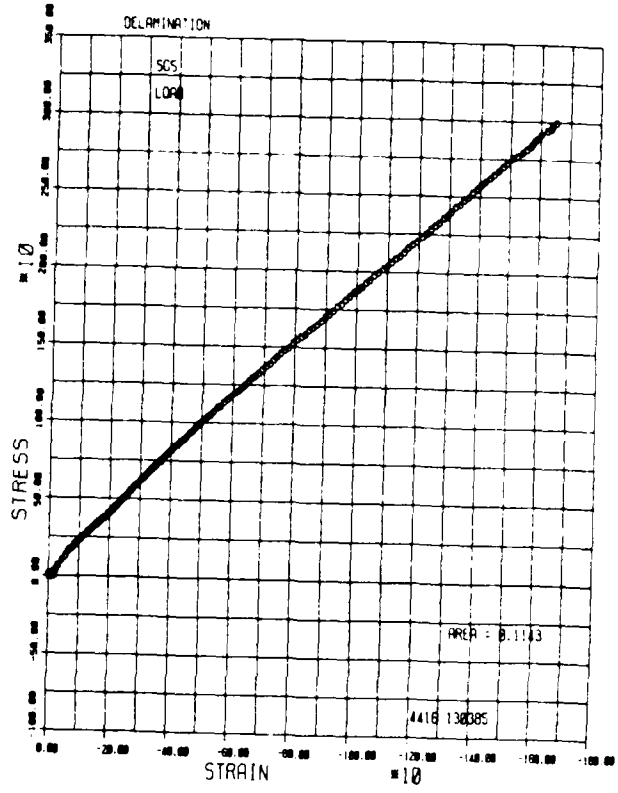

(b) Transverse Gage 5

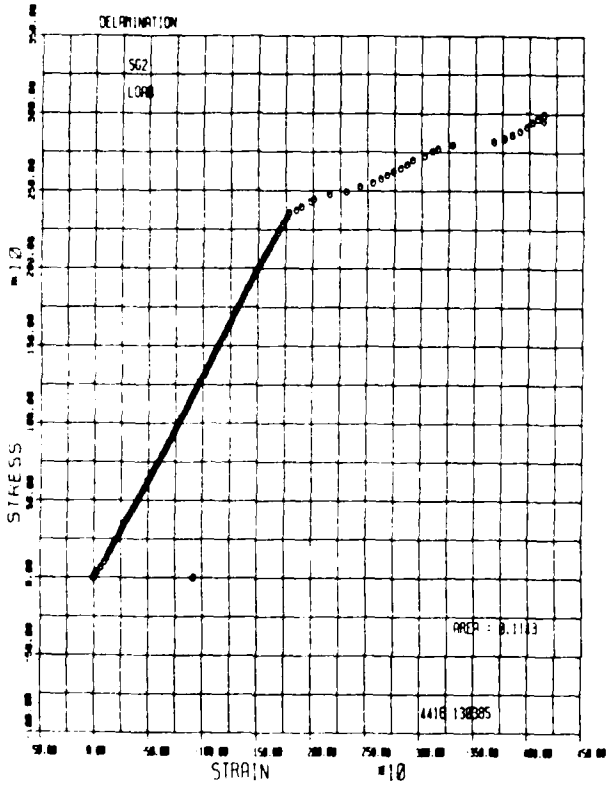

(c) Transverse Gage 2

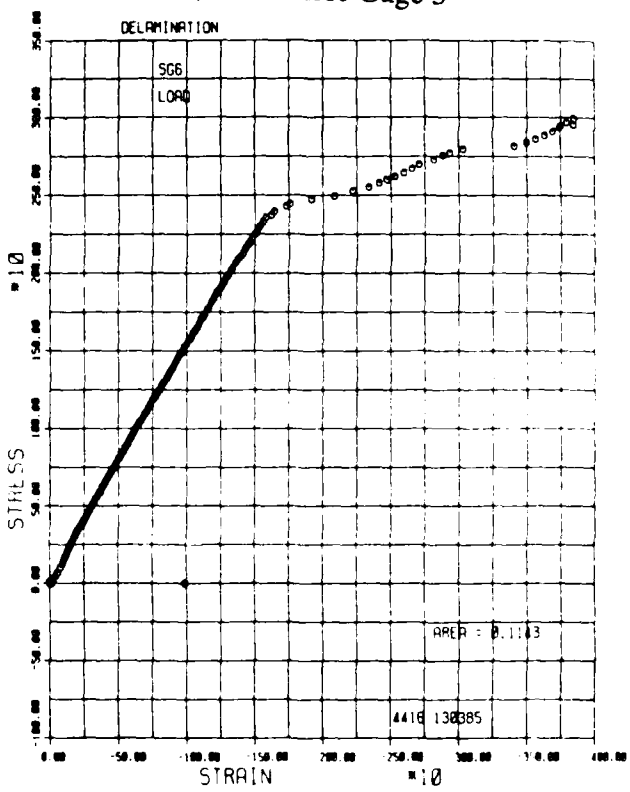

(d) Transverse Gage 6

Figure 19. Stress-Strain Curves of Transverse Gages of Specimen C-4

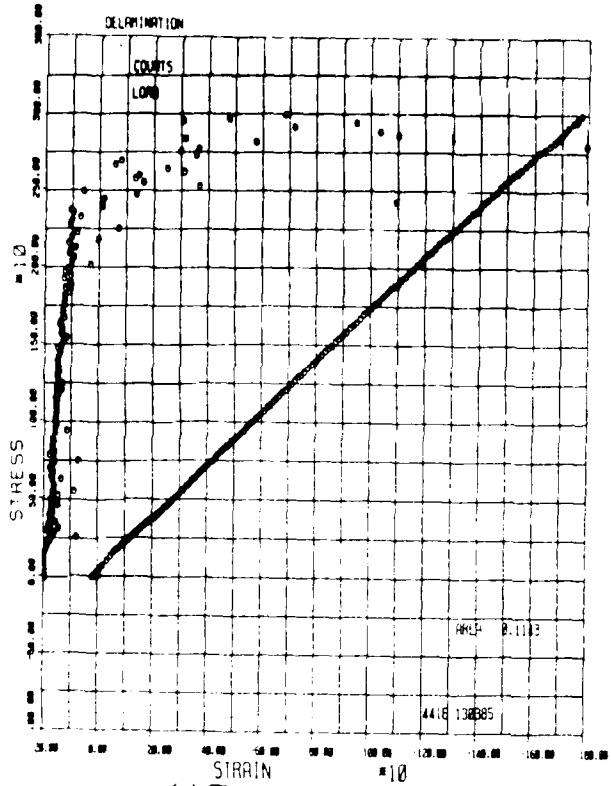

(a) Transverse Gage 3 (B) Acoustic Emission (C)

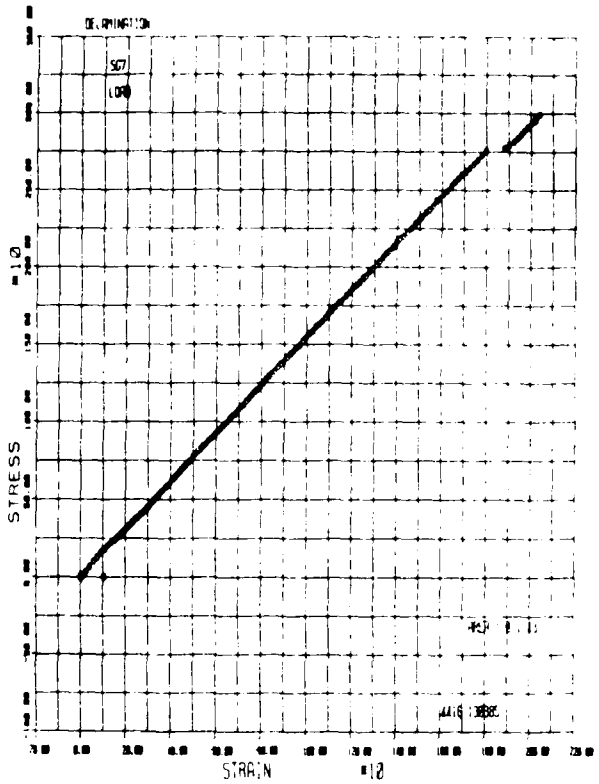

(b) Transverse Gage 7

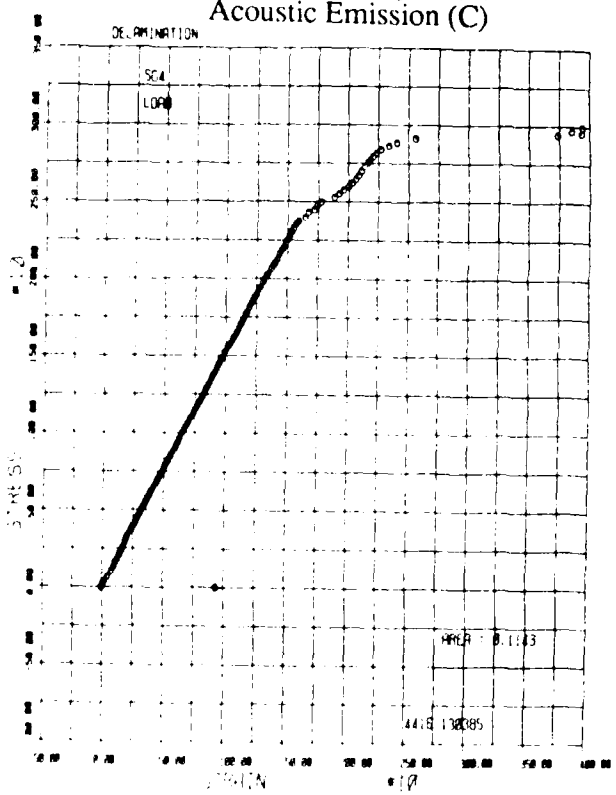

(c) Transverse Gage 4

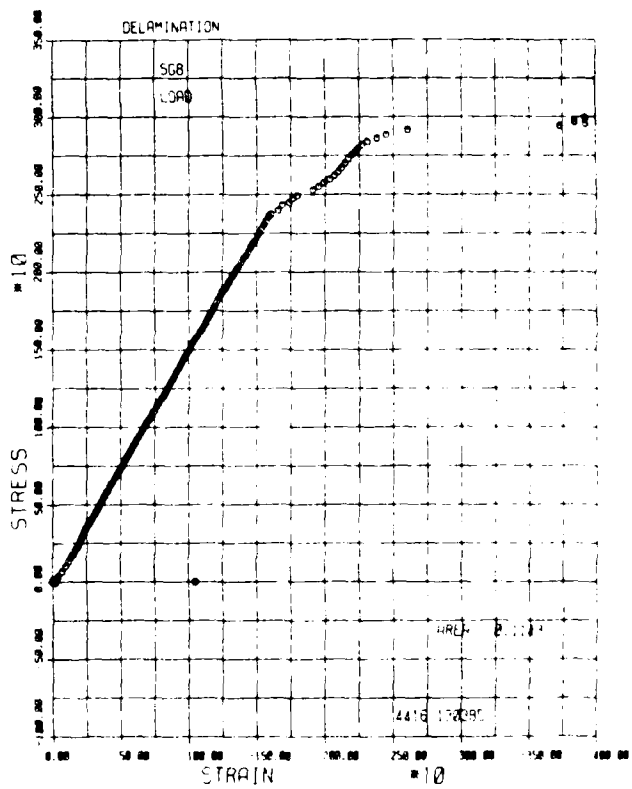

(d) Transverse Gage 8

Figure 20. Stress-Strain Curves of Transverse Gages and Acoustic Emission of Specimen C-4

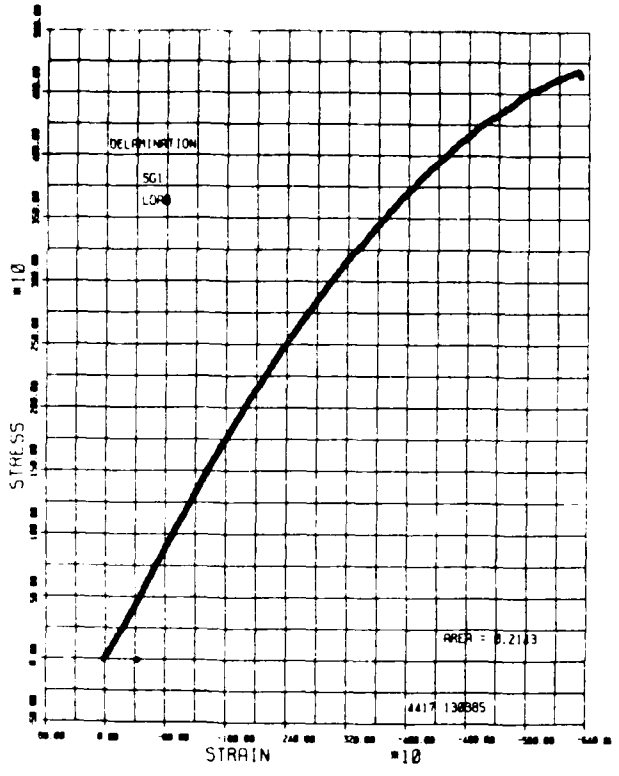

(a) Transverse Gage 1

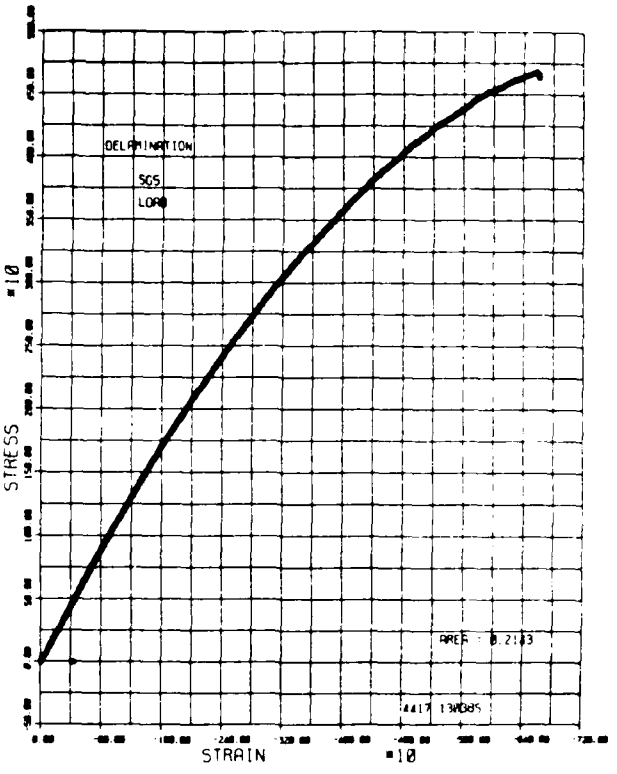

(b) Transverse Gage 5

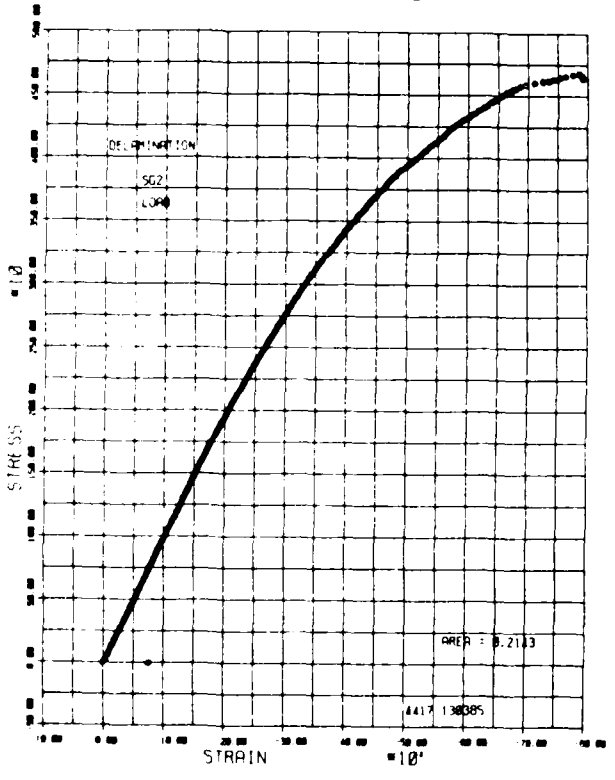

(c) Transverse Gage2

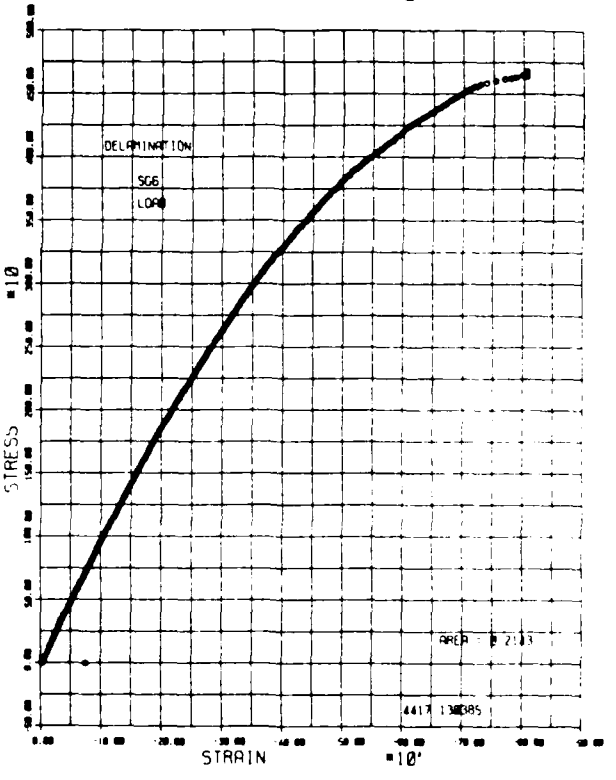

(d) Transverse Gage 6

Figure 21. Stress-Strain Curves of Transverse Gages of Specimen D-4

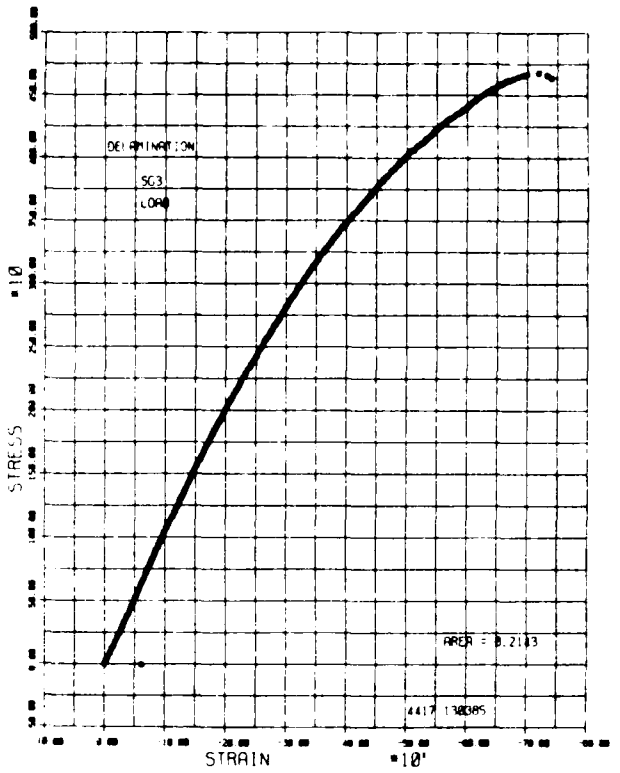

(a) Transverse Gage 3

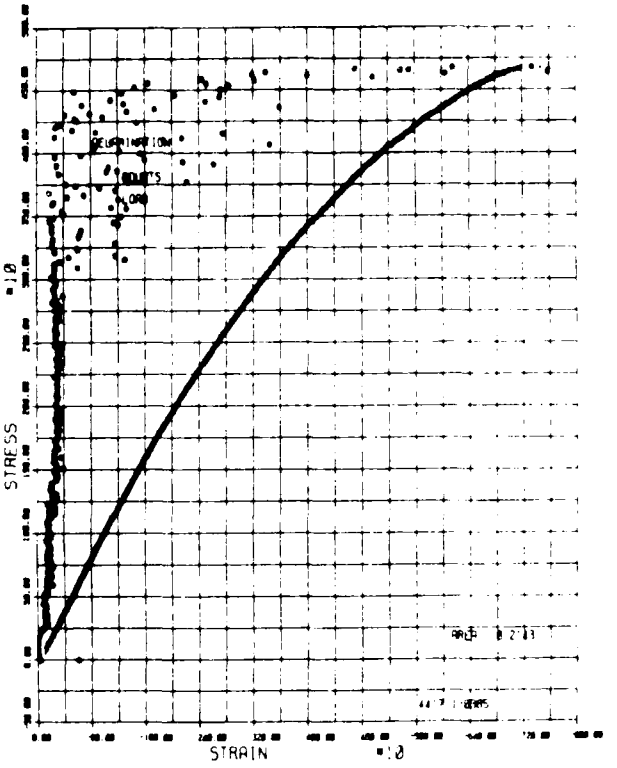

(b) Transverse Gage 7 (B)
Acoustic Emission (C)

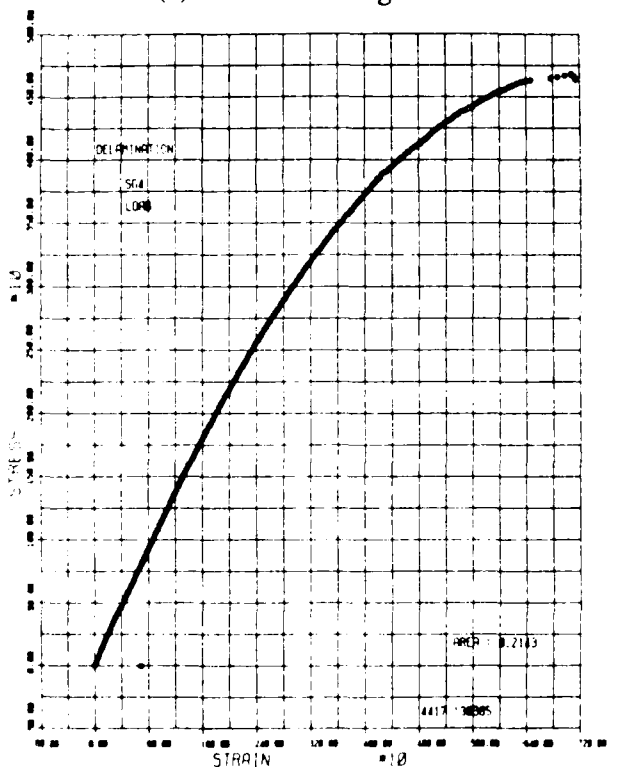

(c) Transverse Gage 4

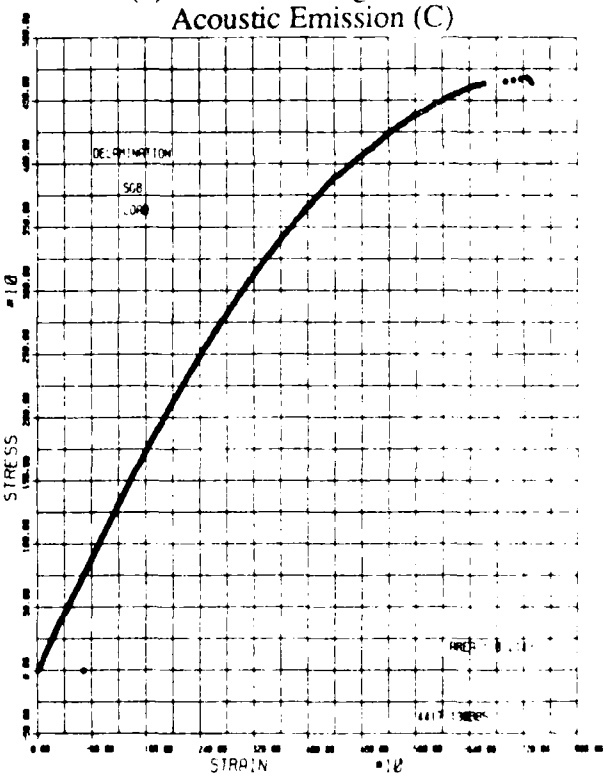

(d) Transverse Gage 8

Figure 22. Stress-Strain Curves of Transverse Gages and Acoustic Emission of Specimen D-4

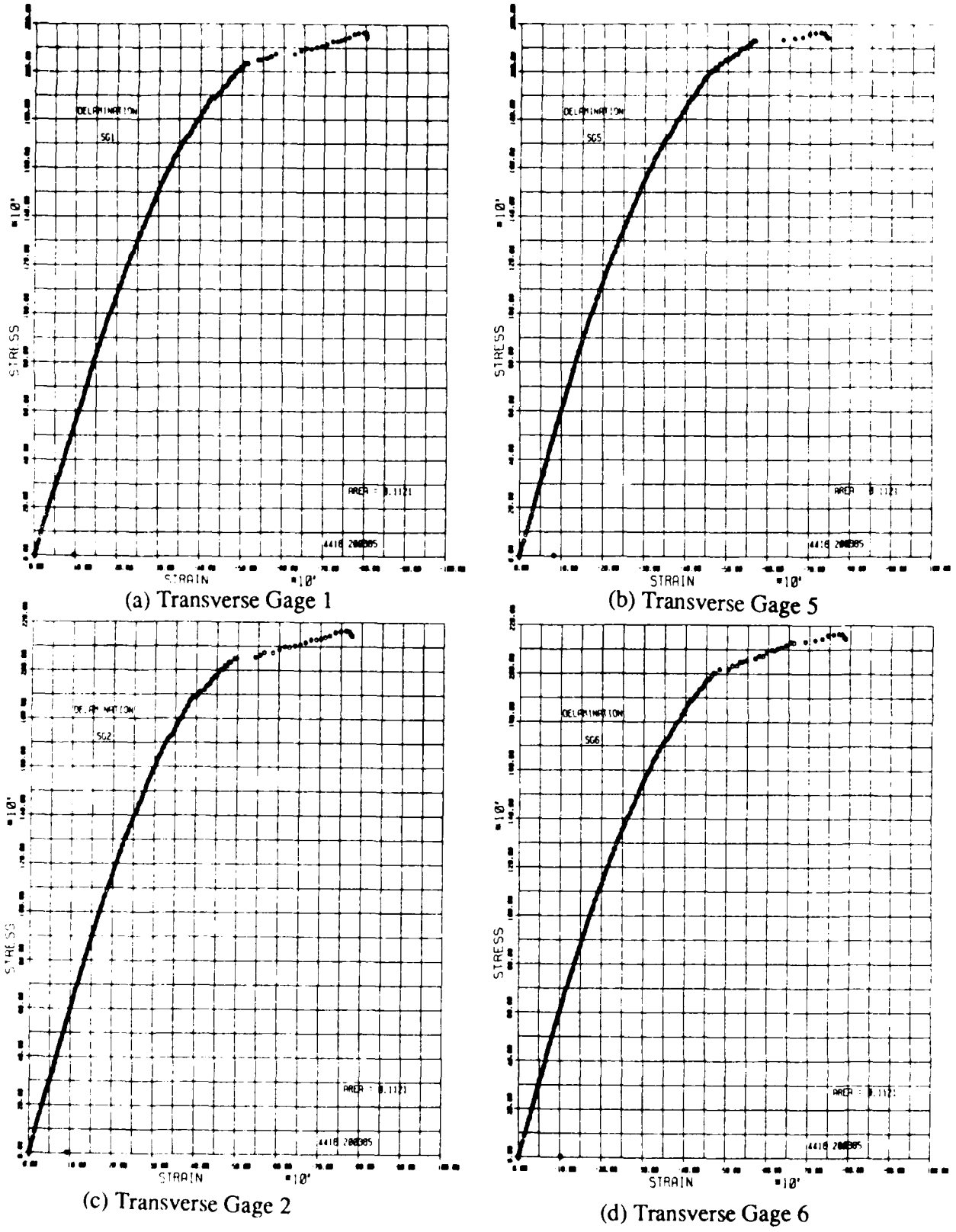

(a) Transverse Gage 1

(b) Transverse Gage 5

(c) Transverse Gage 2

(d) Transverse Gage 6

Figure 23. Stress-Strain Curves of Transverse Gages of Specimen A-5

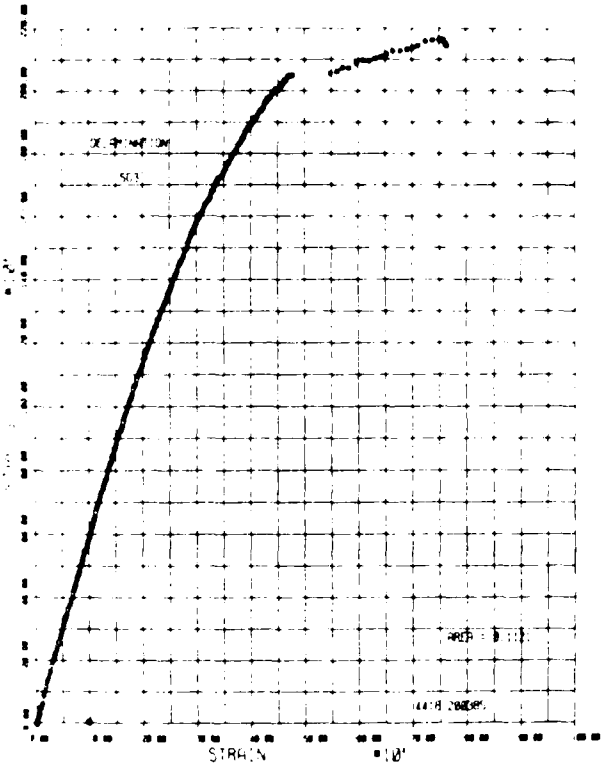

(a) Transverse Gage 3

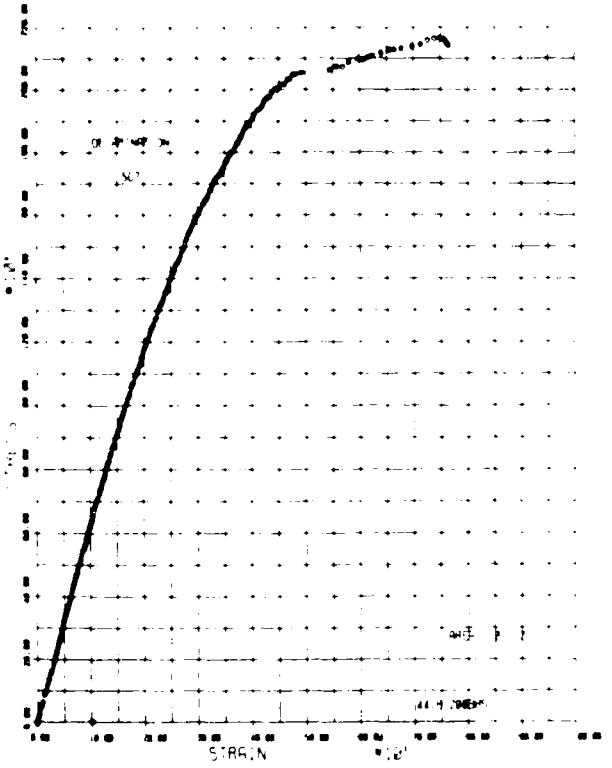

(b) Transverse Gage 7

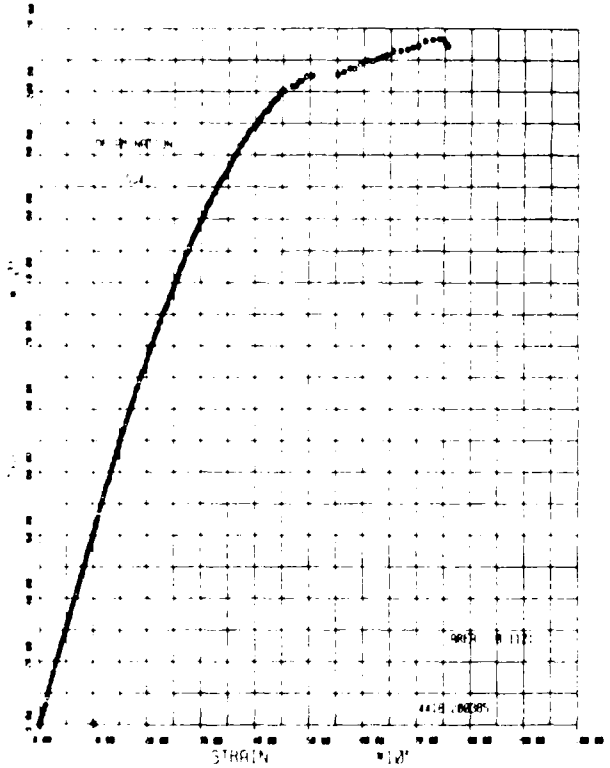

(c) Transverse Gage 4

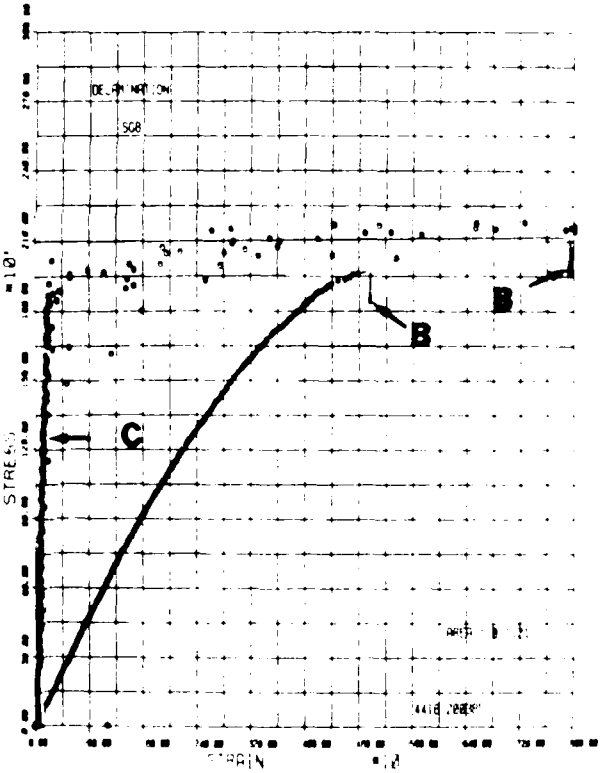

(d) Transverse Gage 8 (B)
Acoustic Emission (C)

Figure 24. Stress-Strain Curves of Transverse Gages and Acoustic Emission of Specimen A-5

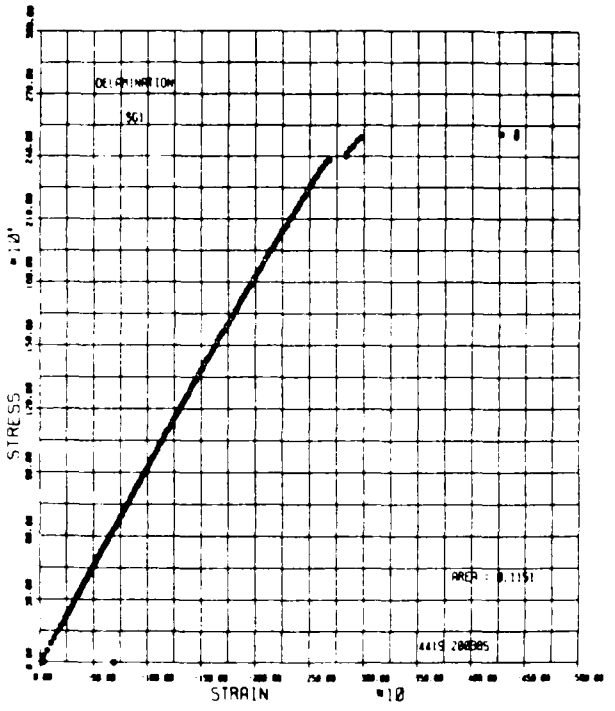

(a) Transverse Gage 1

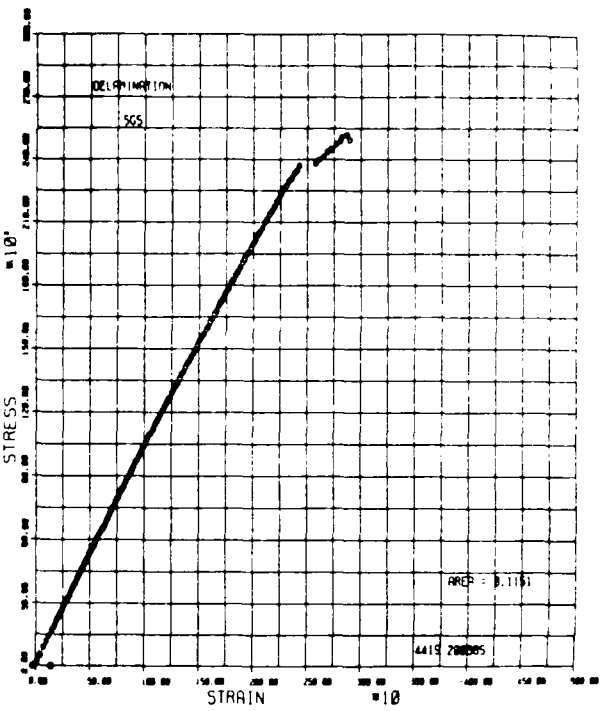

(b) Transverse Gage 5

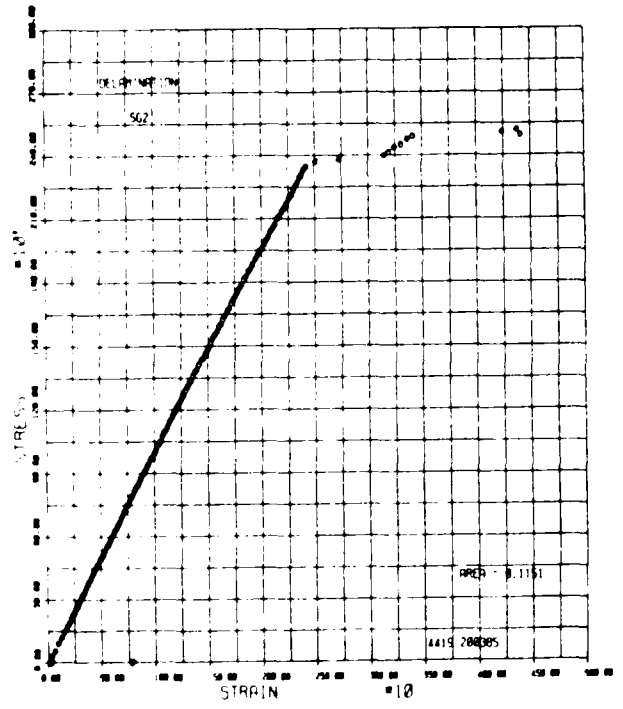

(c) Transverse Gage 2

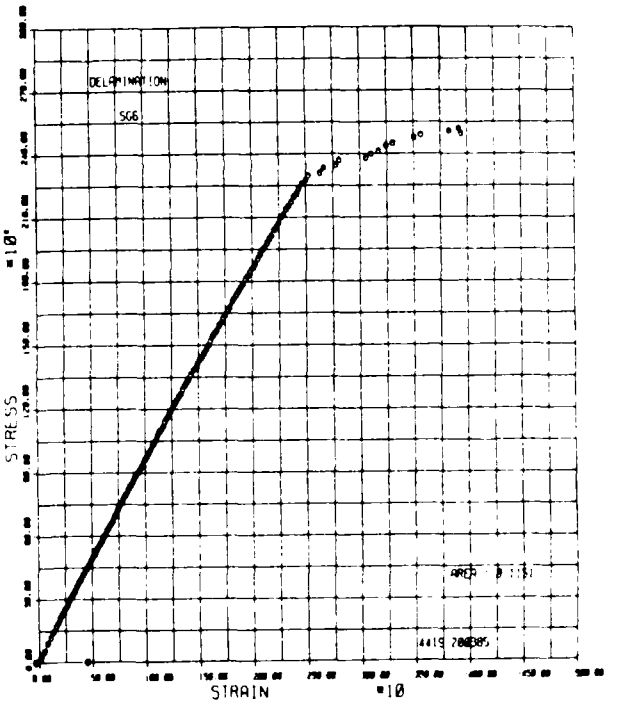

(d) Transverse Gage 6

Figure 25. Stress-Strain Curves of Transverse Gages of Specimen B-5

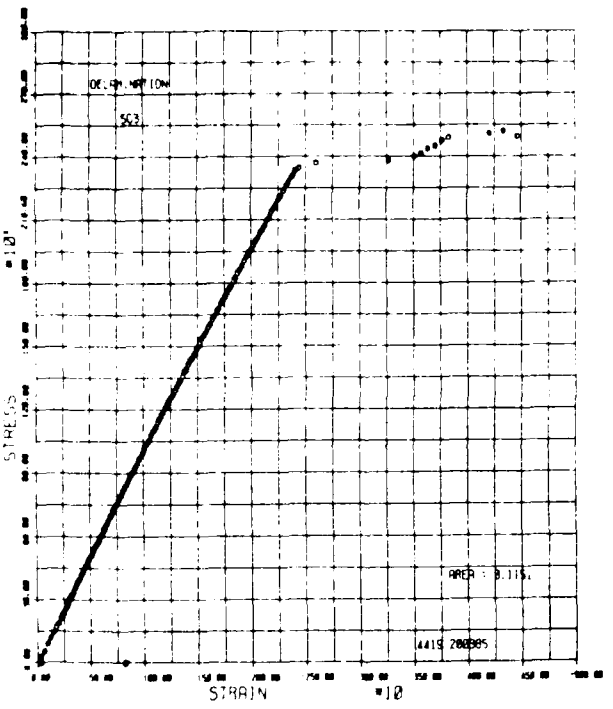

(e) Transverse Gage 3

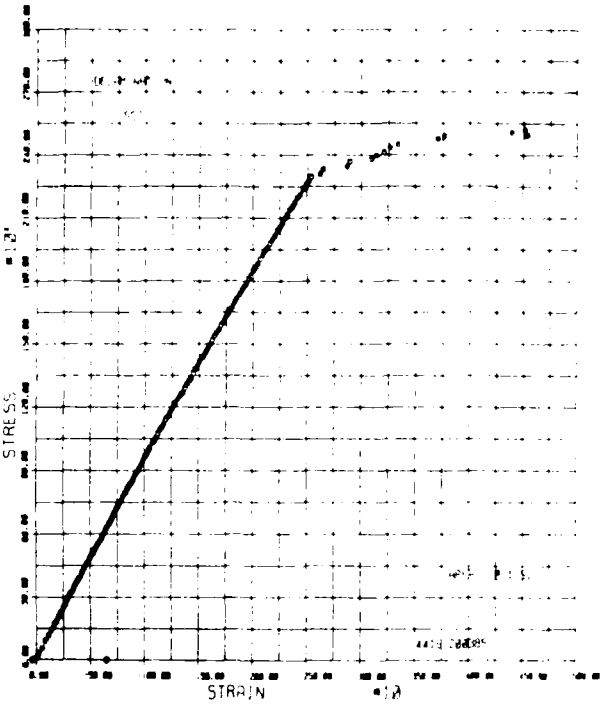

(f) Transverse Gage 7

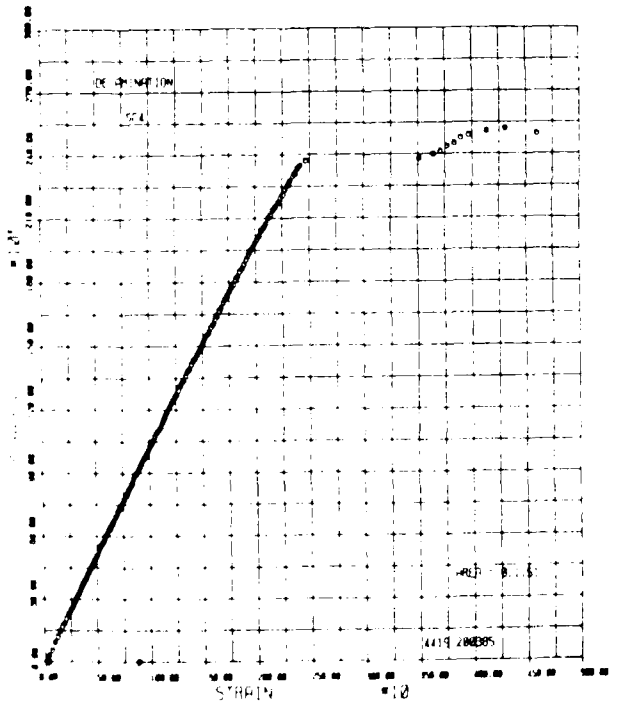

(g) Transverse Gage 4

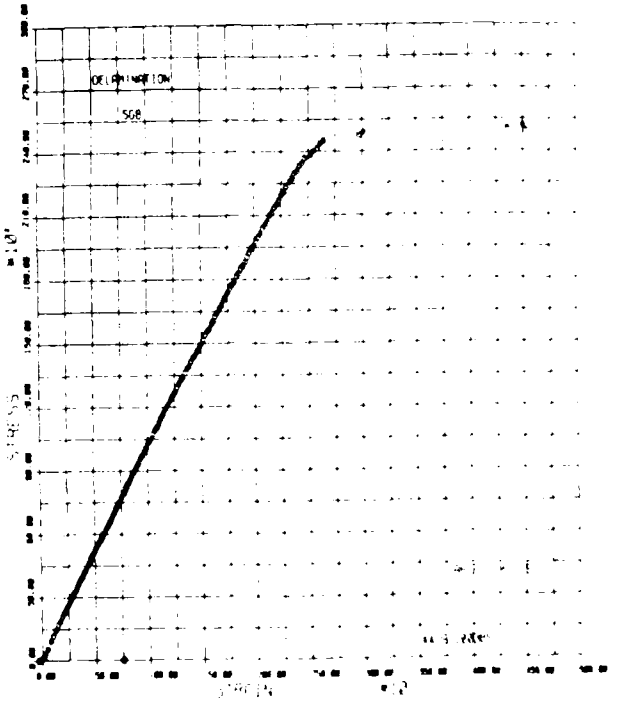

(h) Transverse Gage 8

Figure 25 (Cont'd). Stress-Strain Curves of Transverse Gages of Specimen B-5

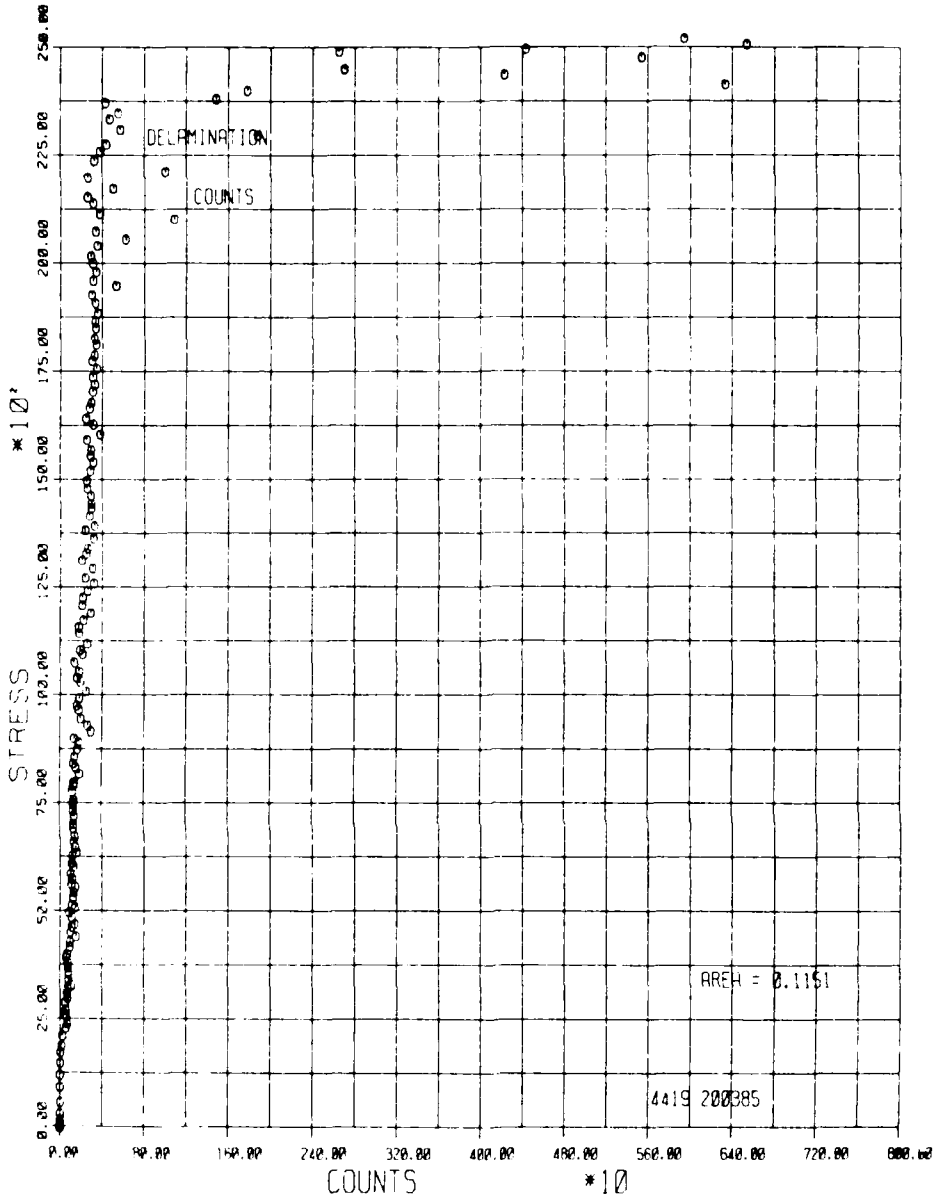

Figure 26. Acoustic Emission of Specimen B-5

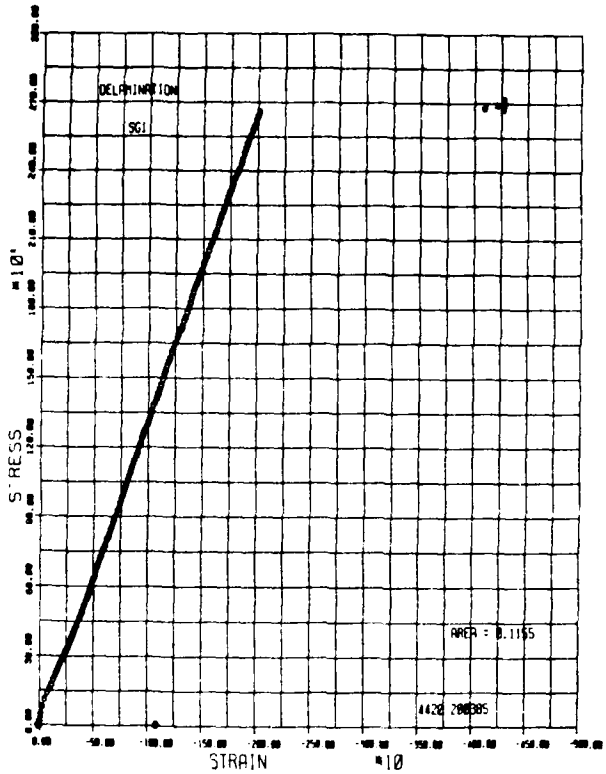

(a) Transverse Gage 1

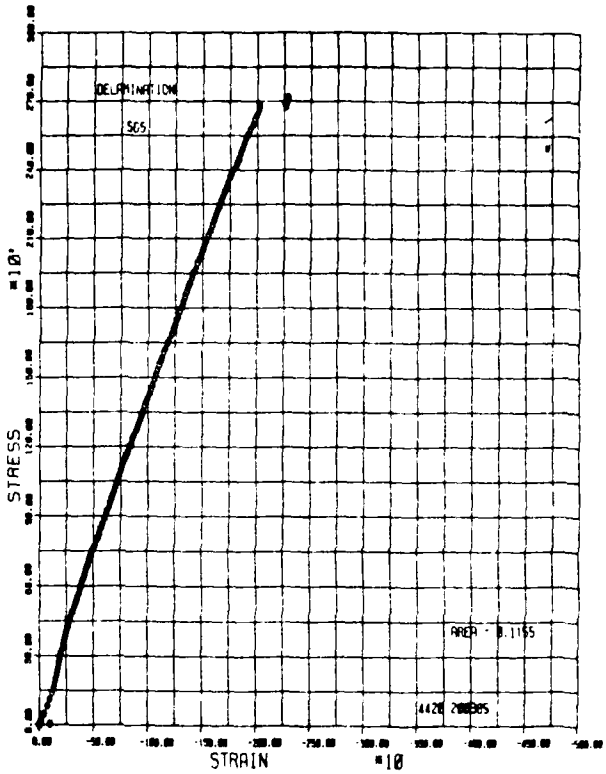

(b) Transverse Gage 5

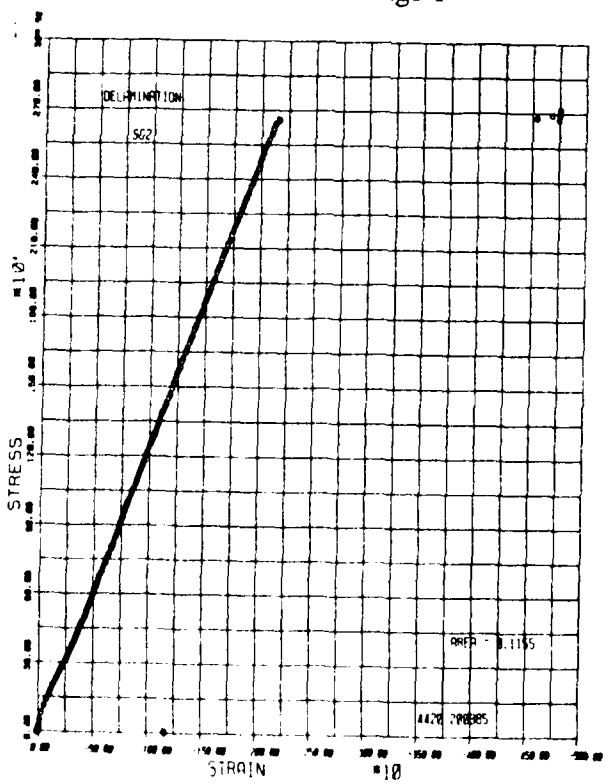

(c) Transverse Gage 2

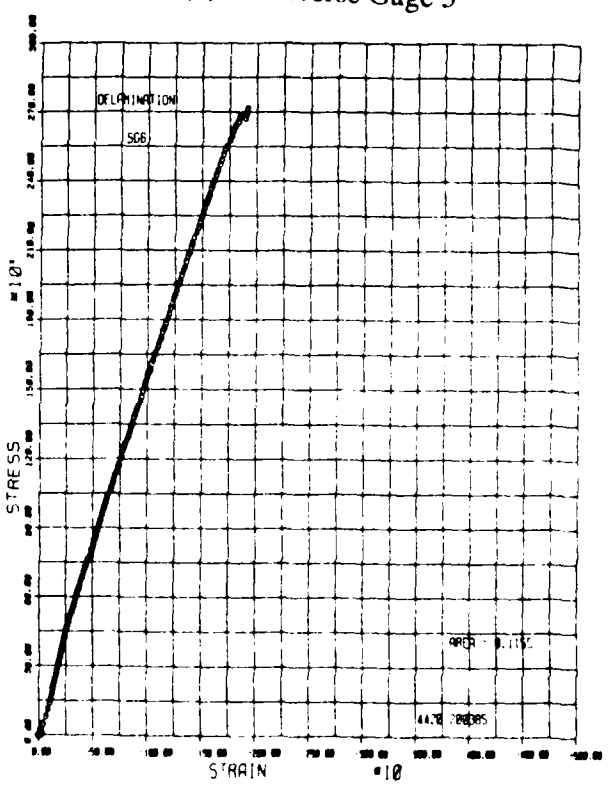

(d) Transverse Gage 6

Figure 27. Stress-Strain Curves of Transverse Gages of Specimen C-5

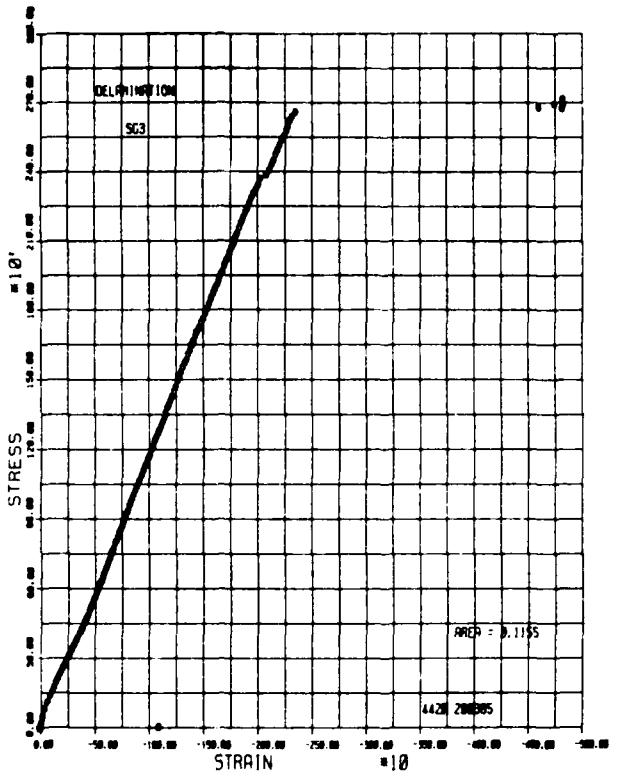

(a) Transverse Gage 3

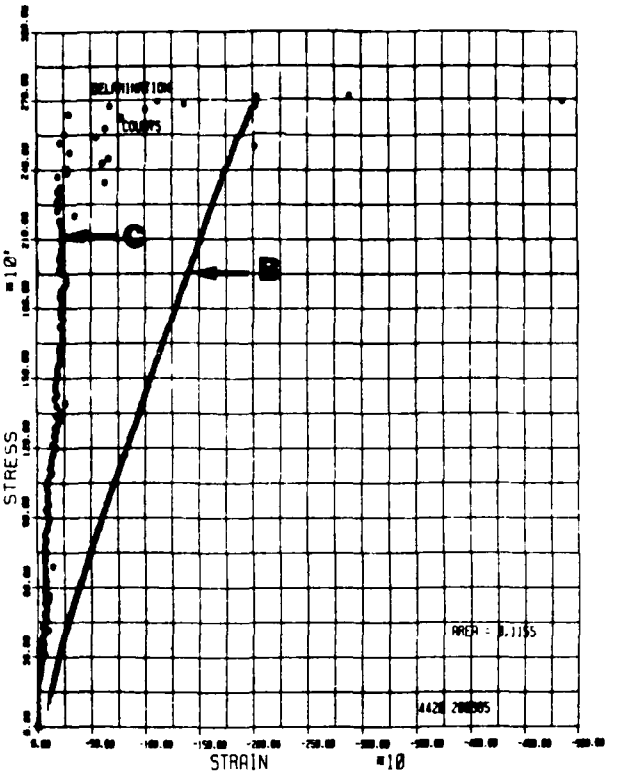

(b) Transverse Gage 7 (B) Acoustic Emission (C)

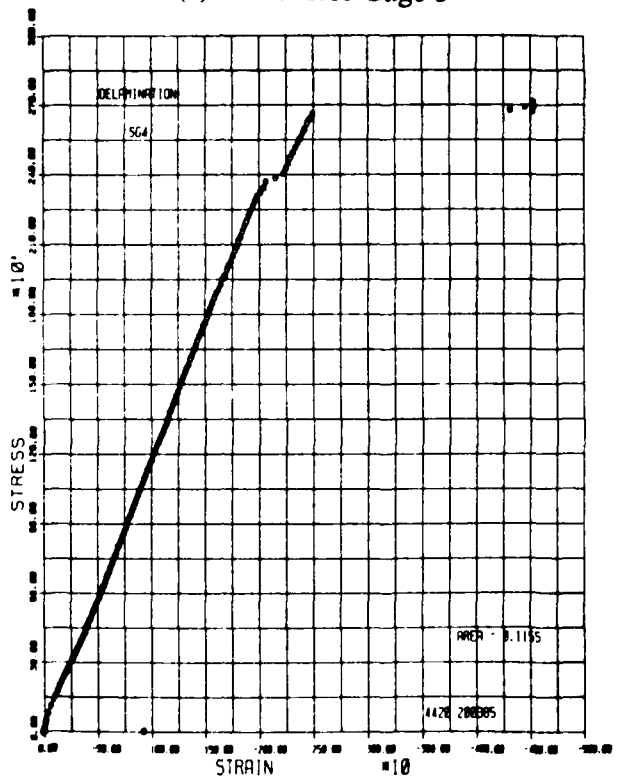

(c) Transverse Gage 4

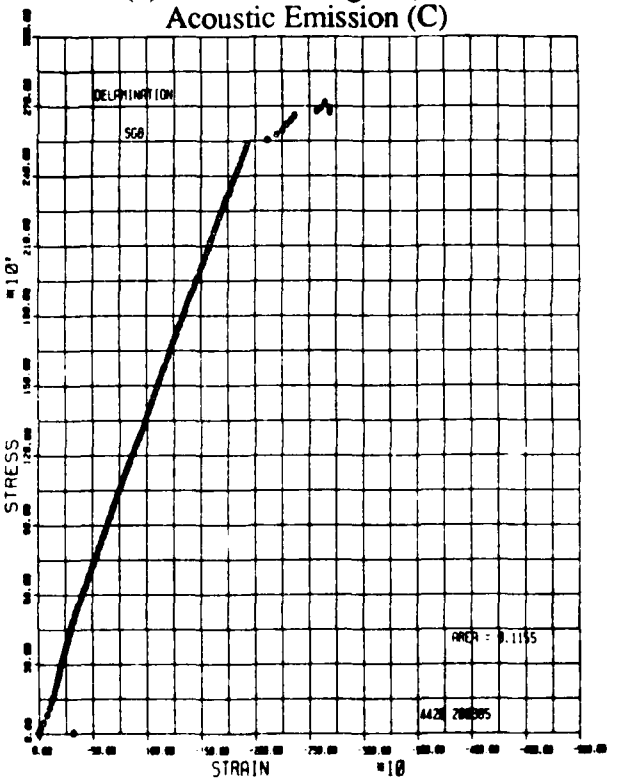

(d) Transverse Gage 8

Figure 28. Stress-Strain Curves of Transverse Gages and Acoustic Emission of Specimen C-5

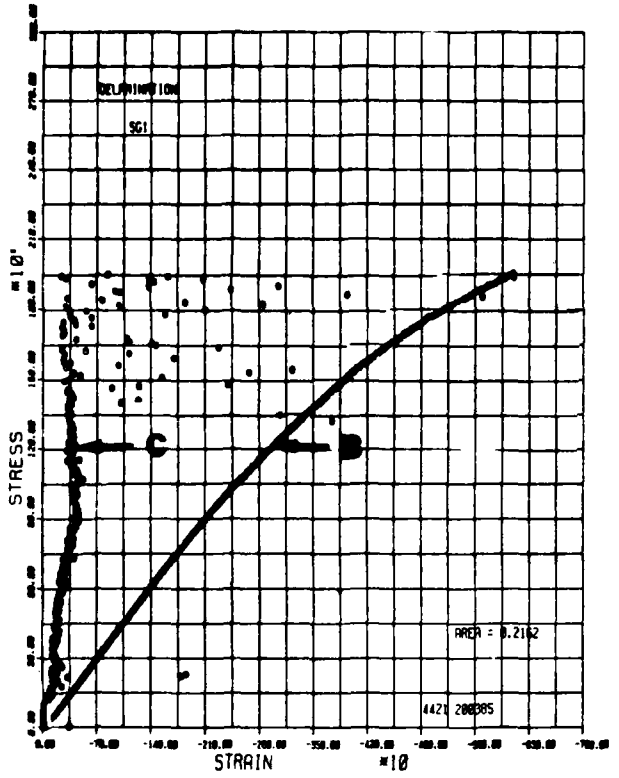

(a) Transverse Gage 1 (B) Acoustic Emission (C)

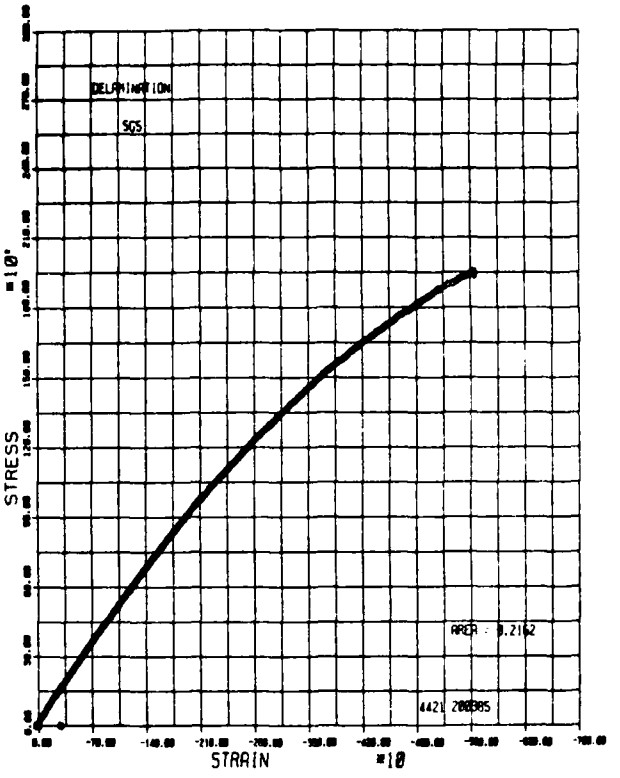

(b) Transverse Gage 5

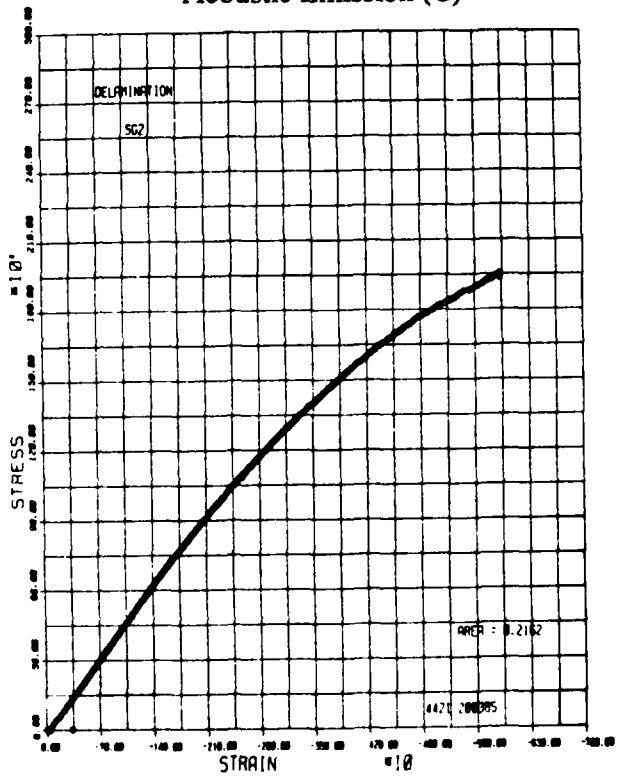

(c) Transverse Gage 2

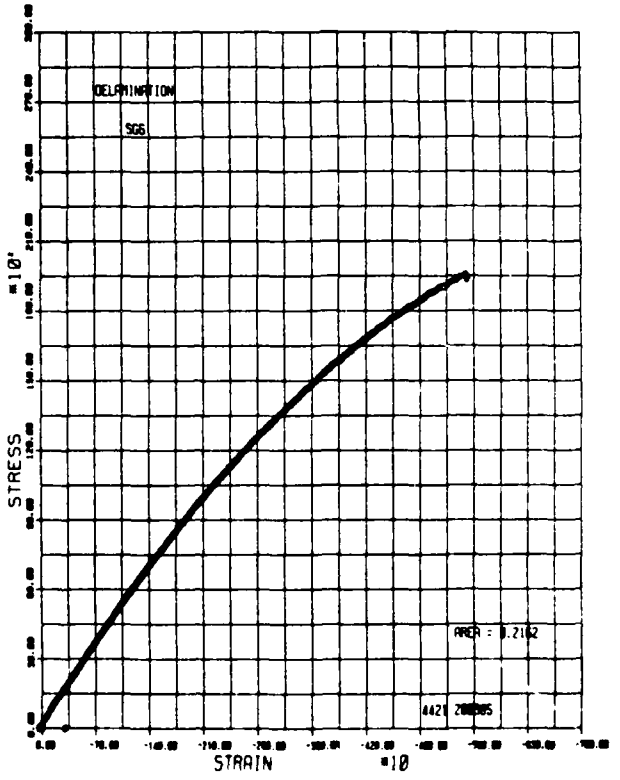

(d) Transverse Gage 6

Figure 29. Stress-Strain Curves of Transverse Gages and Acoustic Emission of Specimen D-5

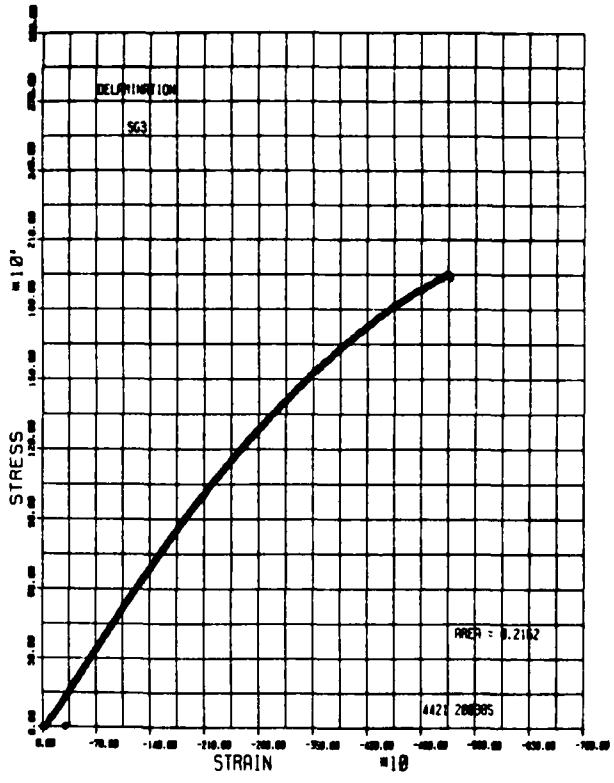

(a) Transverse Gage 3

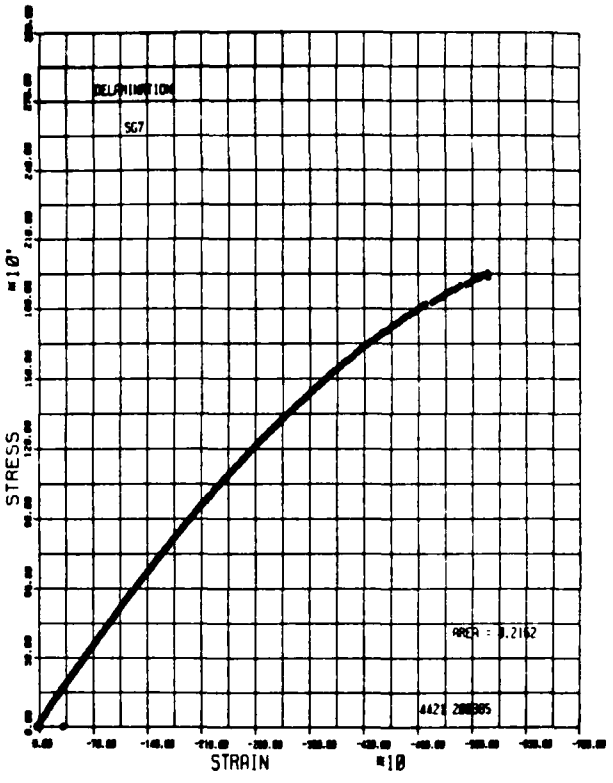

(b) Transverse Gage 7

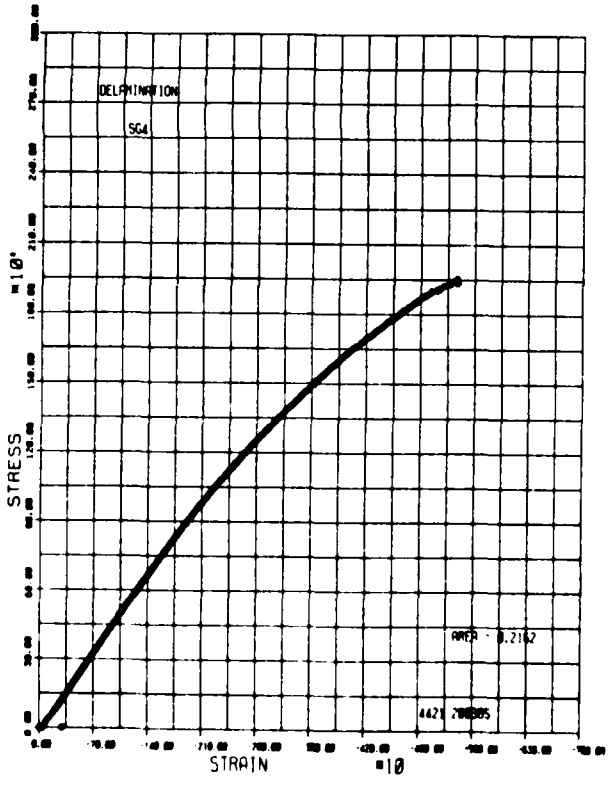

(c) Transverse Gage 4

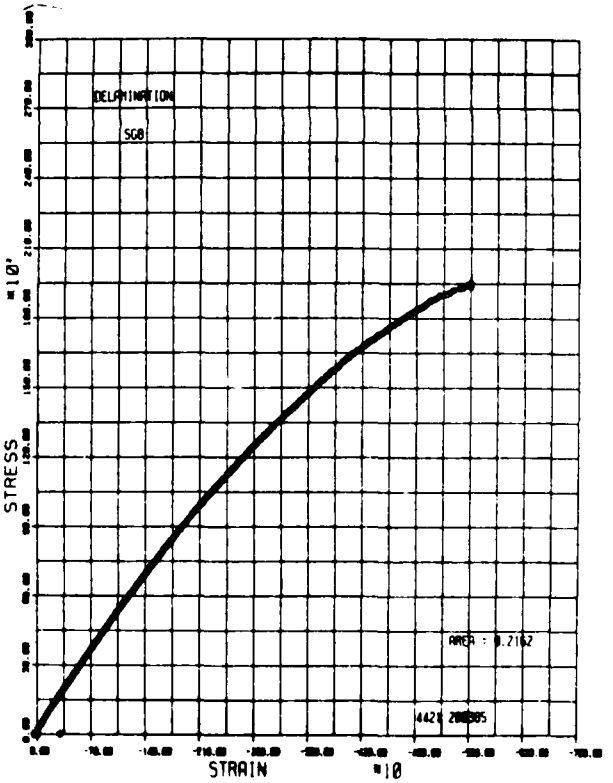

(d) Transverse Gage 8

Figure 30. Stress-Strain Curves of Transverse Gages of Specimen D-5

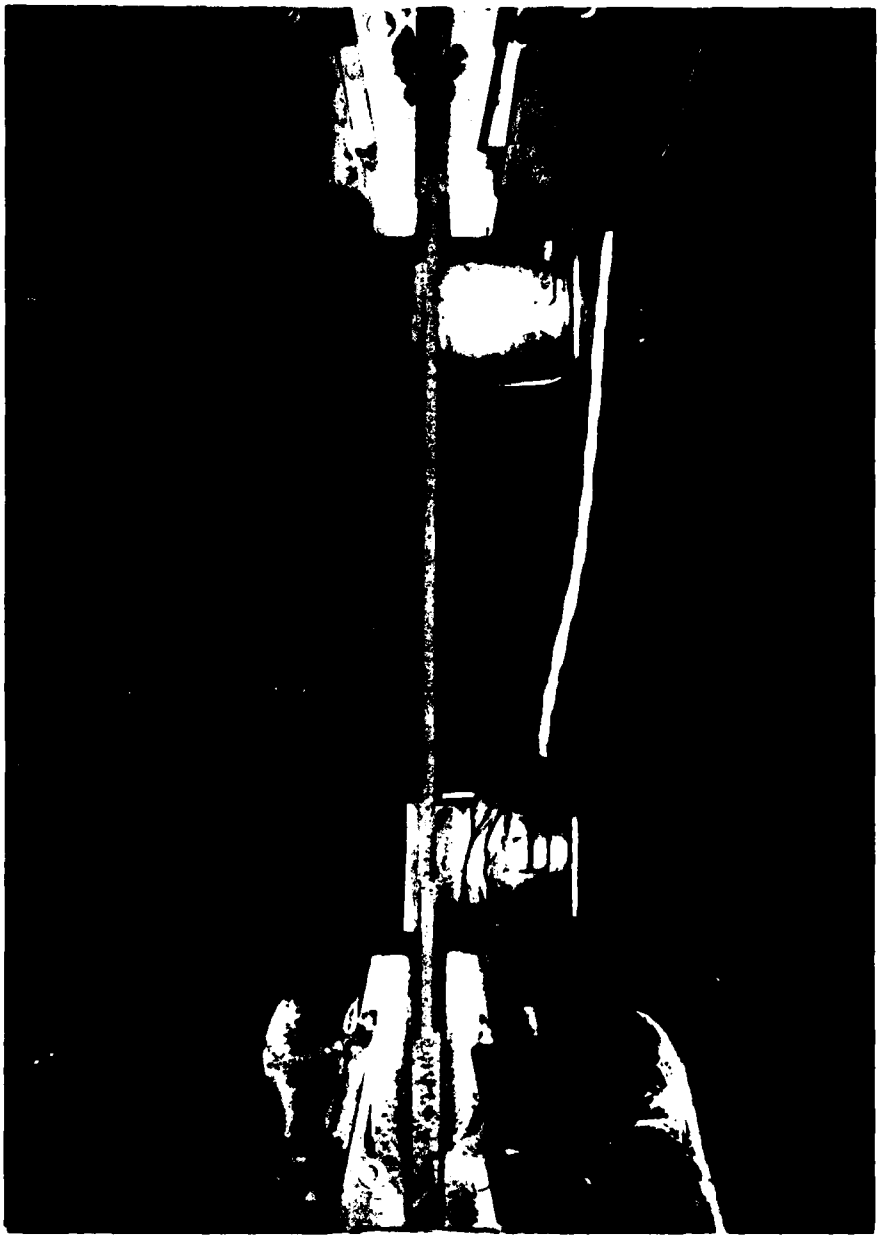

Figure 31. Specimen with Acoustic Tranducers and Grips

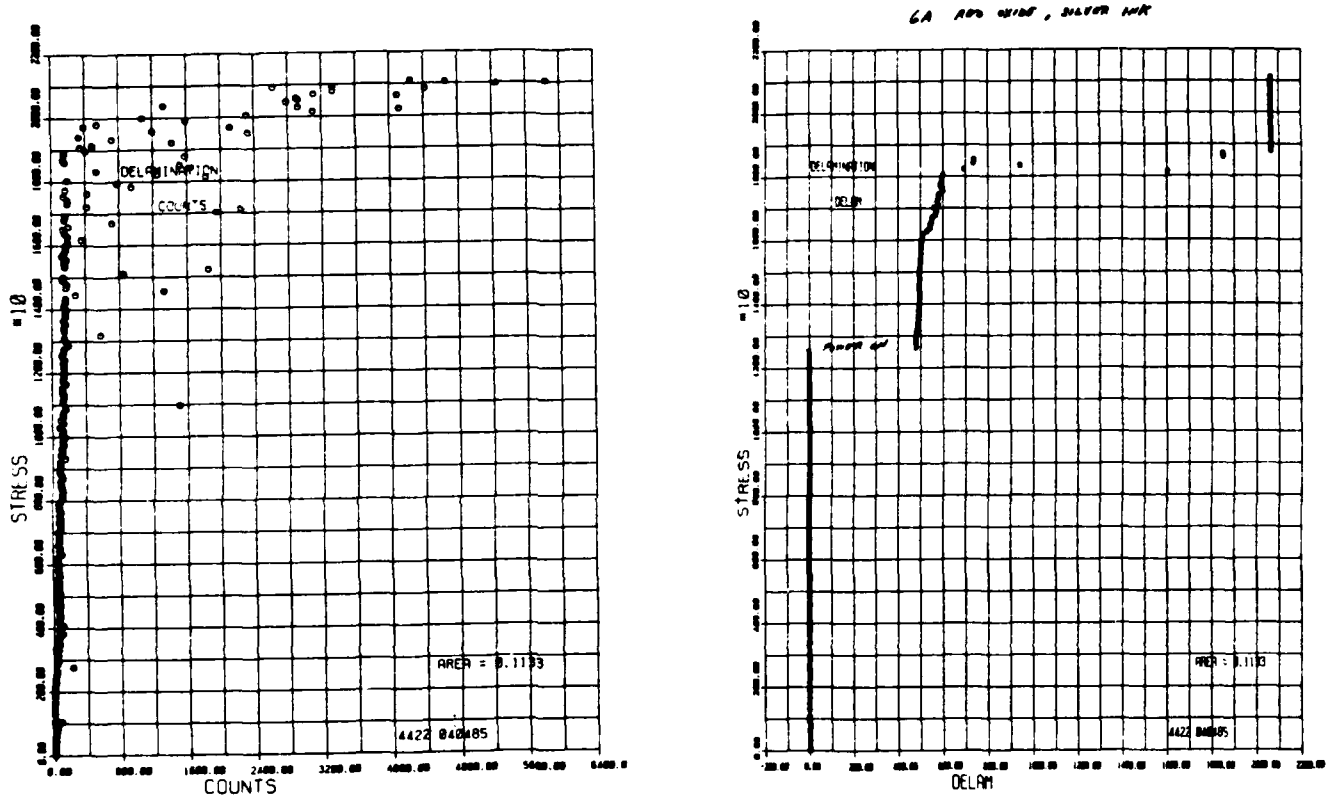

Figure 32. Stress versus Acoustic Emission Count and Silver Ink Response of Specimen A-6

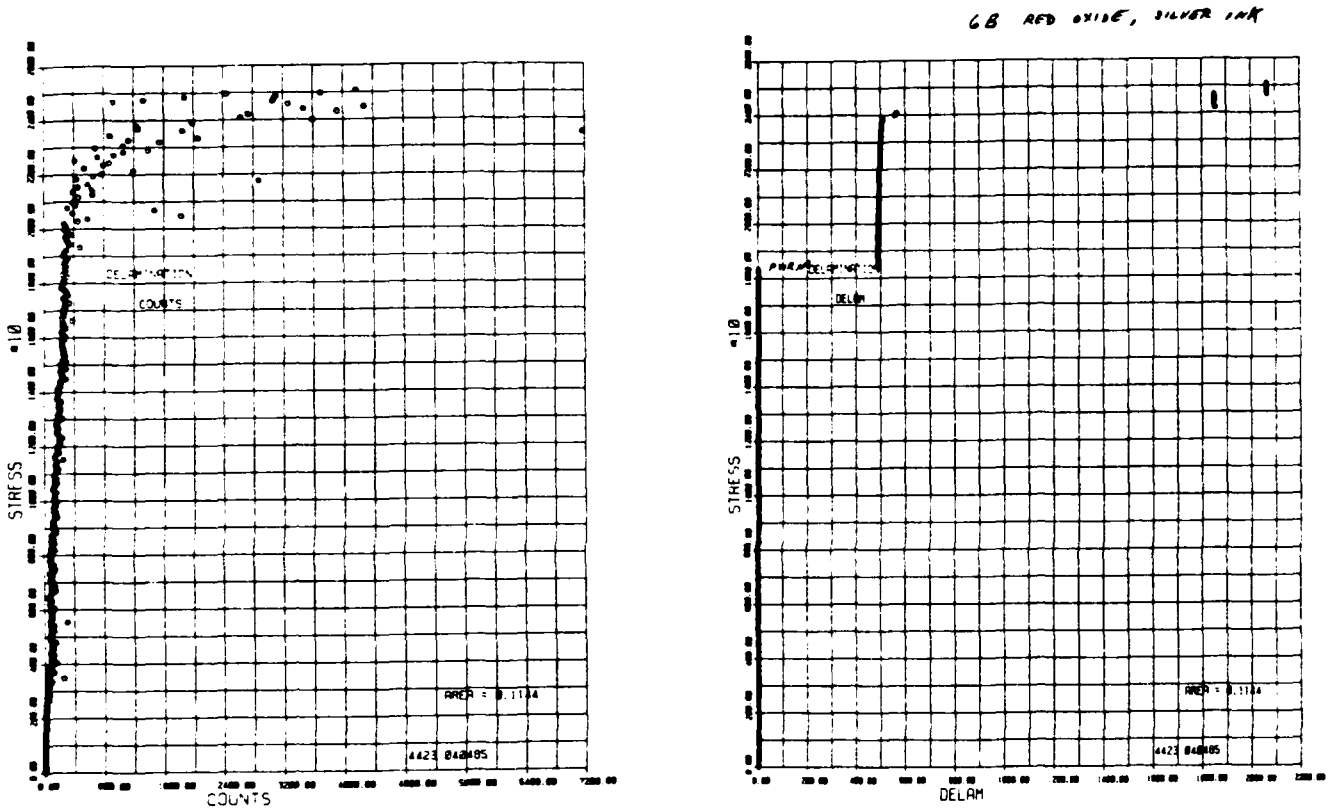

(a) Acoustic Emission Count

(b) Silver Ink

Figure 33. Stress versus Acoustic Emission Count and Silver Ink Response of Specimen B-6

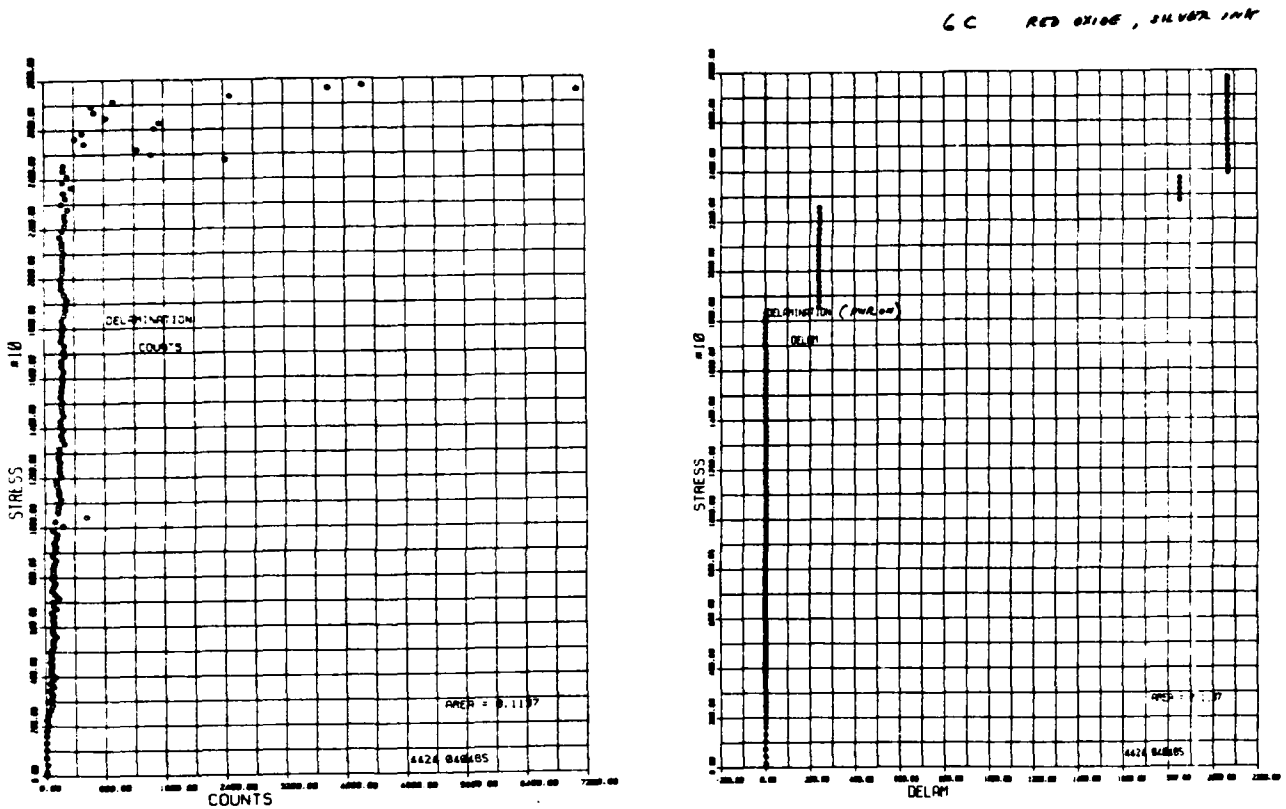

(a) Acoustic Emission Count

(b) Silver Ink

Figure 34. Stress versus Acoustic Emission Count and Silver Ink Response of Specimen C-6

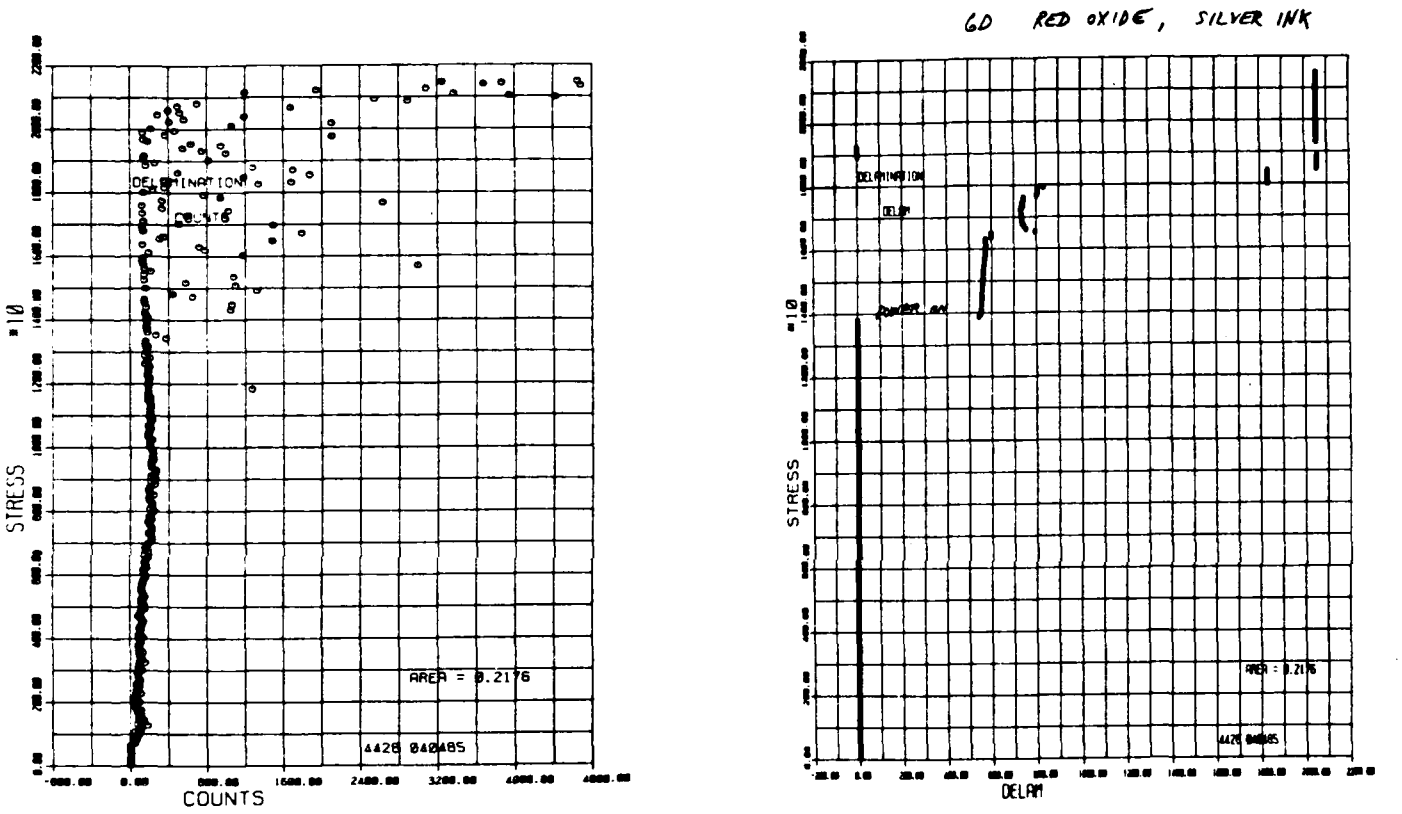

(a) Acoustic Emission Count

(b) Silver Ink

Figure 35. Stress versus Acoustic Emission Count and Silver Ink Response of Specimen D-6

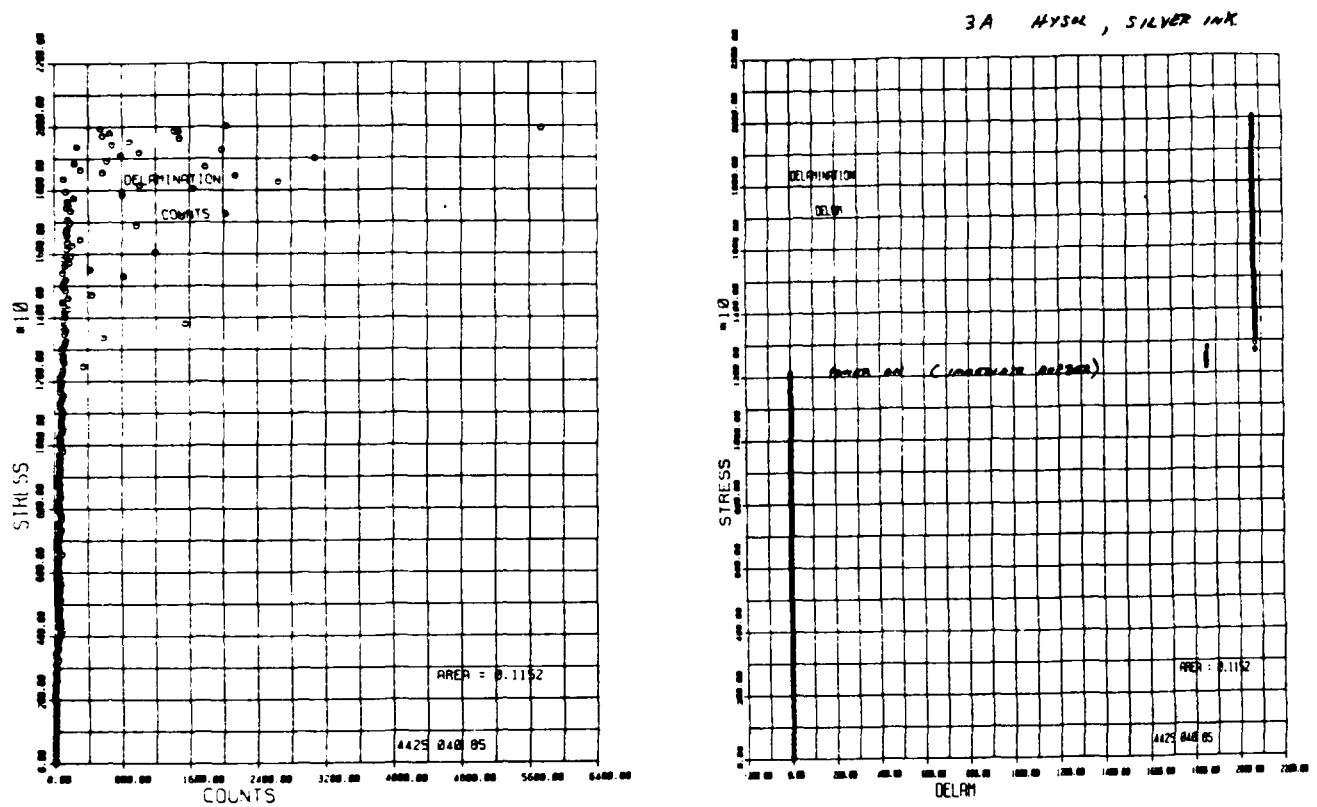

(a) Acoustic Emission Count

(b) Silver Ink

Figure 36. Stress versus Acoustic Emission Count and Silver Ink Response of Specimen A-3

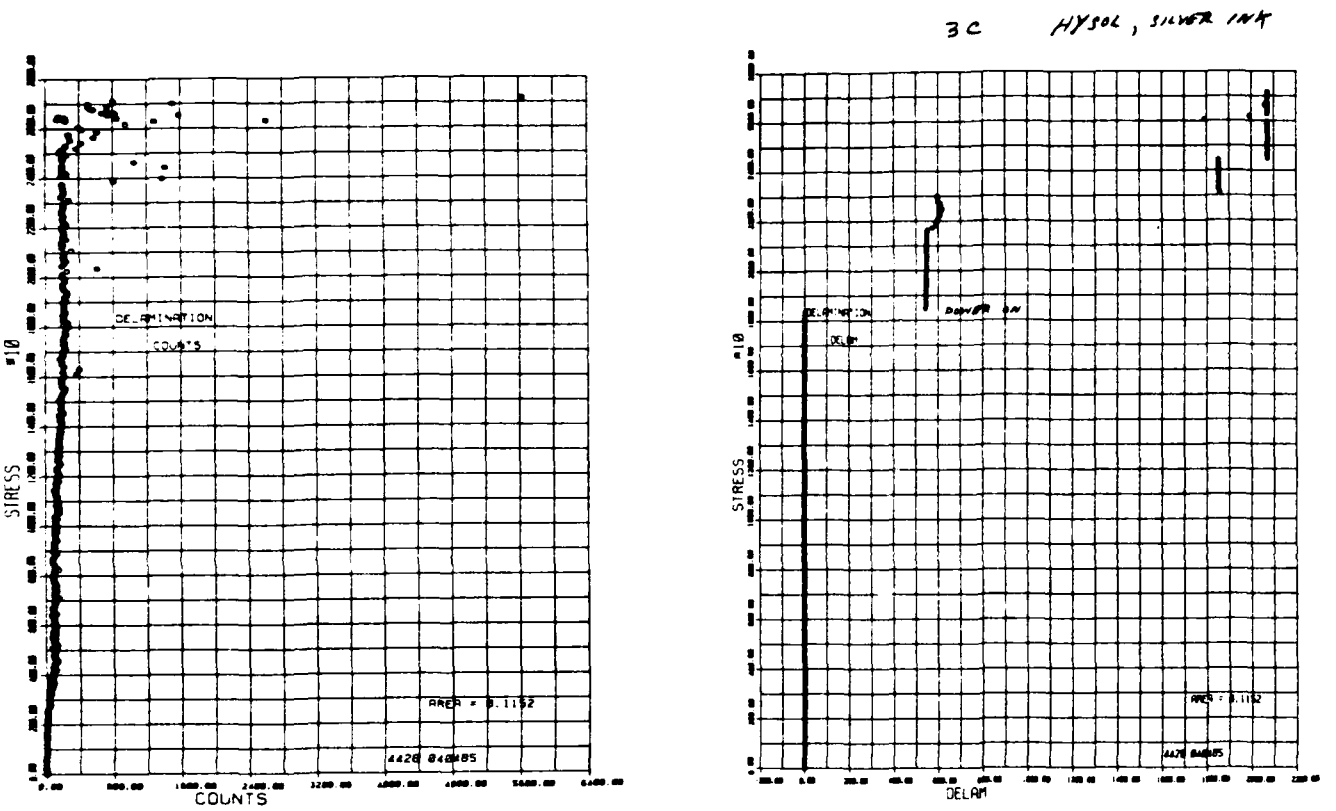

(a) Acoustic Emission Count

(b) Silver Ink

Figure 37. Stress versus Acoustic Emission Count and Silver Ink Response of Specimen C-3

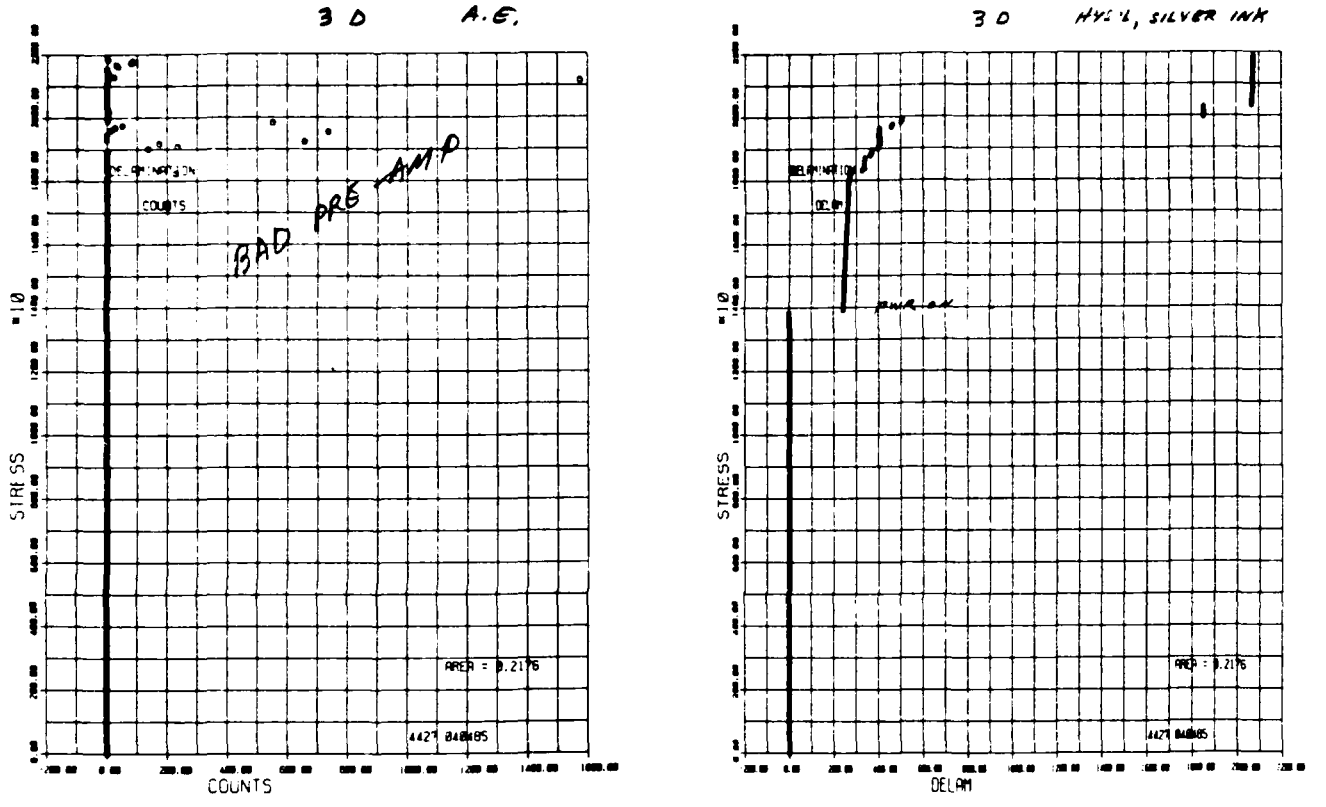

(a) Acoustic Emission Count

(b) Silver Ink

Figure 38. Stress versus Acoustic Emission count and Silver Ink Response of Specimen D-3

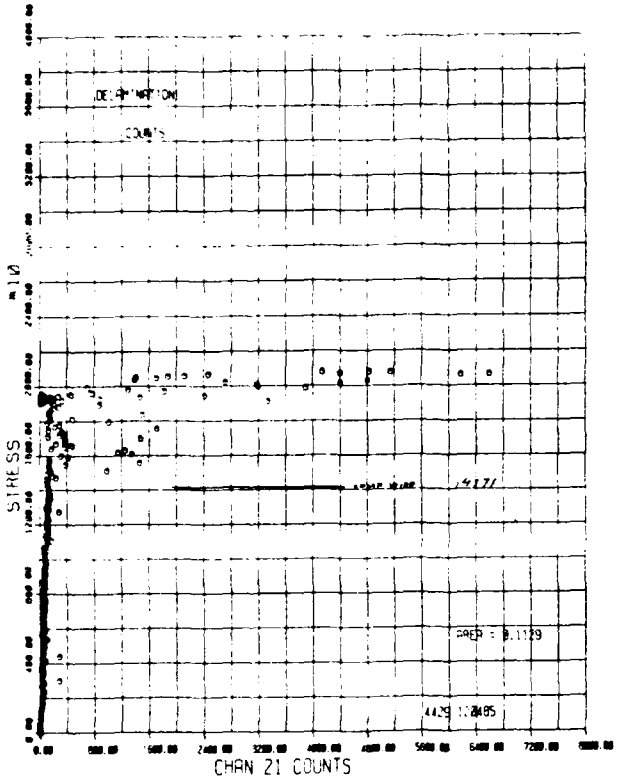

(a) Acoustic Emission Count and Silver Ink

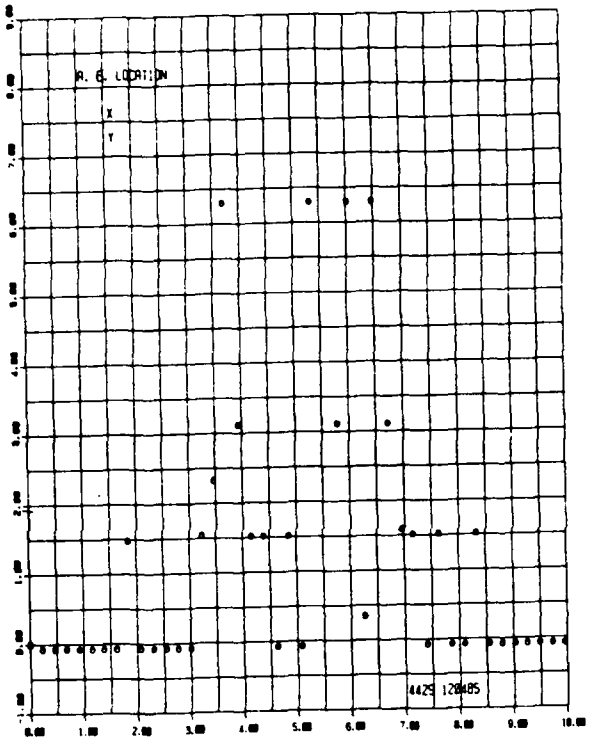

(b) Location of Counts

Figure 39. Stress versus Acoustic Emission Count and Silver Ink Response and Location of Counts of Specimen A-7

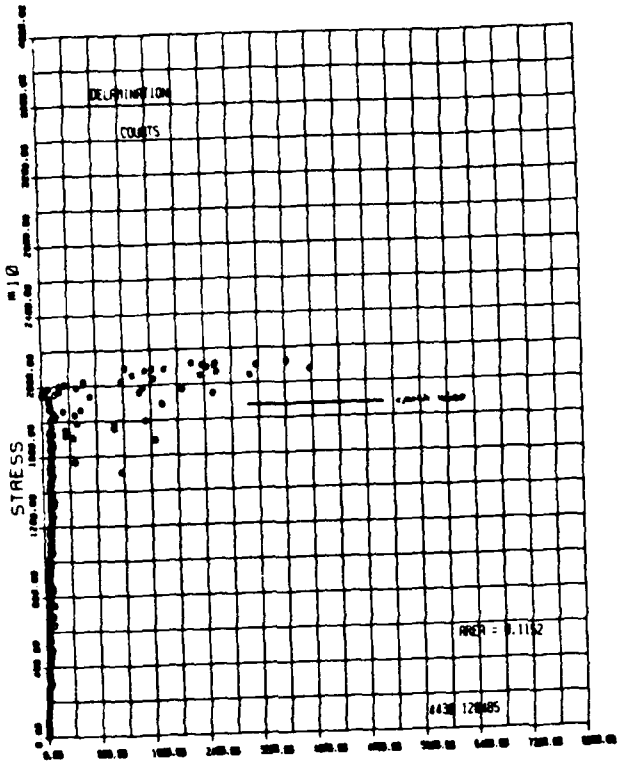

(a) Acoustic Emission Count and Silver Ink

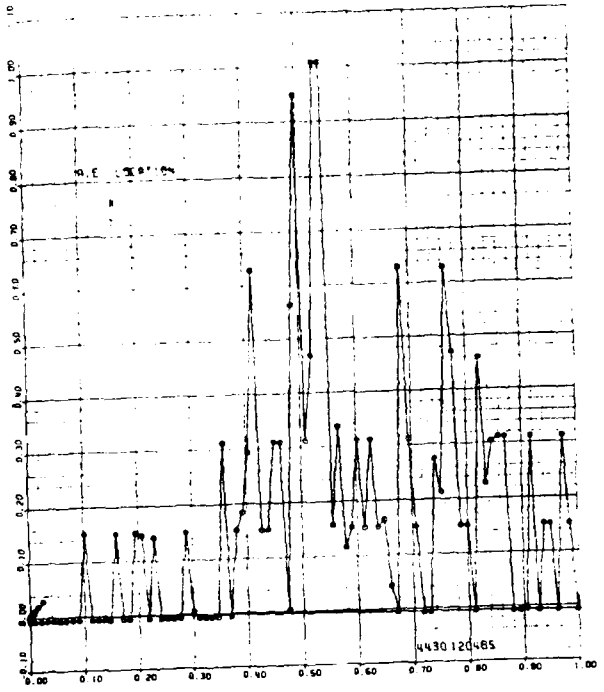

(b) Location of Counts

Figure 40. Stress versus Acoustic Emission Count and Silver Ink Response and Location of Counts of Specimen A-8

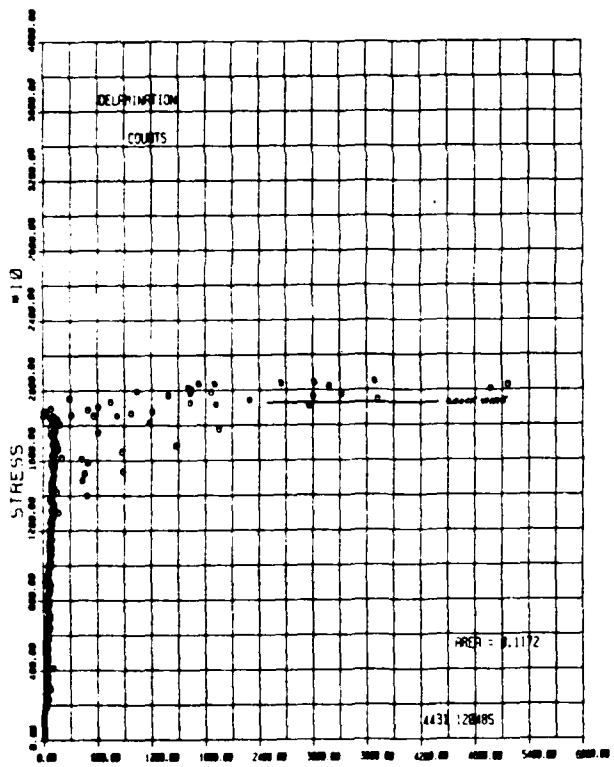

(a) Acoustic Emission Count and Silver Ink

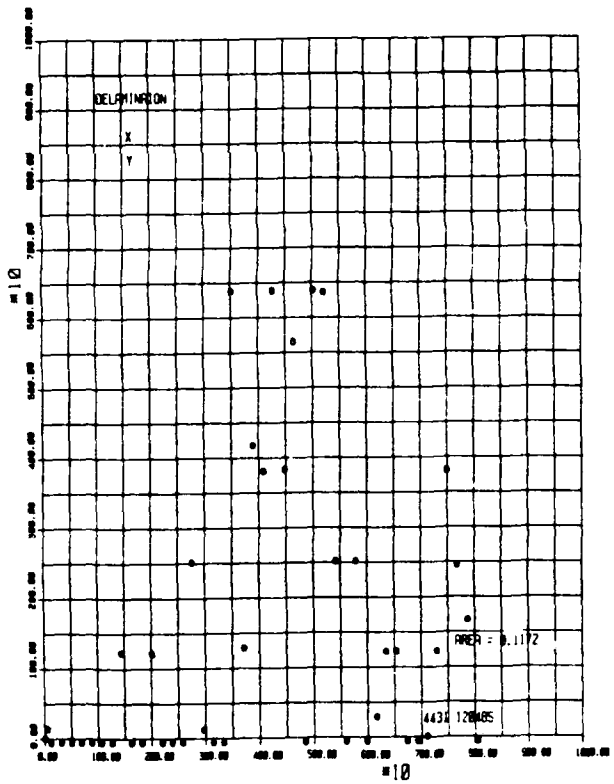

(b) Location of Counts

Figure 41. Stress versus Acoustic Emission Count and Silver Ink Response and Location of Counts of Specimen A-9

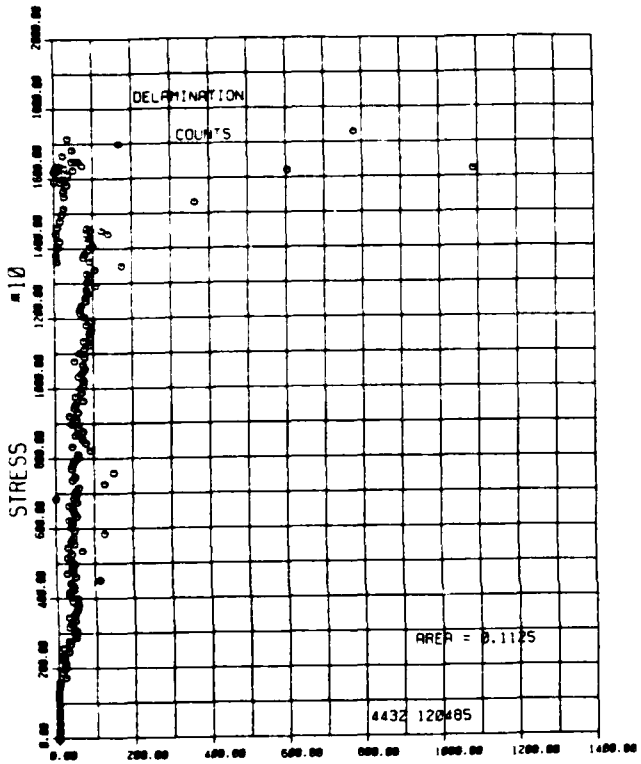

(a) Acoustic Emission Count

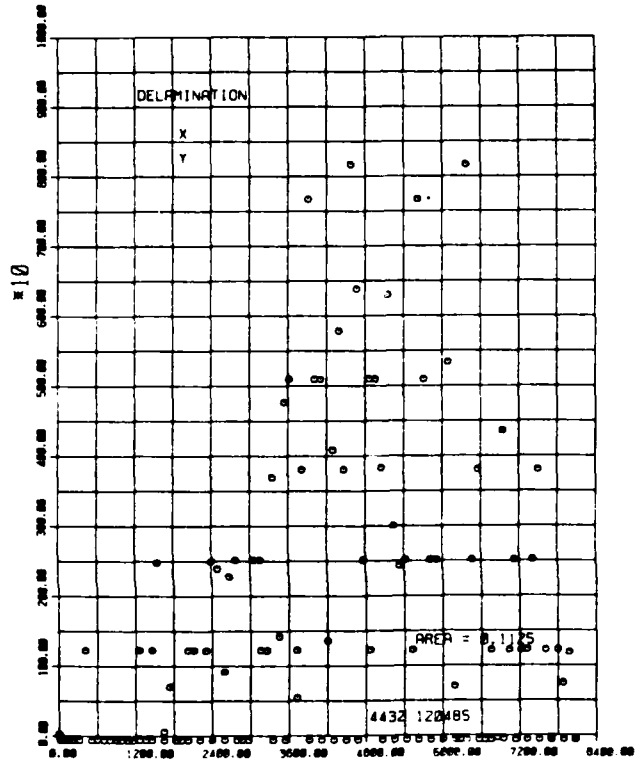

(b) Location of Counts

Figure 42. Stress versus Acoustic Emission Count and Location of Counts of Specimen A-10

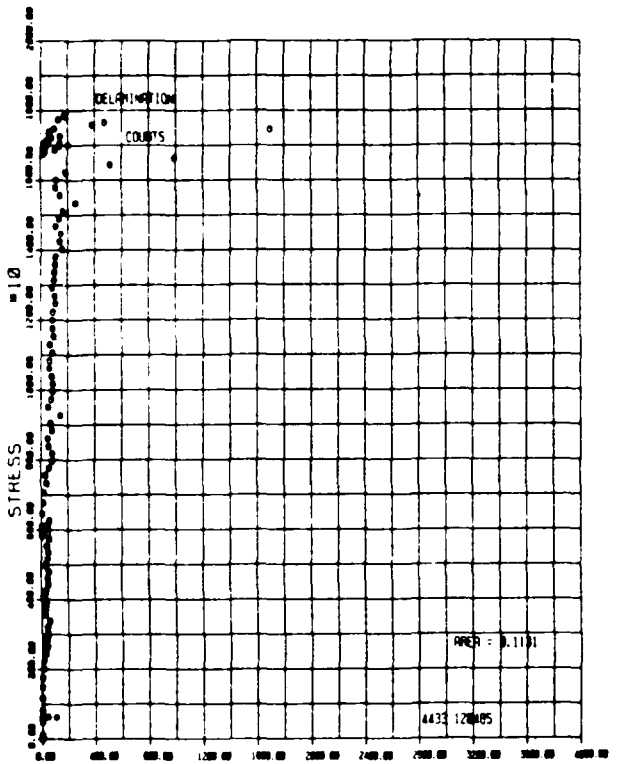

(a) Acoustic Emission Count

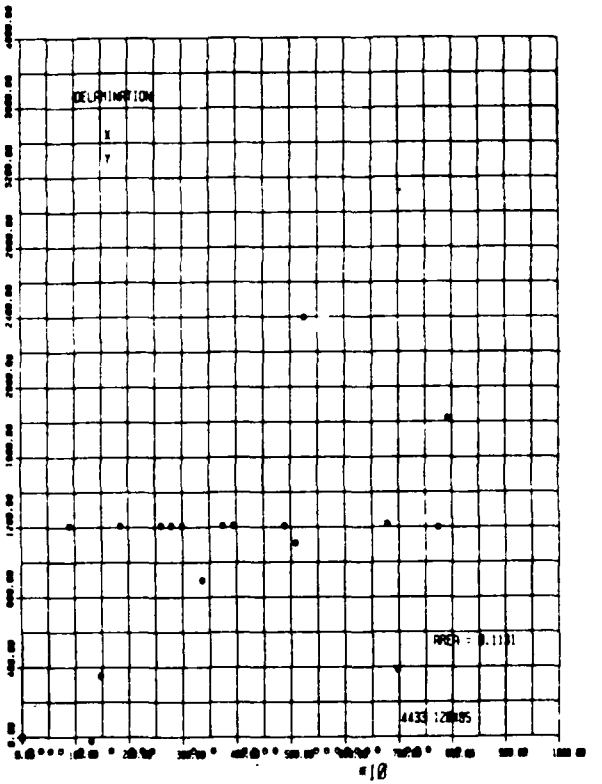

(b) Location of Counts

Figure 43. Stress versus Acoustic Emission Count and Location of Counts of Specimen A-11

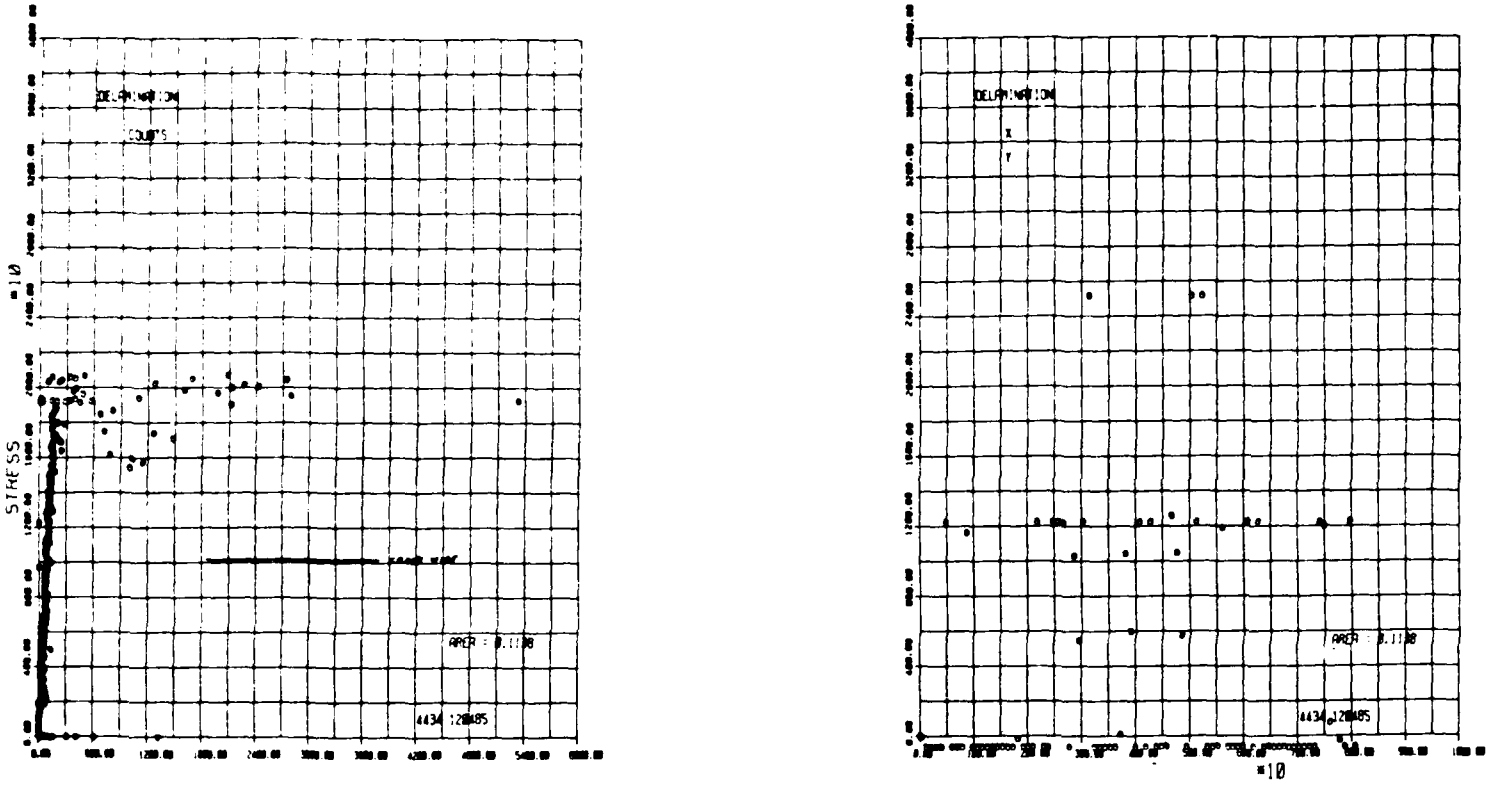

(a) Acoustic Emission Count and Silver Ink

(b) Location of Counts

Figure 44. Stress versus Acoustic Emission Count and Silver Ink Response and Location of Counts of Specimen A-12

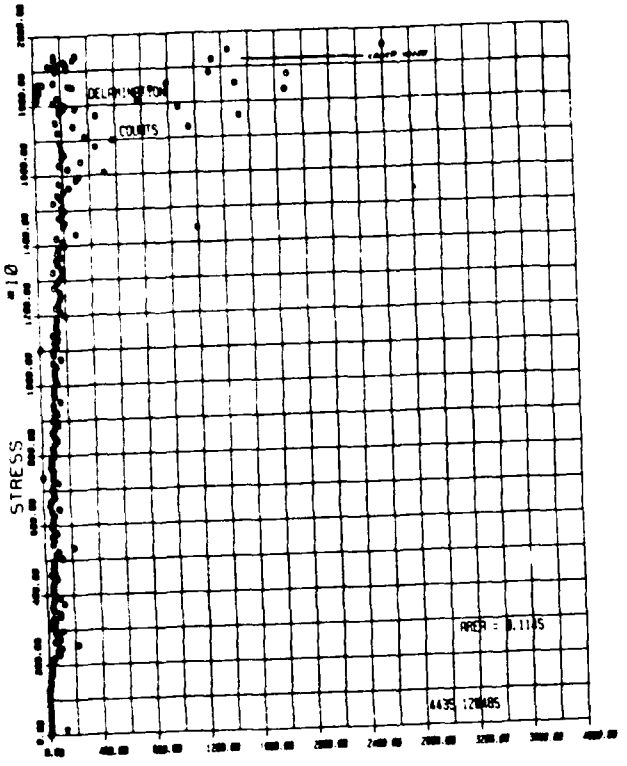

(a) Acoustic Emission Count and Silver Ink

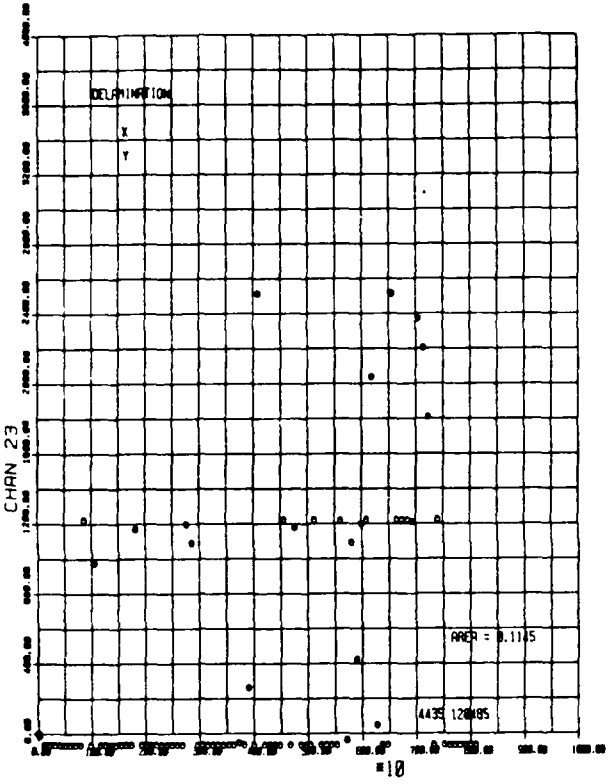

(b) Location of Counts

Figure 45. Stress versus Acoustic Emission Count and Silver Ink Response and Location of Counts of Specimen A-13

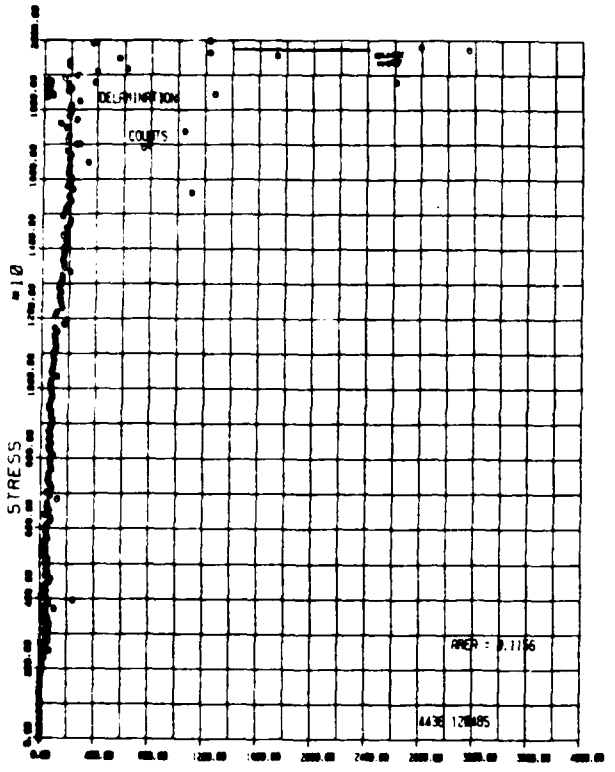

(a) Acoustic Emission Count and Silver Ink

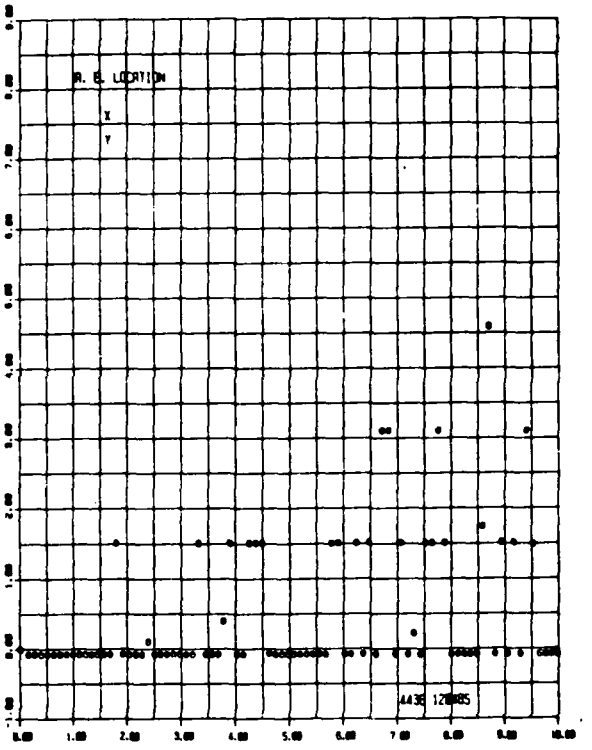

(b) Location of Counts

Figure 46. Stress versus Acoustic Emission Count and Silver Ink Response and Location of Counts of Specimen A-14

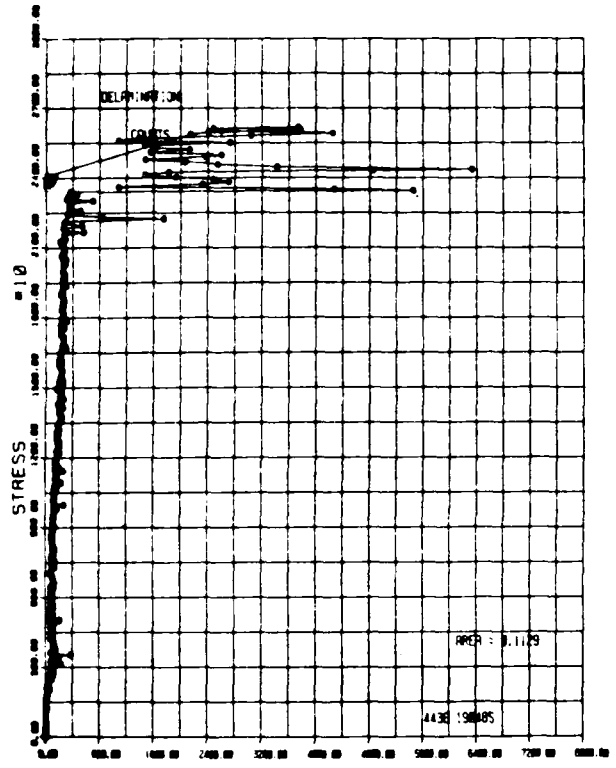

(a) Acoustic Emission Count

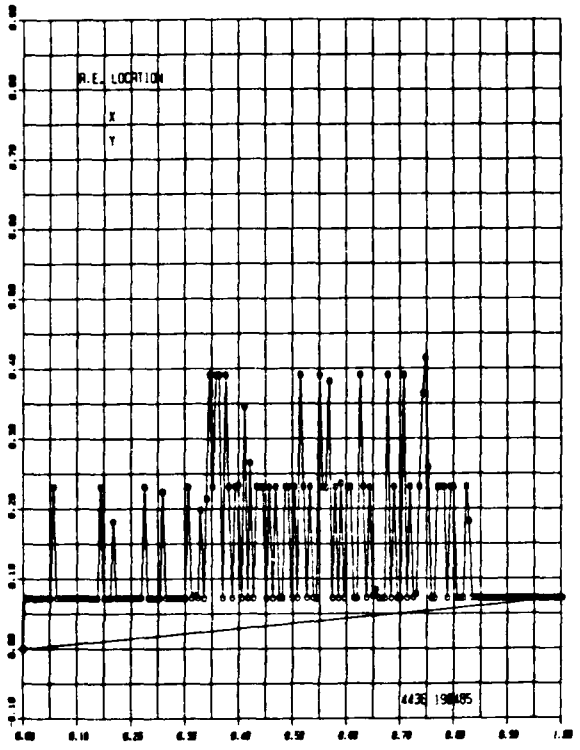

(b) Location of Counts

Figure 47. Stress versus Acoustic Emission Count and Location of Counts of Specimen B-8

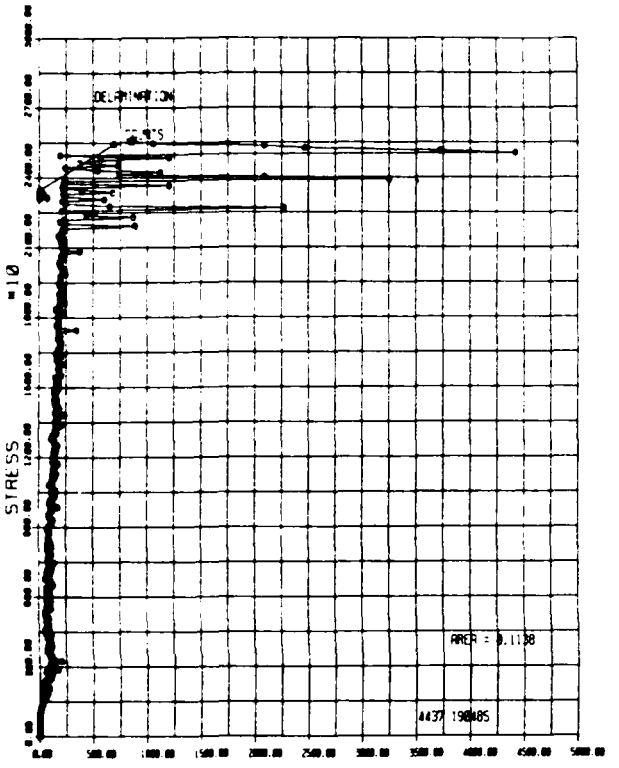

(a) Acoustic Emission Count

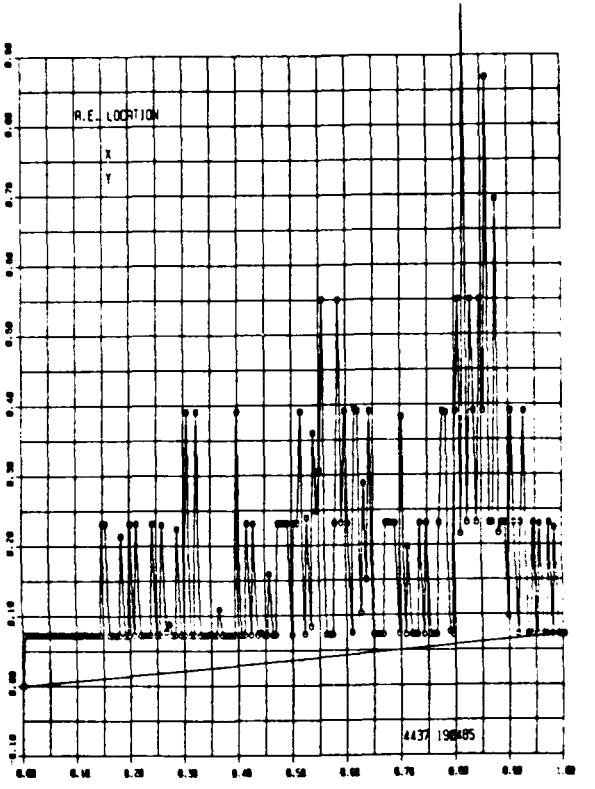

(b) Location of Counts

Figure 48. Stress versus Acoustic Emission Count and Location of Counts of Specimen B-9

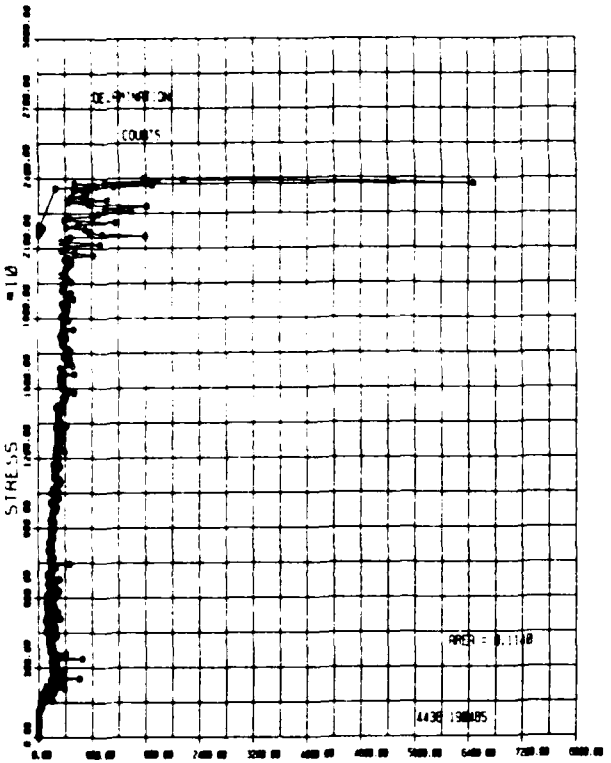

(a) Acoustic Emission Count

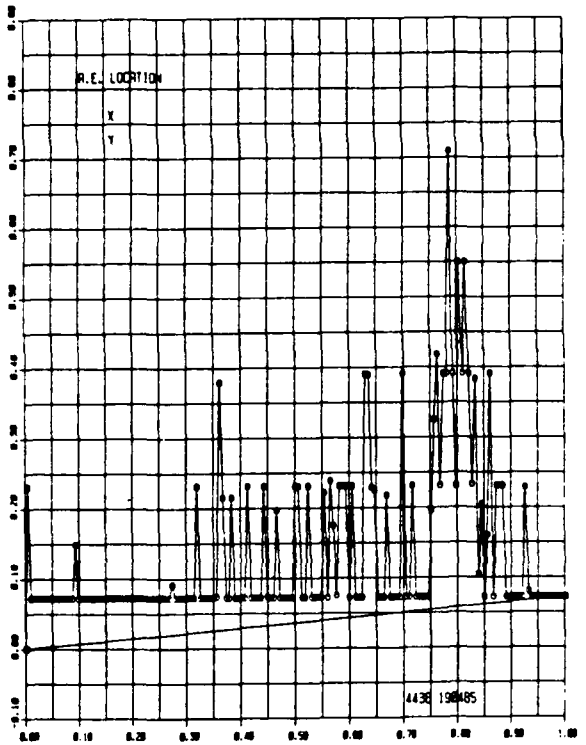

(b) Location of Counts

Figure 49. Stress versus Acoustic Emission Count and Location of Counts of Specimen B-10

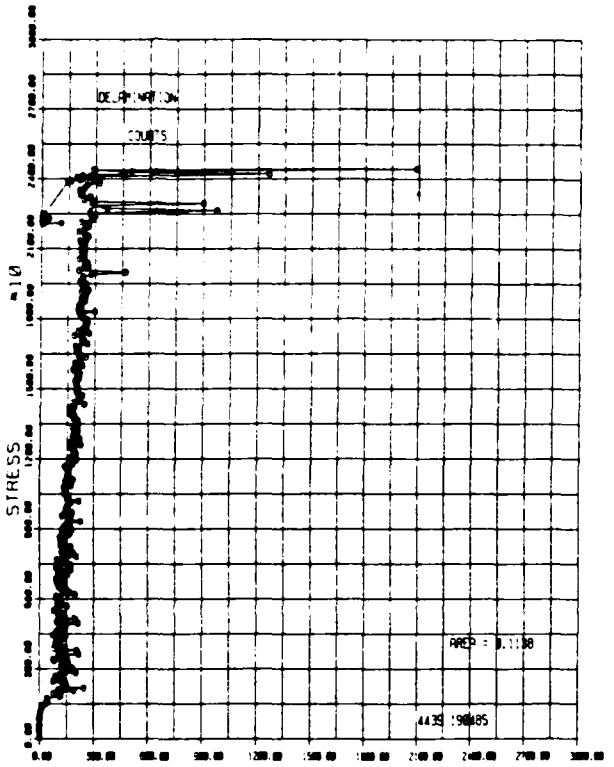

(a) Acoustic Emission Count

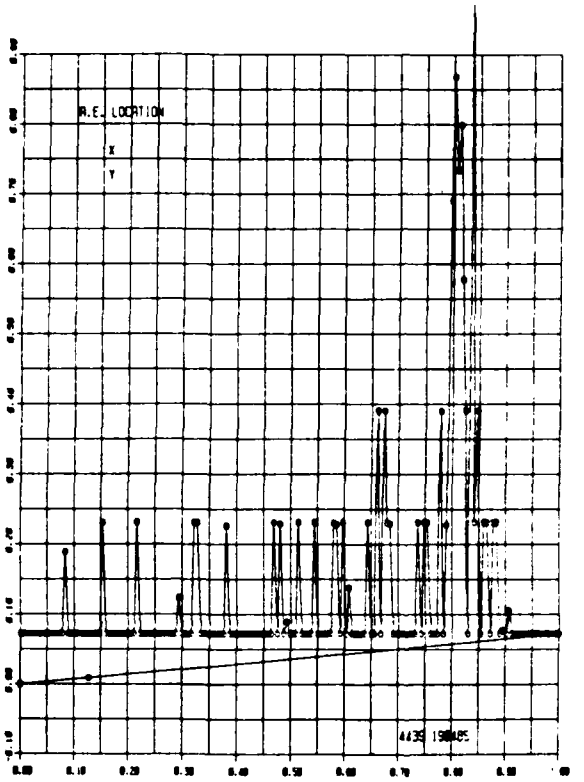

(b) Location of Counts

Figure 50. Stress versus Acoustic Emission Count and Location of Counts of Specimen B-11

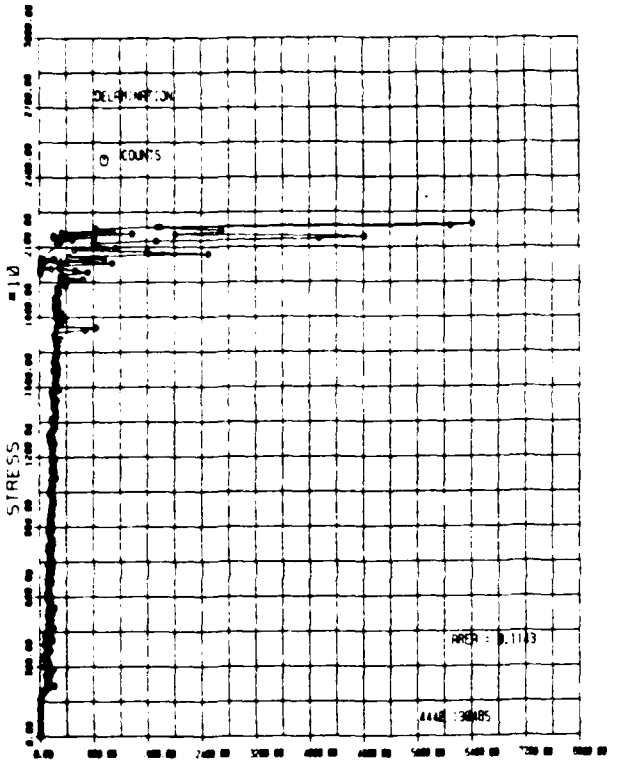

(a) Acoustic Emission Count

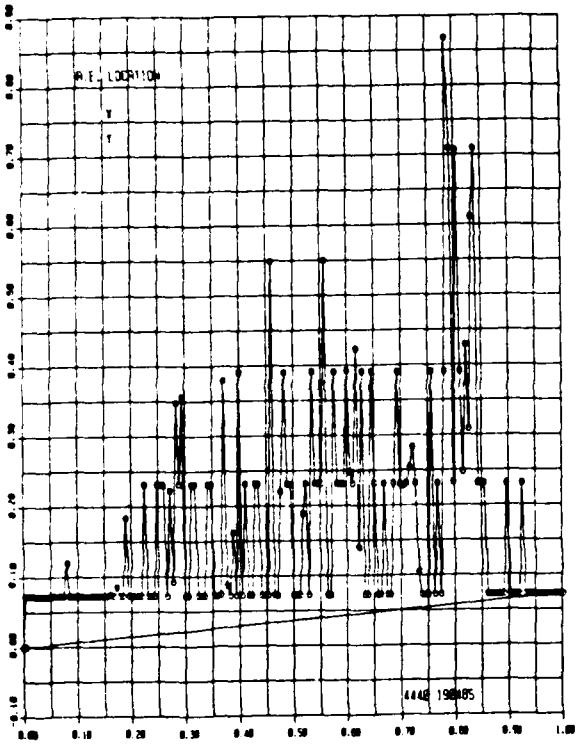

(b) Location of Counts

Figure 51. Stress versus Acoustic Emission Count and Location of Counts of Specimen B-12

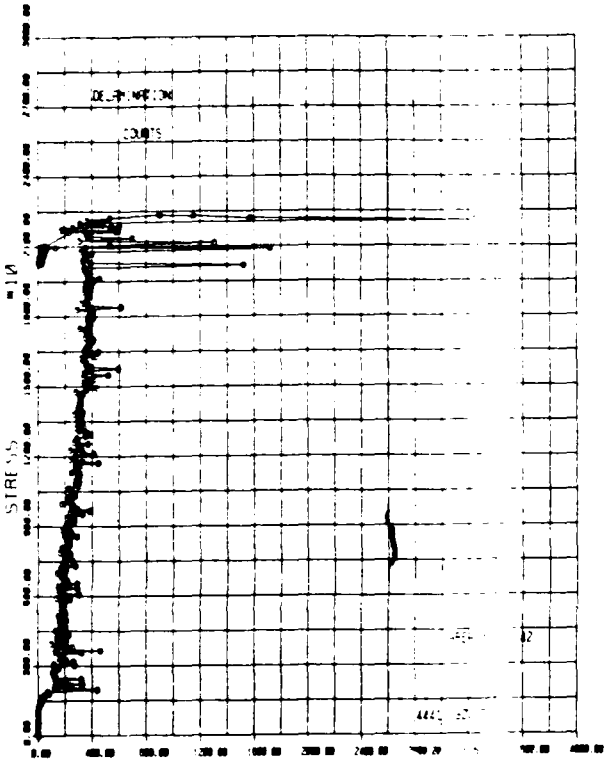

(a) Acoustic Emission Count

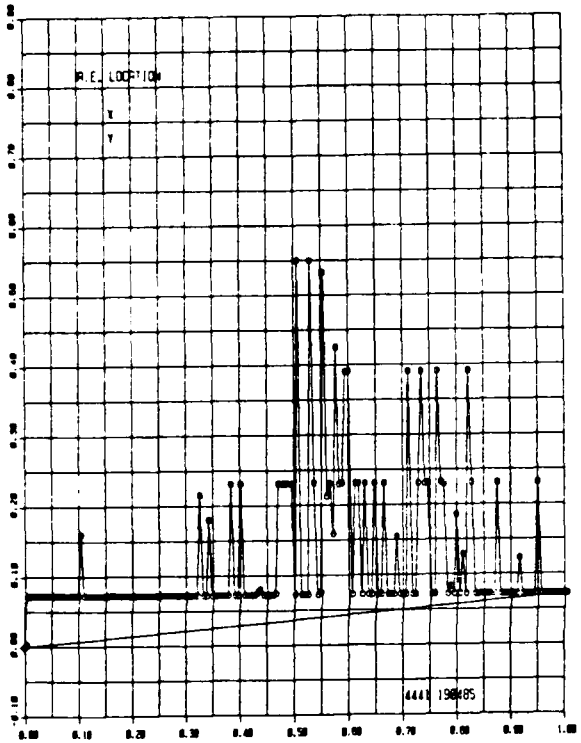

(b) Location of Counts

Figure 52. Stress versus Acoustic Emission Count and Location of Counts of Specimen B-13

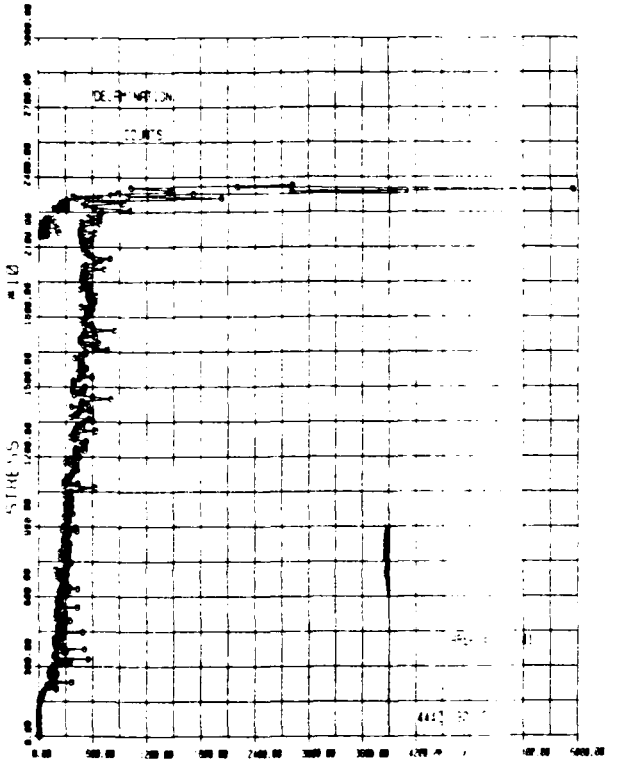

(a) Acoustic Emission Count

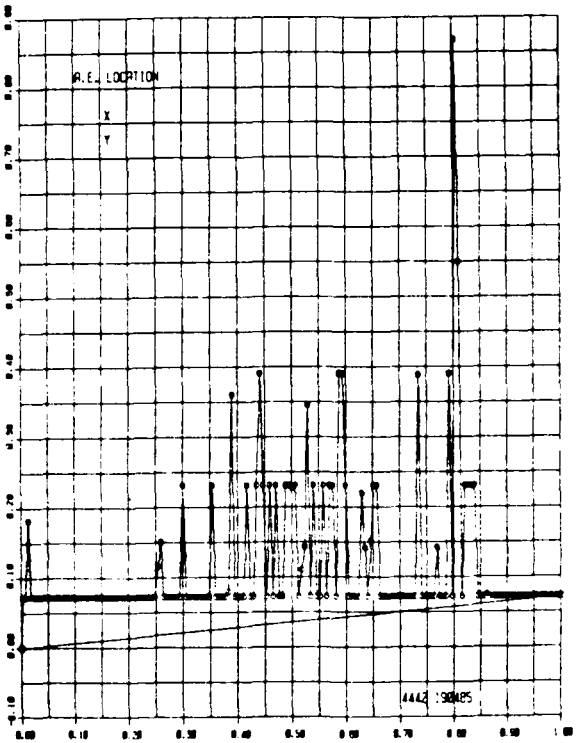

(b) Location of Counts

Figure 53. Stress versus Acoustic Emission Count and Location of Counts of Specimen B-14

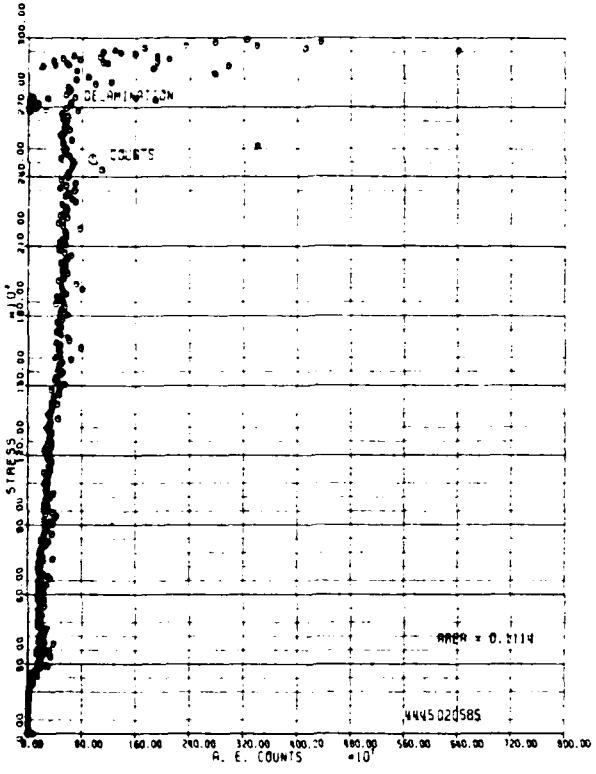

(a) Acoustic Emission Count

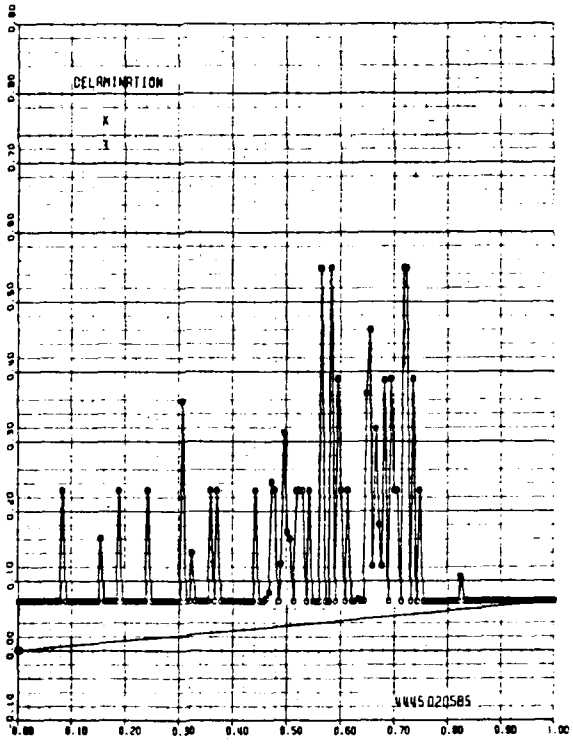

(b) Location of Counts

Figure 54. Stress versus Acoustic Emission Count and Location of Counts of Specimen C-7

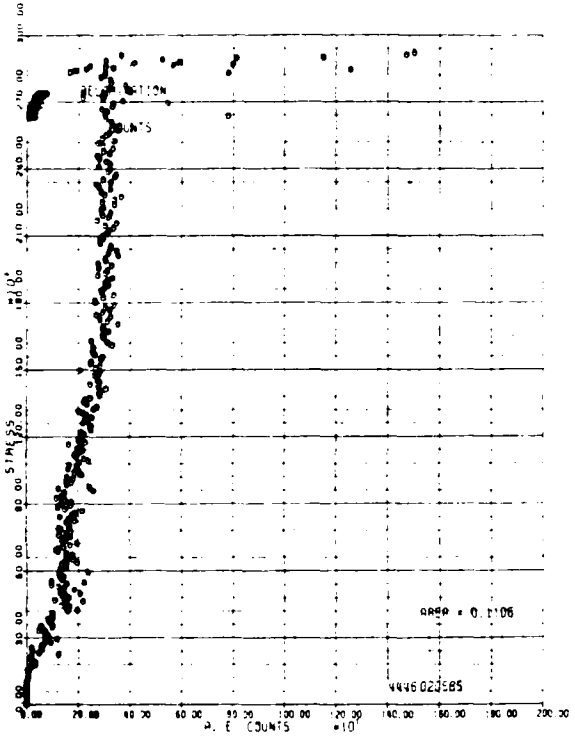

(a) Acoustic Emission Count

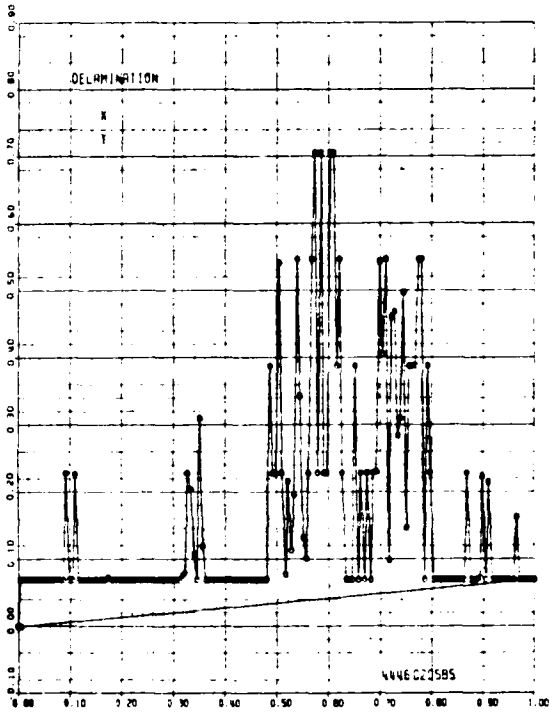

(b) Location of Counts

Figure 55. Stress versus Acoustic Emission Count and Location of Counts of Specimen C-8

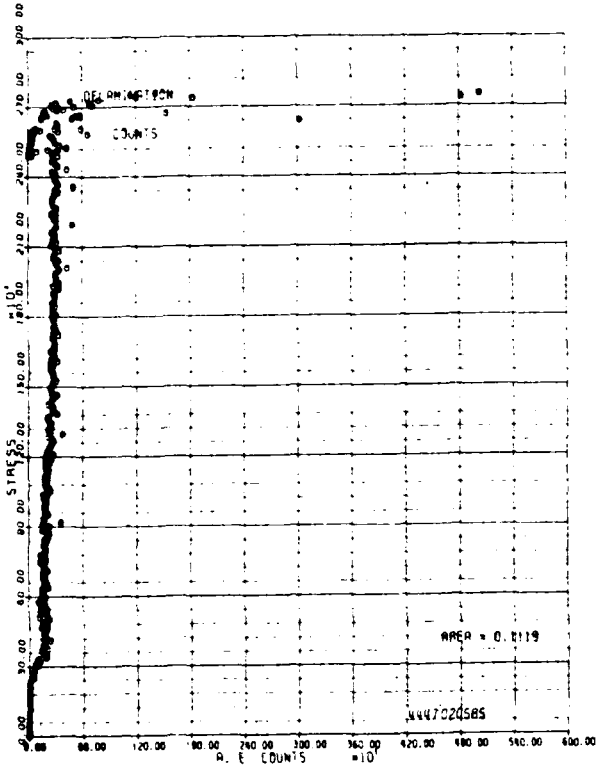

(a) Acoustic Emission Count

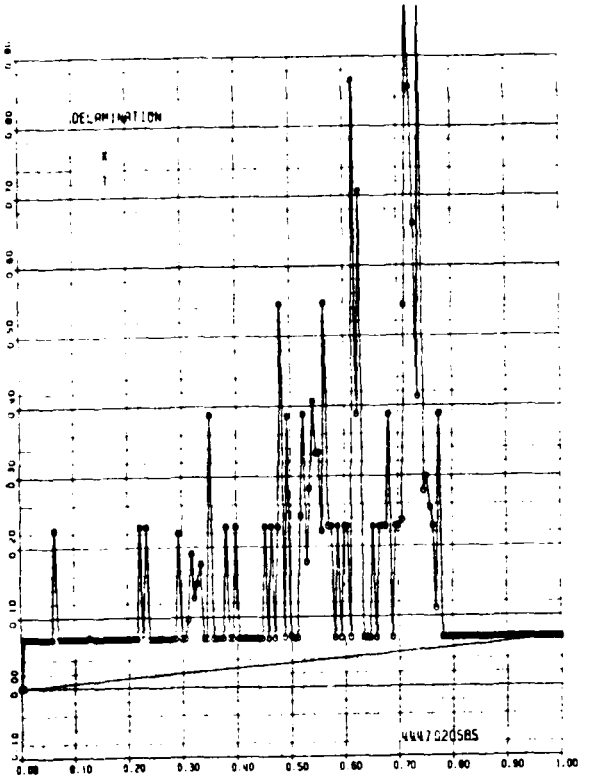

(b) Location of Counts

Figure 56. Stress versus Acoustic Emission Count and Location of Counts of Specimen C-9

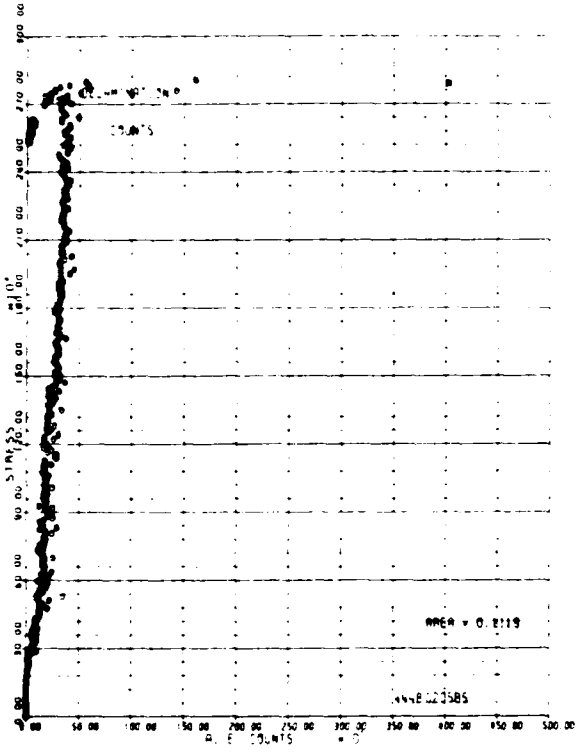

(a) Acoustic Emission Count

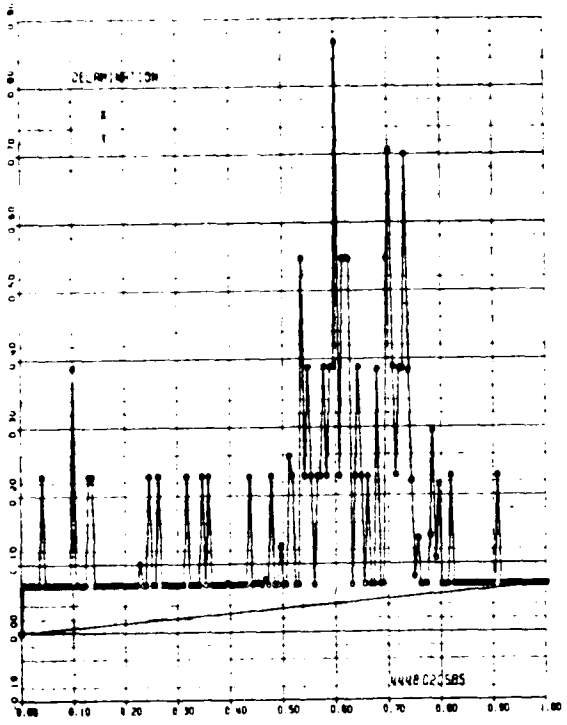

(b) Location of Counts

Figure 57. Stress versus Acoustic Emission Count and Location of Counts of Specimen C-10

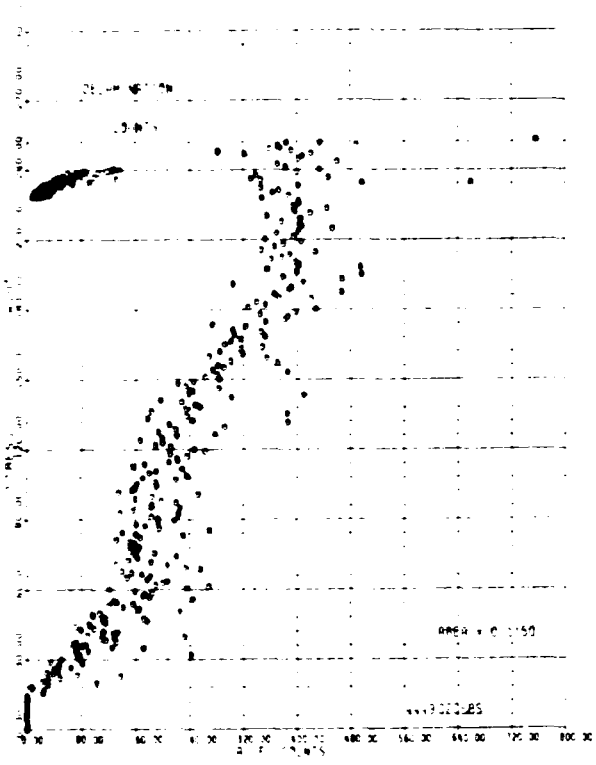

(a) Acoustic Emission Count

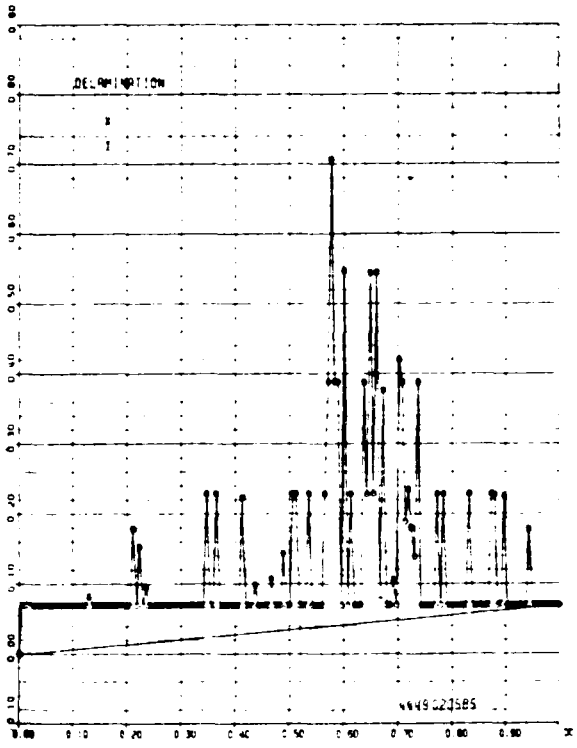

(b) Location of Counts

Figure 58. Stress versus Acoustic Emission Count and Location of Counts of Specimen C-11

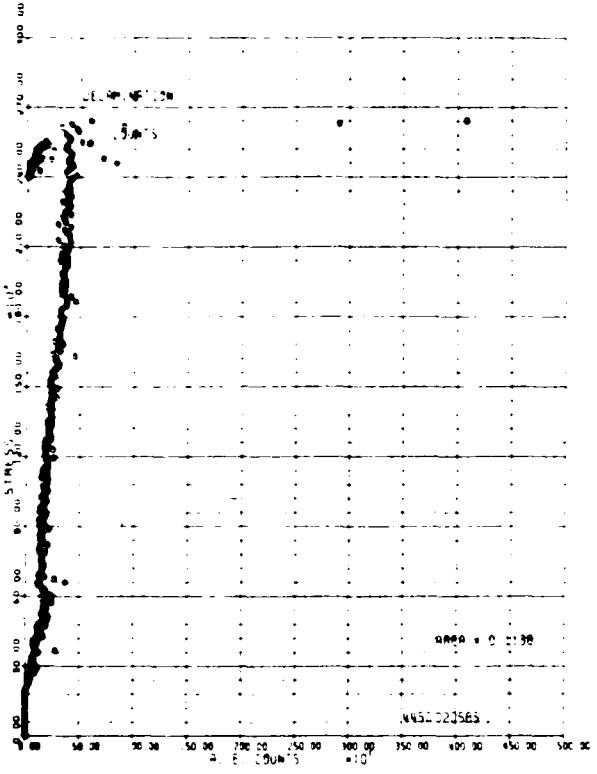

(a) Acoustic Emission Count

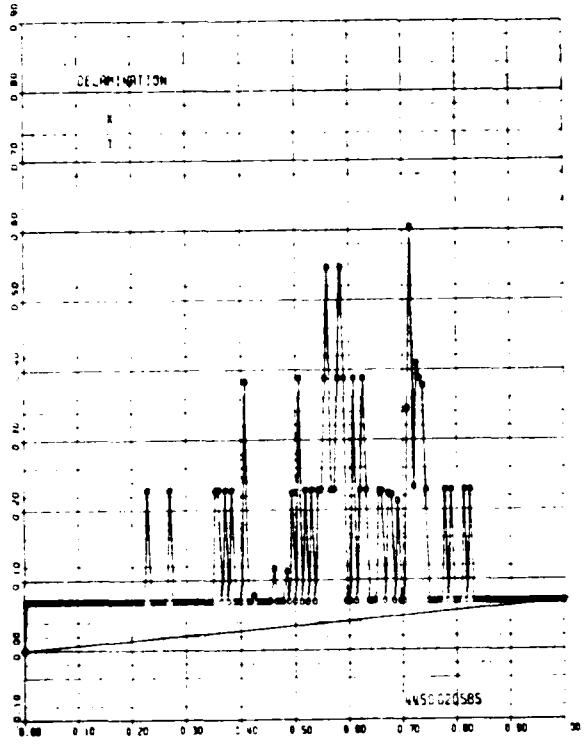

(b) Location of Counts

Figure 59. Stress versus Acoustic Emission Count and Location of Counts of Specimen C-12

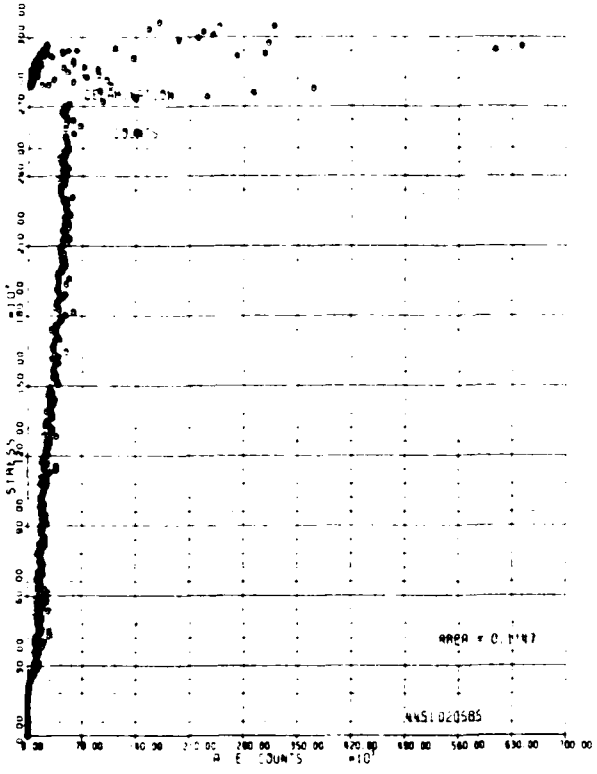

(a) Acoustic Emission Count

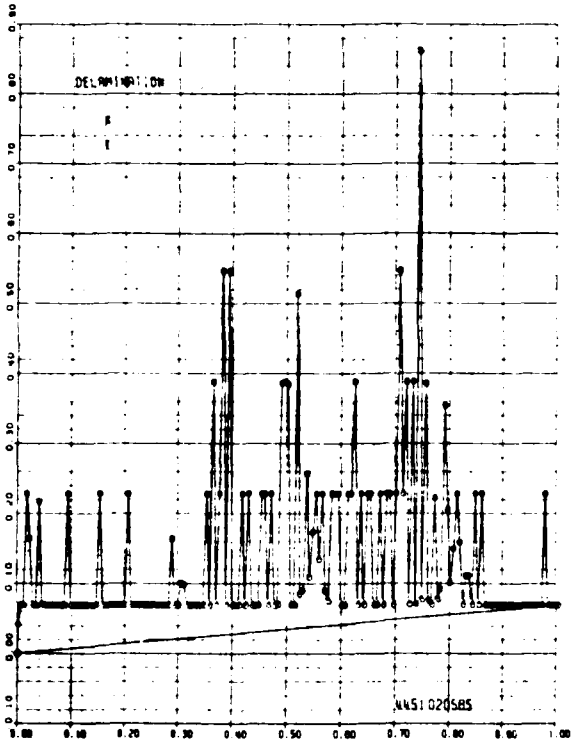

(b) Location of Counts

Figure 60. Stress versus Acoustic Emission Count and Location of Counts of Specimen C-13

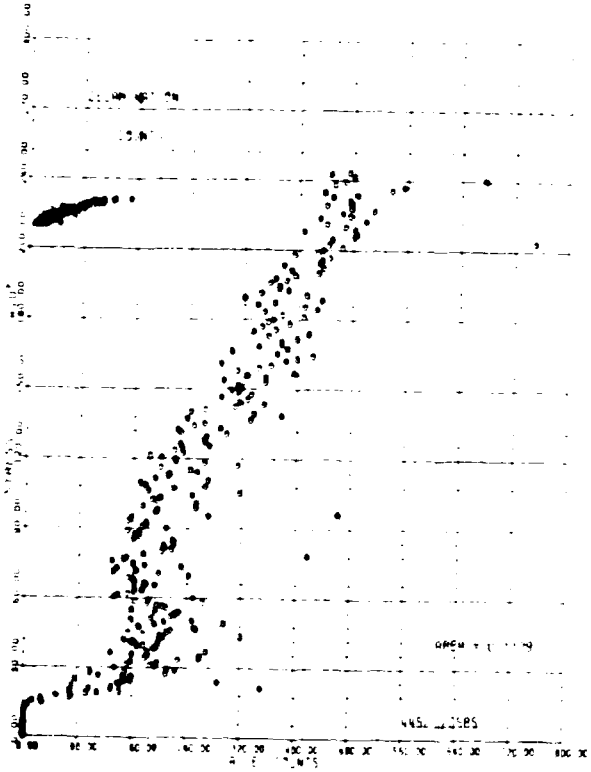

(a) Acoustic Emission Count

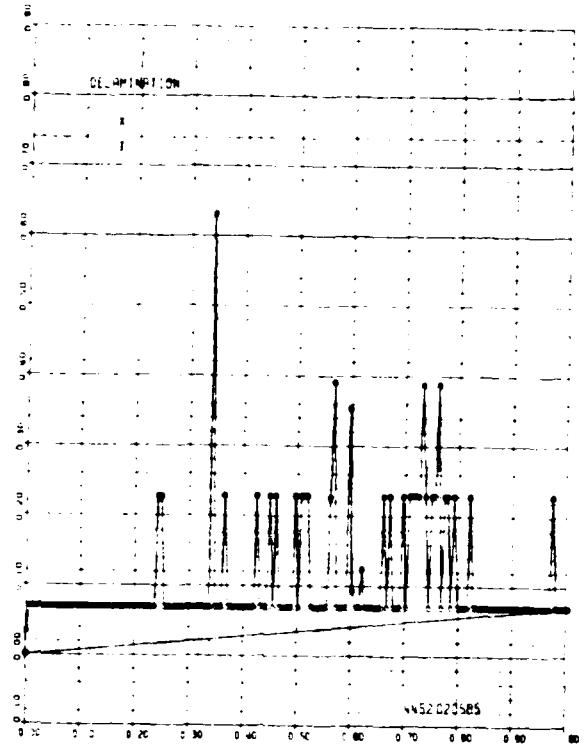

(b) Location of Counts

Figure 61. Stress versus Acoustic Emission Count and Location of Counts of Specimen C-14

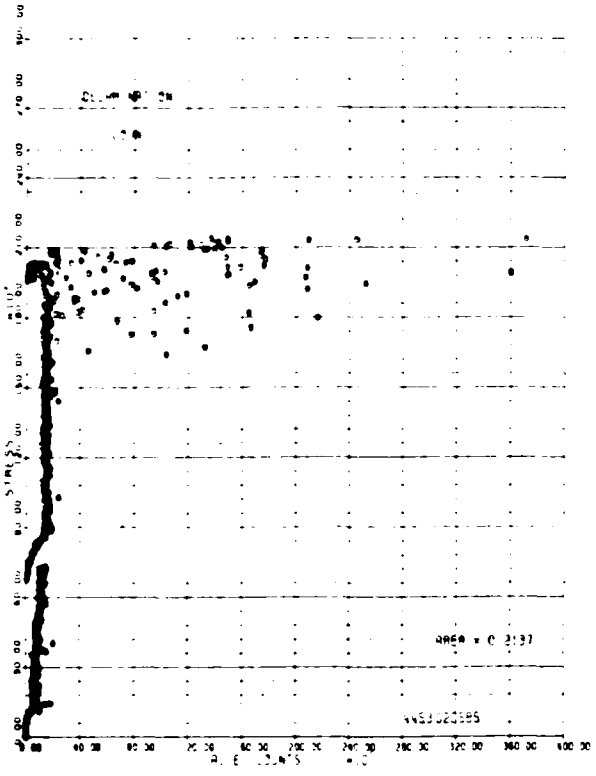

(a) Acoustic Emission Count

(b) Location of Counts

Figure 62. Stress versus Acoustic Emission Count and Location of Counts of Specimen D-7

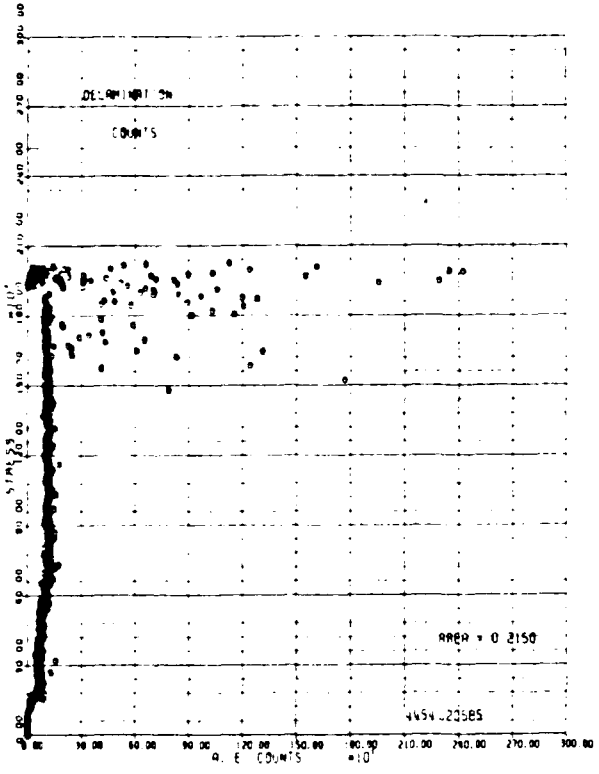

(a) Acoustic Emission Count

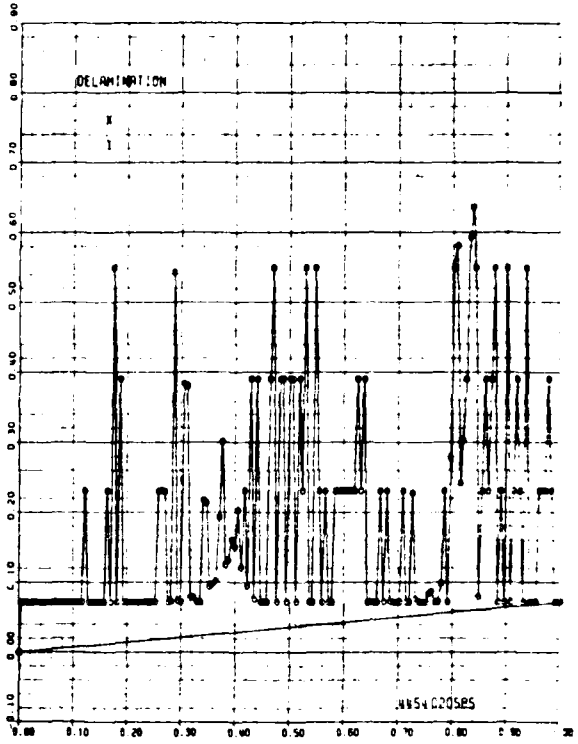

(b) Location of Counts

Figure 63. Stress versus Acoustic Emission Count and Location of Counts of Specimen D-8

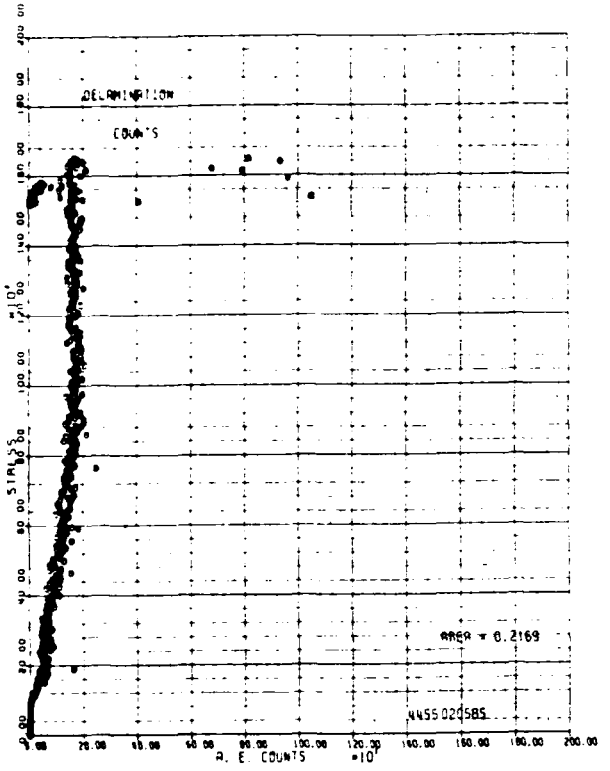

(a) Acoustic Emission Count

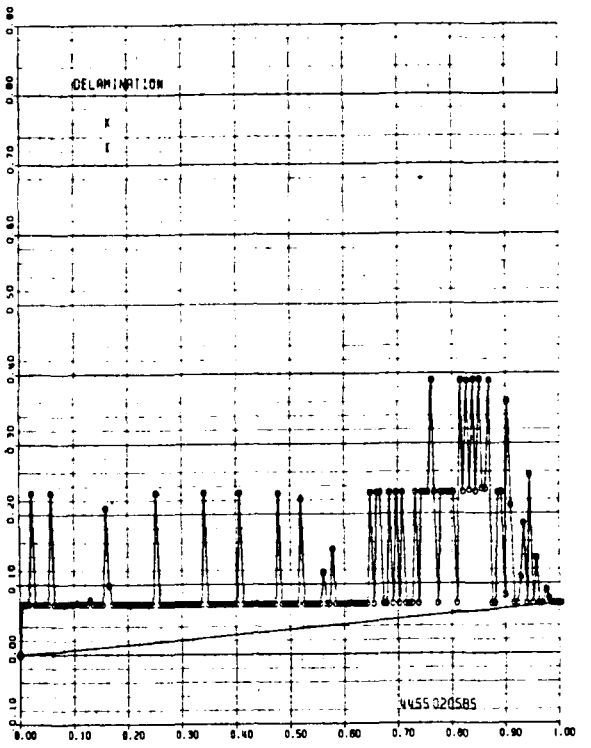

(b) Location of Counts

Figure 64. Stress versus Acoustic Emission Count and Location of Counts of Specimen D-9

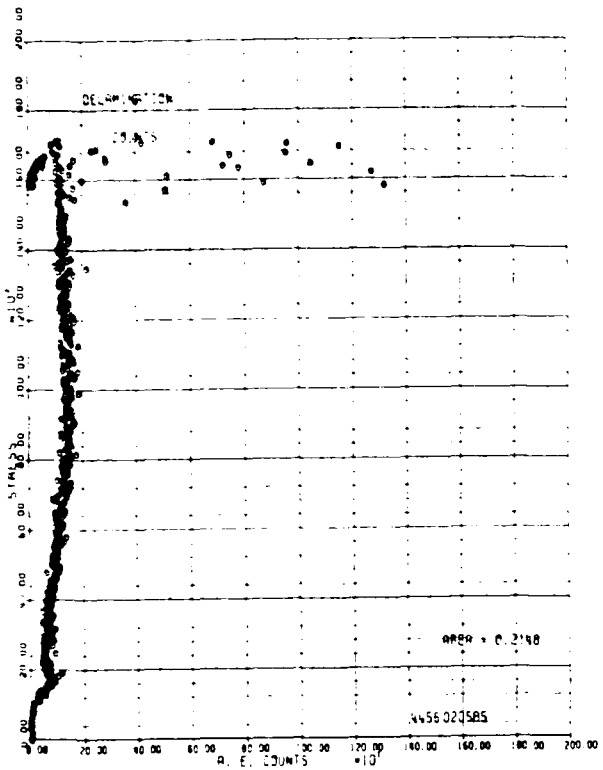

(a) Acoustic Emission Count

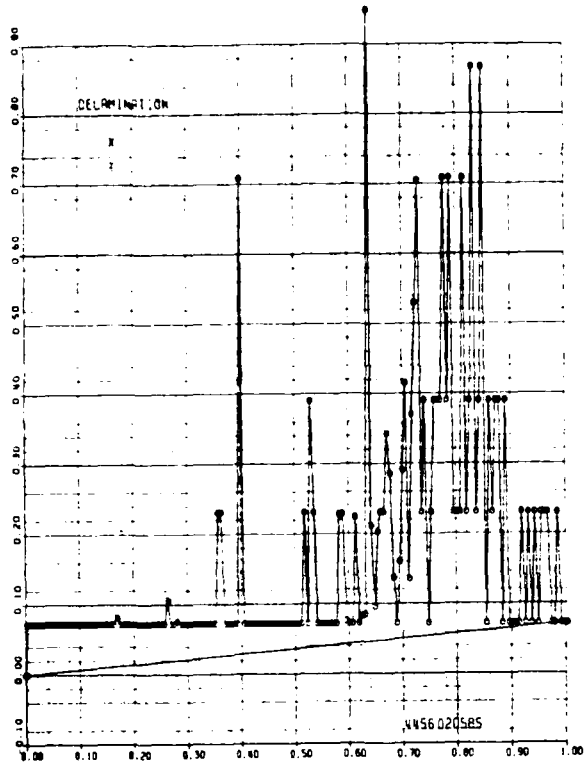

(b) Location of Counts

Figure 65. Stress versus Acoustic Emission Count and Location of Counts of Specimen D-10

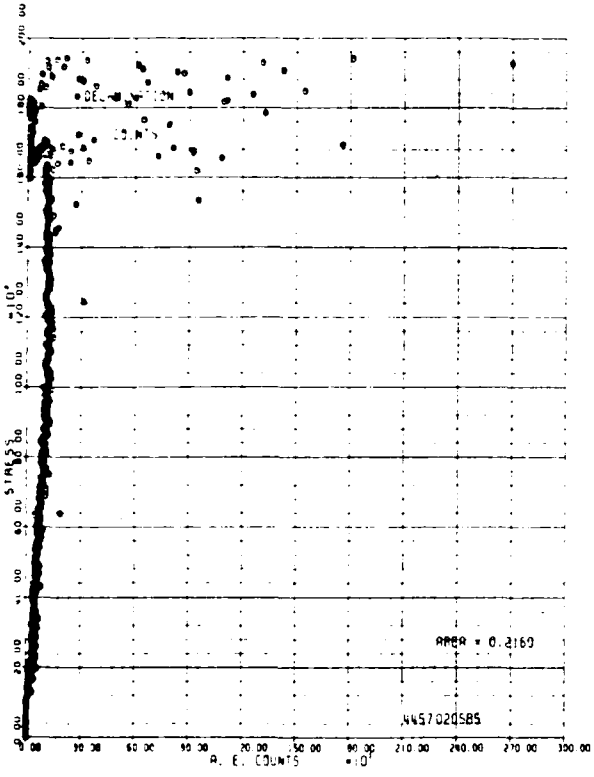

(a) Acoustic Emission Count

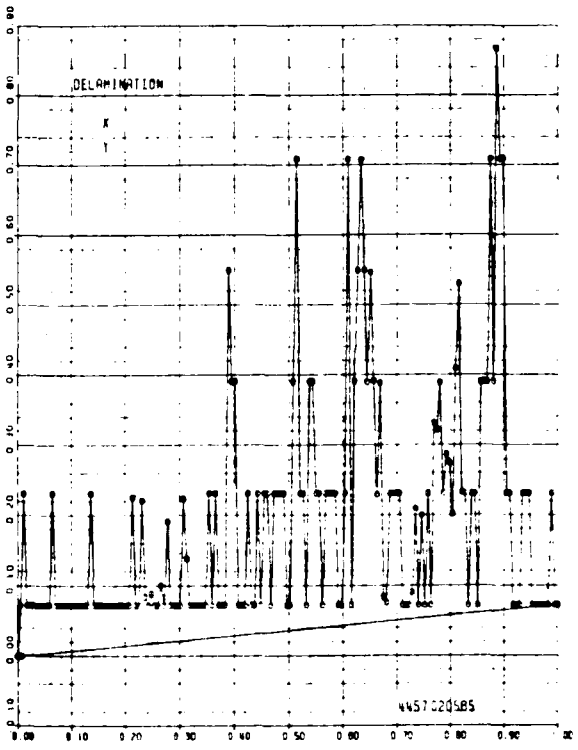

(b) Location of Counts

Figure 66. Stress versus Acoustic Emission Count and Location of Counts of Specimen D-11

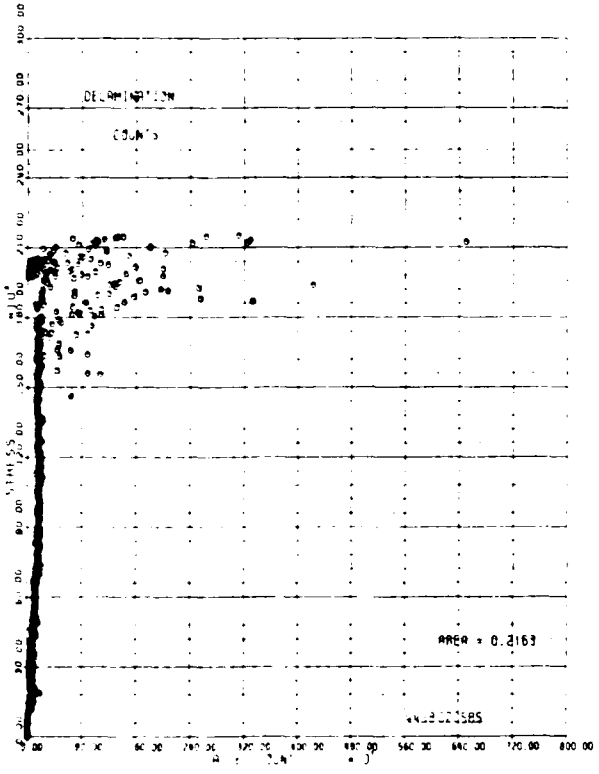

(a) Acoustic Emission Count

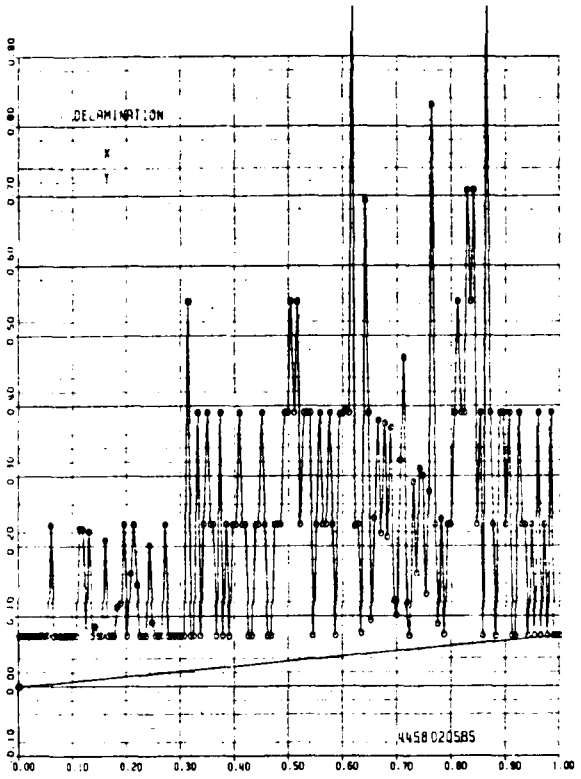

(b) Location of Counts

Figure 67. Stress versus Acoustic Emission Count and Location of Counts of Specimen D-12

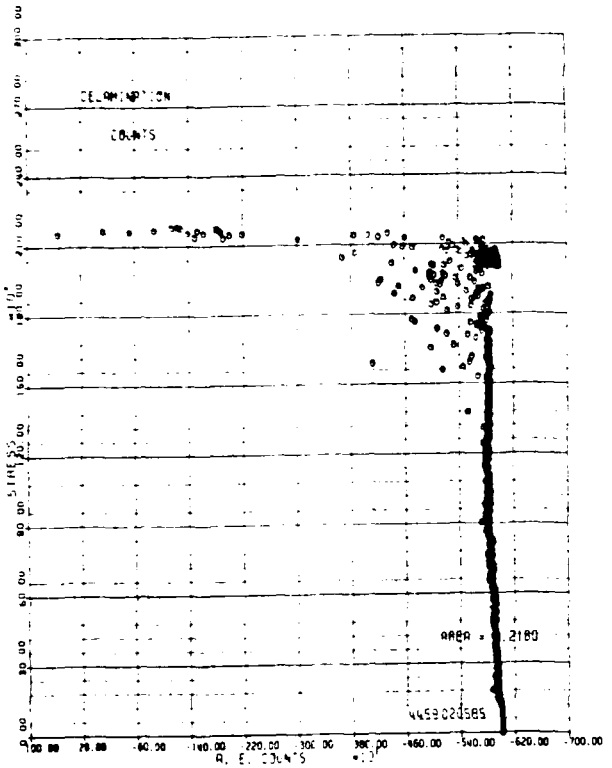

(a) Acoustic Emission Count

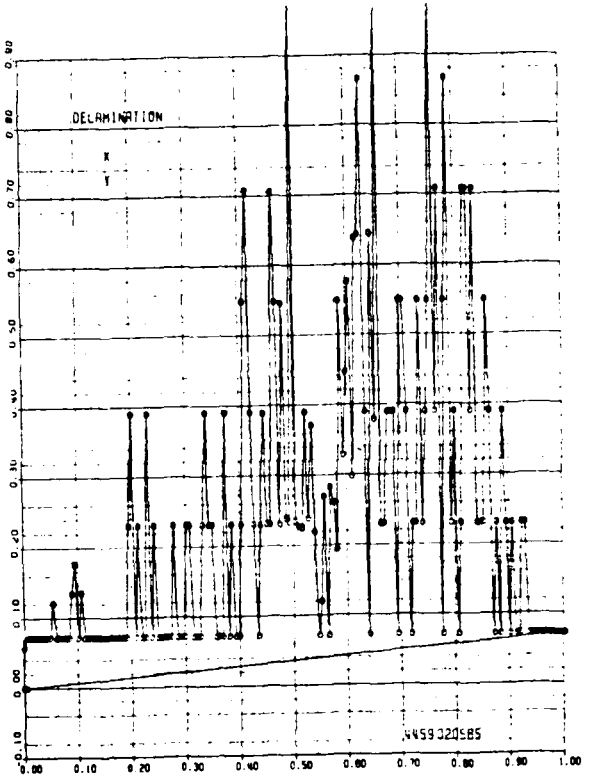

(b) Location of Counts

Figure 68. Stress versus Acoustic Emission Count and Location of Counts of Specimen D-13

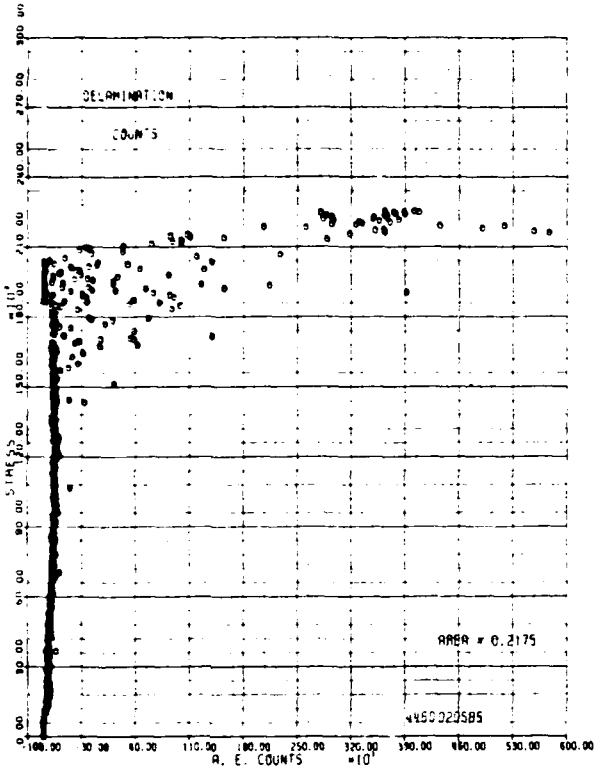

(a) Acoustic Emission Count

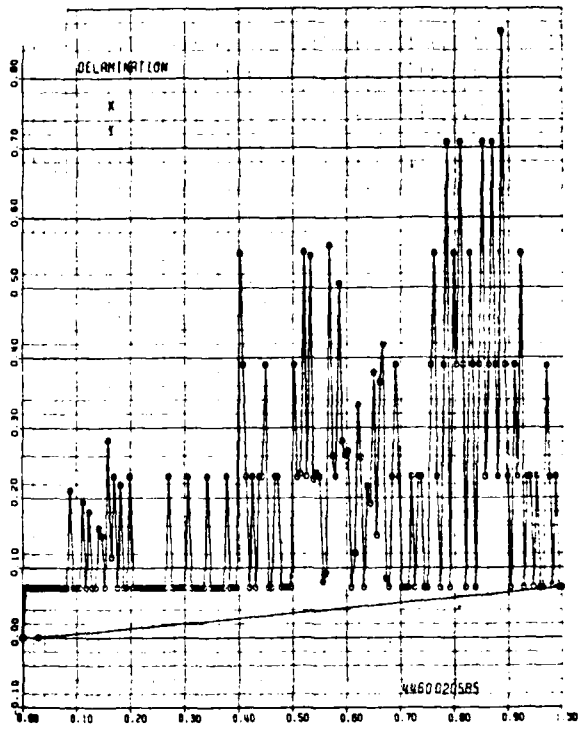

(b) Location of Counts

Figure 69. Stress versus Acoustic Emission Count and Location of Counts of Specimen D-14

Figure 70. Delaminated Specimen A-9

(a) Unloaded Specimen after Test

(b) Loaded Specimen

Figure 71. Delaminated Specimen A-13

(b) Loaded Specimen

(a) Unloaded Specimen after Test

Figure 72. Delaminated Specimen B-9

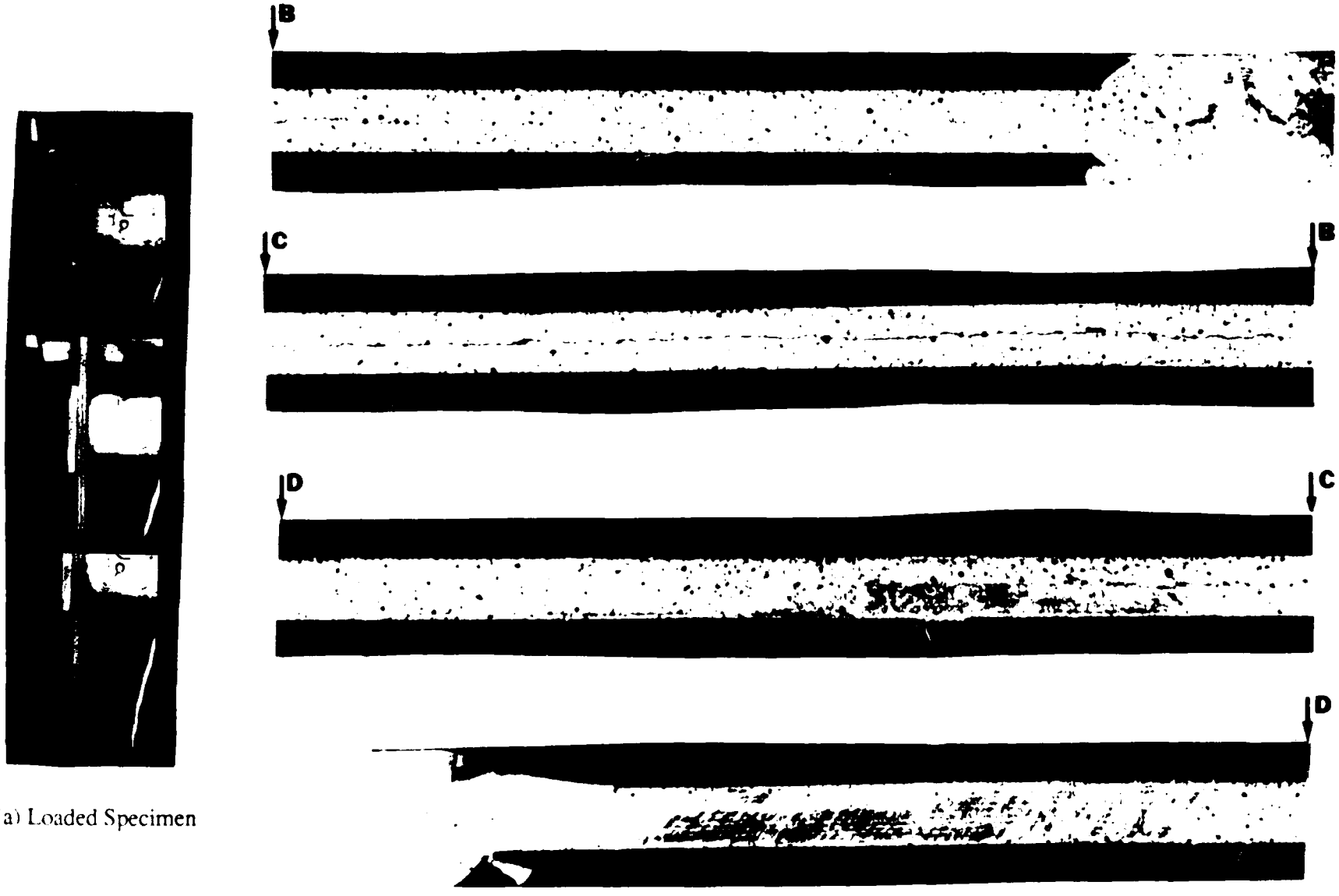

(a) Loaded Specimen

(b) Unloaded Specimen after Test

Figure 73. Delaminated Specimen C-9

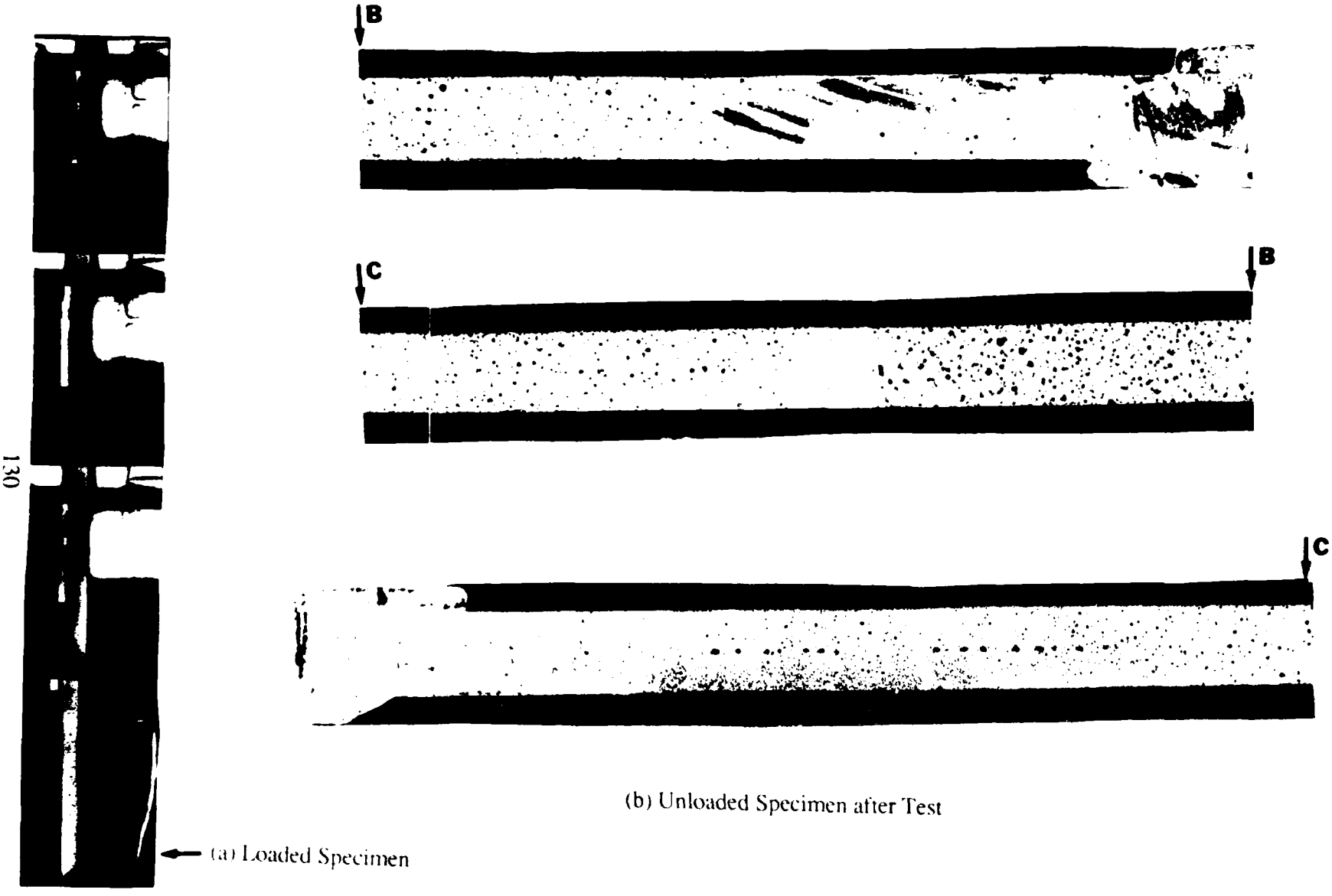

Figure 74. Delaminated Specimen D-9

(a) Loaded Specimen

(b) Unloaded Specimen after Test

Figure 75. Delaminated Specimen D - 14

(a) A-9 (b) A-13 (c) B-9 (d) C-9 (e) D-9 (f) D-13

Figure 76. Enhanced X-ray Photos of Specimens Shown in Figures 70 thru 75

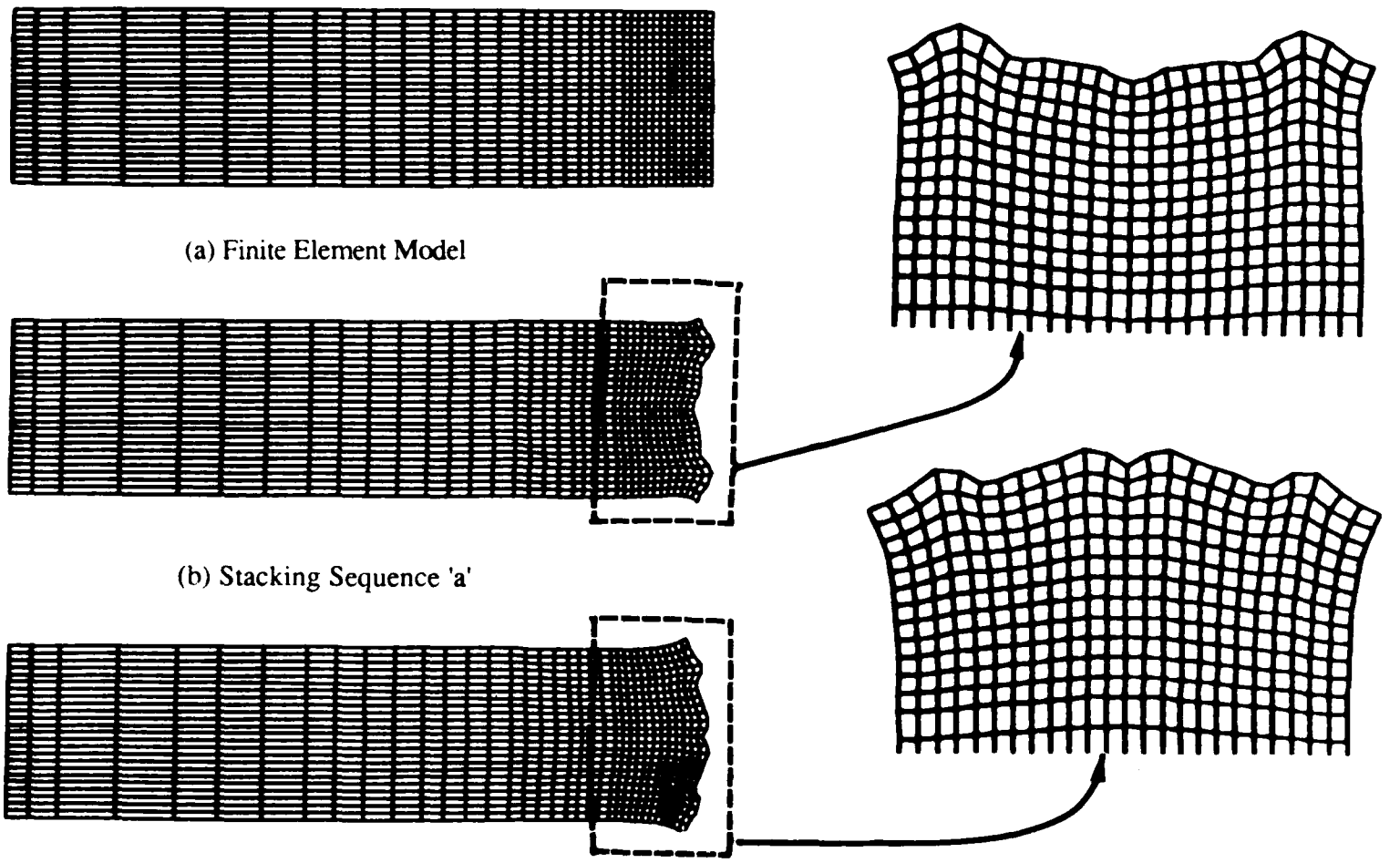

(a) Finite Element Model

(b) Stacking Sequence 'a'

(c) Stacking Sequence 'b'

Figure 77. Effect of Stacking Sequence upon Deformation and Resulting Peeling Stresses of a Laminate

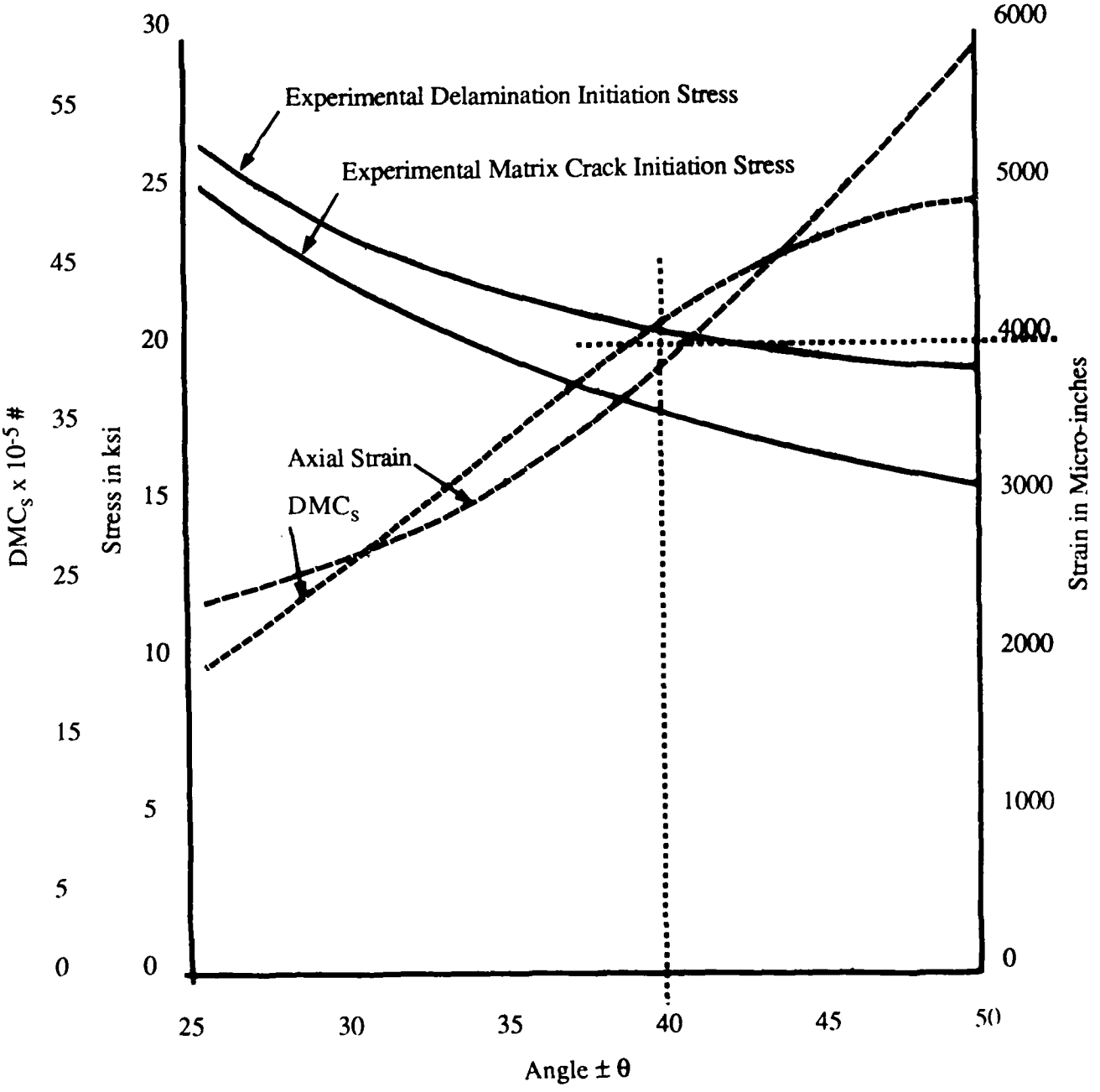

Figure 78. Variations of Delamination Initiation Stress, Matrix Crack Initiation Stress, Axial Strain for Matrix Cracking, and DMC_s in $(\pm\theta_5/90)_s$ Laminates

U.S.Government Printing Office 1987 548-054/80516